Modeling the Effects of Blade Dissimilarity on Rotor Vibrations for CH-47 Chinook Using a Viscous Vortex Particle Method

T. Pruijsers

Delft University of Technology

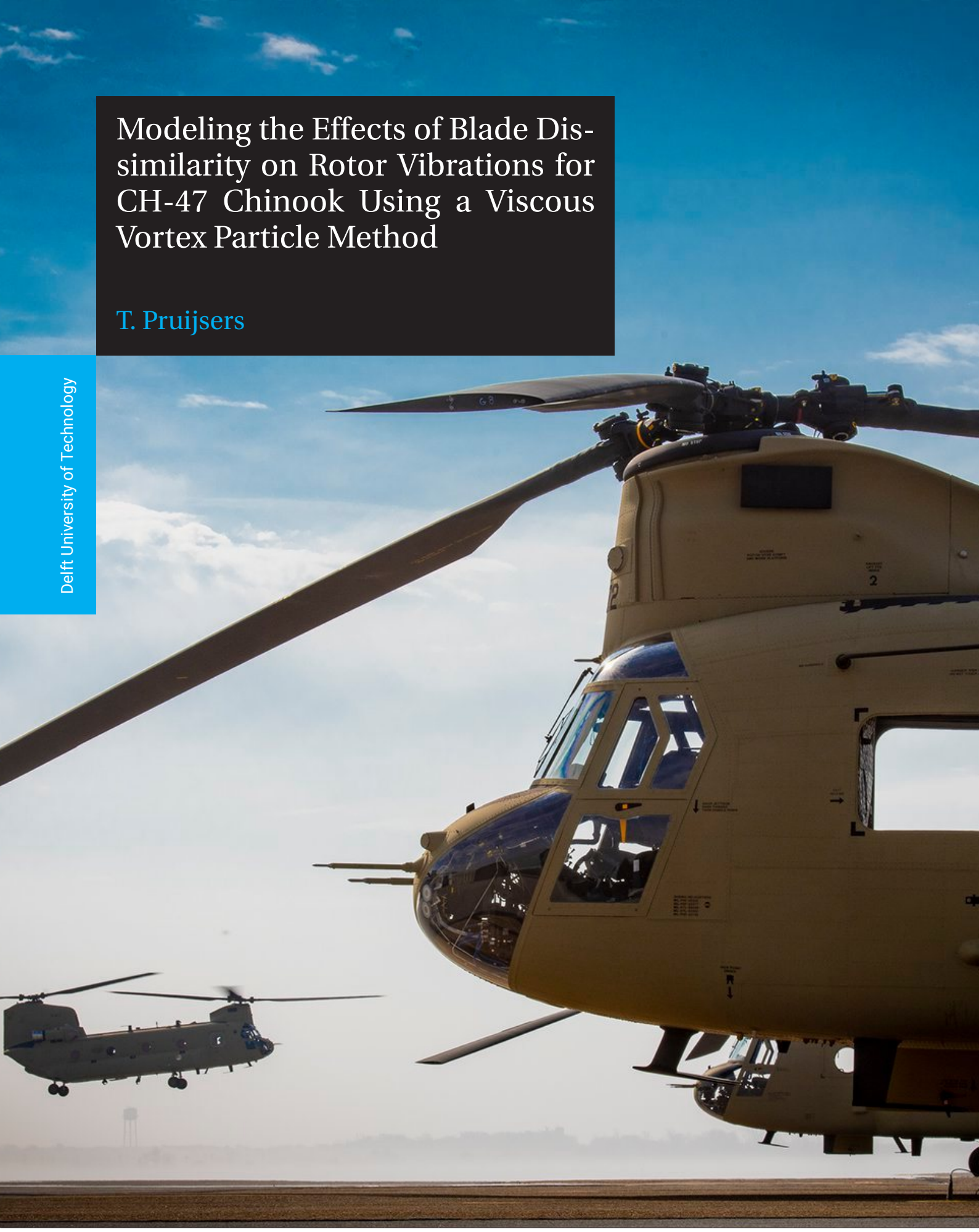

TU Delft Delft University of Technology

Challenge the future

Modeling the Effects of Blade Dissimilarity on Rotor Vibrations for CH-47 Chinook Using a Viscous Vortex Particle Method

by

T. Pruijsers

In partial fulfillment of the requirements for the degree of

Master of Science
in Aerospace Engineering

at the Delft University of Technology,
to be defended publicly on Tuesday April 26, 2021 at 09:00 AM.

Thesis Committee:	Prof. Dr. Ir. L.L.M. Veldhuis,	TU Delft	Committee Chair
	Dr. Ir. R. De Breuker,	TU Delft	Daily Supervisor
	Ir. R.J.J. Bakker,	NLR	Company Supervisor
	Dr. Ir. O.K. Bergsma,	TU Delft	Independent Committee Member

This thesis is confidential and cannot be made public until April 26, 2023.

TU Delft

nlr

Preface

This thesis report marks the end of a long journey. During my time at the University of Delft I have had the opportunity of learning many new skills, got to meet amazing people and was able to experience many inspiring ventures. I am sure I will be able to look back on this period with fond memories for the rest of my life.

I would like to express my sincere gratitude to the persons who have guided me through this thesis research. Firstly to Richard Bakker who offered me the opportunity to work on my thesis at the Rotorcraft department of the NLR. During the thesis work was always a great help whenever I had any questions. Secondly to Roeland de Breuker who guided me throughout the process with his knowledge and recommendations.

Furthermore, I would like to thank my parents, Marcel and Dionne for their support all of these years and my girlfriend Sonja for always believing in me.

Delft, April 2021

Abstract

Excessive rotor vibration causes increased component wear and operator discomfort. Therefore it is required to reduce the measured vibrations to below a certain threshold before the helicopter is ready for normal operations. For the 1/rev frequency this is done by applying the rotor tracking and balancing procedure. During this procedure adjustments are made to trim tab, tip weights and the pitch link in order to balance out the effects of dissimilarities between each blade. The RTB process however is time consuming and costly. Often a successful procedure required multiple test flights and in some cases balance for certain blade sets is not achieved at all. To address this the NLR has initiated the ARBI research project, which aims to accurately measure blade parameters in order to be able to predict its vibratory behavior in order to try and predict matching blade sets from inventory.

This research contributes to this project by evaluating the relation between a change in blade aeromechanical parameters and the resulting vibration levels. The first helicopter type for which ARBI will be specified is the CH-47 Chinook helicopter in service with the Royal Netherlands Air Force. This adds extra complexity, since there exists hardly any previous research into the effects of blade defects on 1/rev vibrations for standard helicopter configurations, let alone for a tandem rotor aircraft. The challenge for a tandem rotor is the rotor to rotor wake interaction.

In order to analyze the effects of blade dissimilarity a model of the rotorcraft was created in FLIGHTLAB, a selective fidelity helicopter simulation software. A relatively new addition to the FLIGHTLAB inflow solves is the Viscous Vortex Particle Method developed by He et al. (2017). According to the author this method is particularly well suited for the modeling of multi rotor systems. The VPM method stores vorticity in particles that travel along the wake of the rotor instead if using a grid and determining vorticity at each grid point, which would be computationally expensive and introduces numerical diffusion. The performance of the VPM model will be compared to a finite state inflow model without accounting for rotor interference in order to examine whether the effects of the wake interaction is significant. In addition, previous works such as by Lee et al. (2009) recommended the use of an elastic fuselage. To examine this recommendation a preliminary investigation was performed using a modal representation of the fuselage.

For both inflow methods the model was repeatedly run in FLIGHTLAB to a trimmed solution. For each trim iteration a single blade parameter was changed for a specific span section and airspeed. This was done to create and overview of which parameters had the greatest impact on 1/rev vibrations. In addition to adjusting the blade properties, the effects of adjusting the trim tab, tip weight and pitch link were also modeled, as the effects of these adjustments are known from test flight measurements. These were then used in order to try and validate the model's performance. Both the effects of pitch link adjustment and the balance weight addition match closely to the reference data. The trim tab effectiveness however was overestimated. This most likely is the result of XFOIL overpredicting the delta airloads for tab deflection, as it is best suited for lower Reynold's numbers.

It was shown that VPM method including interference modeling performed comparably to a finite state inflow model that did not include interference modeling when it comes to predicting the sensitivity of blade adjustments. Therefore it appears that rotor wake interaction only has a minor impact on 1/rev vibrations. Furthermore, the VPM model overestimated the vibrations in hover by quite a margin, which was not the case for the finite state model. The inclusion of a modal fuselage did have an effect on the results for blade adjustments. The change in vibration however was minor and did not lead to closer approximation of the flight test results in all cases. Based on this result and the increased computational cost for the fully elastic fuselage additional justification is necessary to develop and include it in future research.

The most influential blade property adjustments from the analysis were a shift in section chordwise CG location and a chordwise shift in elastic axis location. Also of significant influence are the section lift and drag coefficients, where the lift coefficient is up to four times more effective than the drag coefficient. The torsional stiffness and twist angle also play a significant role and their effects on 1/rev vibration are of similar magnitude as the increase in section drag coefficient. The flapwise and lag bending stiffness have a very minor influence on the 1/rev vibration. Further research into the occurrence of specific defects needs to be performed in order to apply the knowledge gained from this work.

Nomenclature

Greek Symbols

α	Vector-Valued Total Vorticity	$[1/s]$
β	Blade Flapping Angle	$[°]$
γ_{src}	Source Vorticity	$[1/s]$
Γ	Circulation	$[m^2/s]$
ϵ_t	Blade Twist Angle	$[°]$
ζ	Lead-Lag Angle	$[°]$
θ	Blade Pitch	$[°]$
θ_{ply}	Laminate Ply Angle	$[°]$
ν	Kinematic Viscosity	$[m^2/s]$
ρ	Air Density	$[kg/m^3]$
ϕ	Azimuth Angle	$[°]$
ψ	Phase Shift	$[°]$
ω	Frequency	$[Hz]$
ω_v	Vorticity	$[1/s]$
Ω	Angular Velocity	$[rad/sec]$

Latin Symbols

A	Amplitude	$[m]$
b	Blade Span	$[m]$
c	Chord	$[m]$
c_d	2-D Drag Coefficient	$[-]$
c_l	2-D Lift Coefficient	$[-]$
D	Rotor System Diameter	$[m]$
d	Rotor System Stagger	$[m]$
E	Young's Modulus	$[Pa]$
e_d	Elastic Axis Offset	$[m]$
G	Torsional Stiffness	$[Nm/rad]$
H	Rotor System Gap	$[m]$
M_c	Chordwise First Mass Moment	$[Nm]$
M_s	Spanwise First Mass Moment	$[Nm]$
n	Rotor System Number of Blades	[-]
r	Rotor Disk Radius	$[m]$
Re	Reynolds Number	$[-]$
T	Thrust	$[N]$
t_i	Laminate Ply Thickness	$[m]$
u	Flow Velocity	$[m/s]$
v	Poisson Ratio	[-]
v_i	Induced Velocity	$[m/s]$

Abbreviations

ARBI	Automated Rotorblade Inspection	[-]
ART	Advanced Rotorcraft Technology, Inc,	[-]
CBM	Condition Based Maintenance	[-]
CFD	Computational Fluid Dynamics	[-]
CG	Center of Gravity	[-]
DCP	Differential Collective Pitch,	[-]
FFT	Fast Fourier Transform,	[-]
GVT	Ground Vibration Test,	[-]
HUMS	Health and Usage Monitoring System	[-]
ISA	International Standard Atmosphere	[-]
MRO	Maintenance, Repair and Overhaul,	[-]
MSPU	Modern Signal Processing Unit	[-]
MTOW	Maximum Take-Off Weight,	[-]
NLR	Royal Netherlands Aerospace Center	[-]
RCAS	Rotorcraft Comprehensive Analysis System	[-]
RNLAF	Royal Netherlands Air Force	[-]
RTB	Rotor Track and Balance	[-]
USBF	Universal Static Balancing Fixture	[-]
VVPM	Viscous Vortex Particle Method	[-]

Contents

List of Figures

List of Tables

1 Introduction

The Royal Netherlands Aerospace Center (NLR) is developing new innovative approaches to improve the efficiency of aircraft Maintenance Repair and Overhaul (MRO). One of the projects being worked on is the Automatic Rotor Blade Inspection robot (ARBI). One of the aims of project ARBI is to try and aid the rotor track and balance (RTB) process for helicopters, which is the process of adjusting the rotor blades in order to minimize in-flight vibrations. A description of this process can be found in Section 2.3. The RTB process is carried out every time after the rotor blades have been removed from the hub, but also when pilots report experiencing high vibration levels while flying.

This vibration is caused by slight dissimilarities of structural and aerodynamic properties between the blades on the rotor. These dissimilarities occur due to component wear and production imperfections. For example water intrusion may affect the mass balance and damage/repairs may influence the blade stiffness distribution. To account for this the RTB process aims to balance the rotor by adjusting the pitch link, trailing edge tab and balance mass for individual blades. Measuring equipment in the helicopter monitors vibration and a software using an optimization algorithm suggests the adjustments to be made based on the measurements.

In its current form the RTB process often requires multiple test flights, with more adjustments made in between. This process is time-consuming and costly, moreover in some cases a solution can not be found at all, as concluded by De Bruin (2010). Additionally, some specific blades in the inventory of the Royal Netherlands Airforce (RNLAF) are known to cause problems. The occurrence of so-called "rogue blades" complicates the process. Rogue blades are defined as blades that sometimes match so poorly with other blades that balance is unobtainable, while when matched with other pairs do not cause any issues. The amount of iterations required could be reduced by trying to find a matching blade set among the blades across the inventory. One property that plays a major role in pairing blade sets is the blade span moment as determined by Buckel (2003). This is measured on a static measuring facility and is a prerequisite before starting the RTB process. Nevertheless the blades do not have uniform properties. This will be further elaborated on in Section 2.3.1. The goal of ARBI is to a reduce the time spent on RTB and the amount of required test flights. The project aims to determine whether it is possible to measure and quantify the blade property imperfections and predict the impact on rotor vibrations. With this knowledge it would be possible to select blade sets from the inventory based on how well they would match, requiring the least amount of adjusting. Additionally, if blade property imperfections could be measured and the effect on vibrations is known, adjustments can be predicted before test flights. This would lead to fewer flights required to reach satisfactory vibration levels.

The ARBI projects aims to design a 3-D optical/thermal rotor blade scanner that can measure both external and internal blade properties. These types of inspection machines are already being developed for wind energy and helicopter blades using thermographic imaging, X-ray and shearography. Examples of their applications are found in works by: Meinlschmidt and Aderhold (2006), Krumm et al. (2019) and Pezzoni and Krupka (2001) respectively. The goal of this research is to aid in setting requirements for the fault detection and quantification method and the required resolution. This is done by individually changing the properties of a single blade by a certain percentage and evaluating the effect it has on vibration levels. It is unknown however, what the realistic parameter variation is in the blades.

1.1. Research Questions

The ultimate aim of this research is to reduce the amount of effort spent on the RTB process for the Chinook helicopter. It is hypothesized that when more knowledge is gained on which blade parameters have the most influence over vibration levels, that this knowledge can be used to tailor blade selection for RTB during the maintenance process. The current balancing process measures far from all blade parameters, as will be presented in Section 2.3. The ability to rank individual blade parameters based on their influence on vibration levels could dictate requirements for new measuring equipment. Therefore the main research question of this research is formulated as:

> MQ: "Which aeromechanical parameters of the CH-47 Chinook helicopter rotor blades have the greatest impact on the system's one-per-rev vibration levels during flight?"

The answer to the main research question can be quantified by computing the 1/rev vibration level of the system in inch per second using FLIGHTLAB. A sensitivity study can be performed on the different parameters within their respective operationally observed ranges to rank them based on their influence on the vibration levels. Examples of causes for blade dissimilarity include: repairs, delaminations, water intrusion and airfoil erosion and other effects due to extended use. On top of that, even brand new blades show dissimilarities due to manufacturing imperfections. The modeling of these parameters will be further elaborated on in Section 2.6.

In support of the main question there are a couple of sub-questions that help answer the main research question. Lee et al. (2009) have shown that the adjustment coefficients on both rotors behave quite differently and adjustments on one rotor influence the vibratory forces on the other, this was also apparent from flight test data. Just as for the balancing adjustments, the natural blade perturbations will behave differently depending on which rotor and will have an influence on the opposite rotor. Therefore a model excluding rotor on rotor interference will be created and compared to a model including rotor on rotor wake interference. One of the sub-questions of this research will be to examine what the difference in results will be between these two modeling approaches:

> SQ1: "What is the effect of the tandem rotor configuration on the 1/rev vibration levels of the rotor systems and how can this effect be captured in a computational model?"

This question will be answered by comparing the coefficient values following from both modeling approaches. From flight test data it is known that the front rotor is influenced much less by the rear rotor than the reversed situation and that the blade adjustment sensitivity coefficients are smaller on the rear rotor. Therefore it is hypothesized that the sensitivity coefficients for blade dissimilarity on the rear rotor will be smaller than those on the front rotor. Based on Lee et al. (2009) the coefficients on the front rotor of the tandem rotor system should be mostly unaffected by rotor interference. It will be of interest to test to what extent this will follow from the results from the FLIGHTLAB analysis. The state of the art Viscous Vortex Particle Method (or VPM) inflow model discussed by He et al. (2017) will be used since it specifically addresses the complexities of multi-rotor aerodynamics.

The investigation by Terpening et al. (2016) recommended future research should include a flexible fuselage to more accurately represent the vibrations felt in the cockpit. A model of the CH-47 fuselage is available in modal form and can be included in the model. Including the fuselage however will result in a greatly increased computation time. Therefore it planned to perform a small number of simulations to investigate the effect on the blade adjustment coefficients. This leads to the final sub-question:

> SQ2: "Does the inclusion of a flexible fuselage increase the accuracy of predicting the vibration coefficients?"

This question will be answered by comparing the results for a rigid fuselage set-up and a model with a flexible fuselage in modal form for a each of the blade adjustments. From the results of this analysis it needs to be concluded whether or not the difference in predicted vibrations is significant enough to justify the extra computation costs for determining the full set of coefficients.

It will be challenging to validate the model since the actual values for the natural perturbation vector are unknown. An indication of the validity of the model can be obtained by computing the blade adjustment sensitivity coefficient matrix. This matrix is the collection of the effects of each of the three RTB adjustments on vertical and lateral vibration on both rotors. These coefficients have been collected during flight testing. Therefore in order to assess the applicability of the model the following sub-question needs to be answered:

SQ3: "What are blade adjustment sensitivity coefficient values predicted by the model and how well do they match flight test data?"

There are three adjustment parameters per blade and three blades on each of the two rotors. Each of the adjustments influences vertical and lateral vibration levels on either rotor hub. This results in twelve sensitivity coefficients per flight condition for a specific blade. Currently HUMS software suggests the adjustment settings during RTB based on its own integrated set of sensitivity coefficients specified by the manufacturer. These values however, are currently not known.

1.2. Research Objective

The project goal is to provide insight into which rotor blade aeromechanical parameters have the largest influence on in-flight vibration of the CH-47 Chinook helicopter. This will be done by means of creating a computational model quantifying blade deformation and vibrations using the program FLIGHTLAB and comparing its results to measurement data from RNLAF operation. In order to limit the scope to what is achievable within the thirty week thesis schedule the helicopter fuselage will be assumed rigid, the rotor rpm constant and the hub hinges and damper equal during all measurements, although a preliminary investigation will be performed using a flexible fuselage in modal form. A sensitivity analysis on the blade parameters can be performed to identify the most significant contributors to the system's vibration levels. To create this model aerodynamic performance and structural data on the blades needs to be collected. Structural data for the rotor blades is available. The aerodynamic coefficient data can be collected by using XFOIL. The aerodynamic analysis includes studying the effects of reduced airfoil lift or increased airfoil drag and the effect of blade trim tabs. Furthermore, the effect of the tandem rotor configuration on the rotor dynamics will be evaluated by comparing an isolated rotor system to a rigidly connected tandem rotor system. The new VPM module included in FLIGHTLAB will be used to resolve the rotor wake and wake-blade interaction.

This research is part of a larger effort to investigate a way to increase RTB process efficiency for rotorcraft. The NLR has previously performed a similar study on a single rotor helicopter. Results from that analysis provided a ranking of the most important parameters, which currently being applied in an experimental setting. This research can strengthen the credibility of their findings if results are similar. Additionally the effects of the tandem rotor configuration can be investigated. The current software used for RTB by the RNLAF only works by measuring vibrations while the rotor system is running and suggests adjustments to the blade tabs and weights based on those measurements. It however, does not provide insight into the cause of the vibration. The novelty of this research is the aim to find causal relations between blade parameters and the vibration levels.

There already exists a basic computational model of the Chinook rotor blade system, however this has not yet been validated. This thesis continues to build on this groundwork. Other projects within this research topic are looking for ways to accurately measure rotor blade properties. The aim of the combined research projects is to gain more knowledge in the relevance of blade parameters and to develop new measurement techniques that offer the opportunity to create a more efficient RTB process.

The problem background will be discussed next in chapter 2. This chapter will introduce the rotorhead dynamics for an articulated rotor system such as the CH-47. Additionally it will touch upon the description and origin of rotor vibration and how the RTB process is currently applied. In chapter 3 the structural and aerodynamic modeling within FLIGHTLAB will be discussed. In addition to the blade structural and aerodynamic theory the principles of the VPM method, that is applied to represent the vorticity distribution in the rotor wake will be introduced. The representation and adjustment of both the rotor adjustments (trim tab, pitch link and tip mass) and the blade structural and aerodynamic properties within the FLIGHTLAB environment will be explained in chapter 4. This chapter also touches on the way a trimmed flight solution is obtained and how the maximum vibration level is then computed. The resulting changes in vibration due to an adjustment for a specific blade property are presented in chapter 5. In this chapter the results for both a model without VPM wake modeling and with are presented and compared. Chapter 5 also includes an investigation into the causal principle behind the increased vibration and whether structural dynamics or aeroelastic behavior plays a more significant part. In Section 6 the predicted effectiveness of trim tab, pitch link and tip weight of the computational model will be compared to data collected from flight tests. This is done in order to examine how well the model represents the effects of RTB adjustments and to provide a degree of confidence for the results obtained in chapter 6. The flight test data will also be compared to a separate FLIGHTLAB model that has a modal fuselage representation in order to examine the effects of its

inclusion. Furthermore a sensitivity analysis is carried out to investigate the significance of changes in the initial conditions of the computations. The conclusions drawn from the research and the recommendations that follow will be discussed in chapter 7.

2

Project Background

This section aims to introduce the principles that play a role in rotor track and balance and discusses some works of researchers that have previously contributed to this field. First a short introduction to the rotor assembly and the dynamics of an articulated rotor system will be given in Section 2.1. The definition of rotor vibration will be elaborated on in Section 2.2. This section will also treat the different types and origins of vibration experienced by pilot while flying in different flight conditions. The rotor tracking and balancing methods that are currently used will be discussed in Section 2.3. This section will introduce the purpose of the trim tab, pitch link and tip mass and in which situation an adjustment to each is applied. The distinction between rotor static and dynamic balancing will also be made clear. The mathematical basis for rotor vibrations for a generic rotor system have been presented by Rosen and Ben Ari in 1997. Even though their work is over twenty years old at this point their work is still very relevant today and is still often cited as a basis for works comprising the current state-of-the-art. Their mathematical description will be summarized in Section 2.4. A description of the tandem rotor system and the rotor geometry of the CH-47 is presented in Section 2.5. The selection of the relevant blade properties to be investigated follows from works by other researchers. These works and which parameters are deemed relevant to this research are discussed in Section 2.6.

2.1. Rotor Dynamics

The rotor of a helicopter is complex system containing many moving parts and there exist many different configurations. Something the majority of helicopters share is that the pilot controls the rotor system using three inputs, namely the collective, the cyclic and the pedals. By manipulating the collective the pilot controls the total rotor thrust and uses it to determine the vertical velocity of the rotorcraft. The cyclic is used to adjust the lateral and longitudinal attitude angle of the helicopter and in combination with the collective is used to adjust the forward and sideways velocity. The pedals are used to rotate the helicopter around its vertical axis in order to change its heading. For a single rotor helicopter the pedal usually controls the tail rotor power. For a tandem rotor system such as the CH-47 the control mechanics become slightly more complicated, as the stick input from the pilot needs to distributed over two separate main rotors. The CH-47 makes use of what is called differential collective pitch (DCP). When the pilot inputs forward cyclic in the Chinook the collective setting on the rear rotor increases and the collective on the forward rotor decreases. In a similar way, pedal inputs cause opposite lateral cyclic pitch on either rotor to create a moment around the center of gravity.

The mechanisms of the collective and the cyclic are similar. Both of the inputs translate to a specific change in pitch angle on the blades, where the collective increases the pitch of the blades collectively and the cyclic only increases pitch at a specific azimuth angle. This uneven pitch distribution then causes rolling motion. This can be best explained by first taking a closer look at an example of a rotor assembly for a helicopter with a single main rotor, such as shown in Figure 2.1.

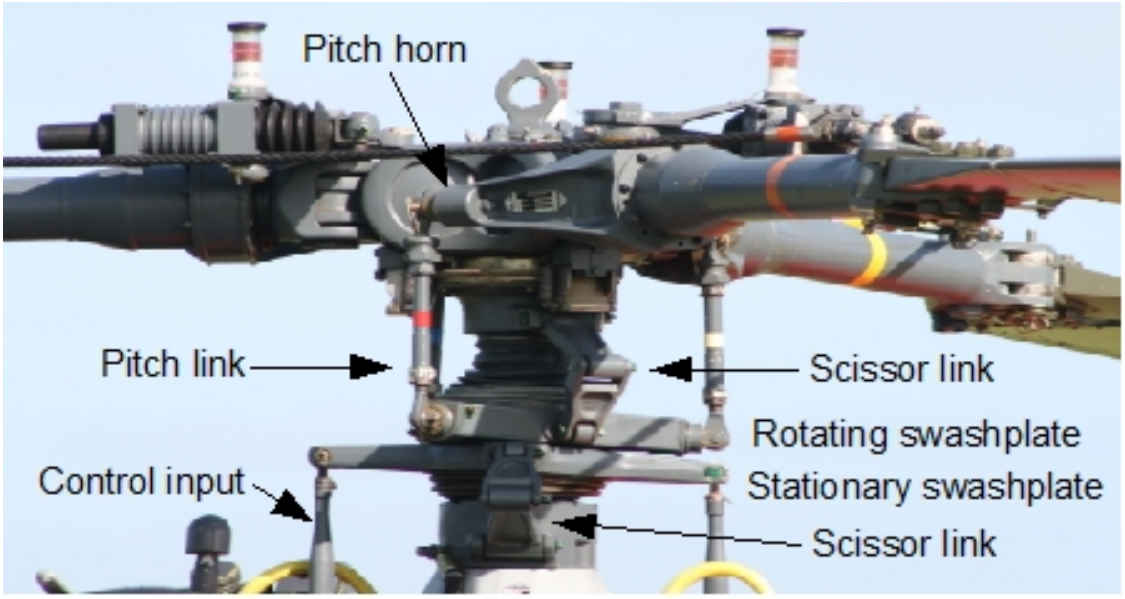

Figure 2.1: Rotorhead and swashplate assembly for a rotorcraft with part names indicated (Helistart.com).

When the pilot increases the collective the entire swashplate will translate up vertically, extending the pitch links. The pitch links are connected to the blade at the pitch horn. This pitch horn extends either forward from the leading edge or aft from the trailing edge of the blade, depending on the helicopter model. The pitch horn translates the vertical motion of the pitch link into a pitch rotation. This in turn increases the lift on all the blades, increasing rotor thrust. When the pilot uses the cyclic the swashplate will tilt, consequently the pitch links will be extended more on one side than on the other. Due to the effects of gyroscopic precession, the increased pitch angle only causes a lift increase 90 degrees later. This means that when a pilot wants to roll to the right with a counter-clockwise spinning rotor that the lateral cyclic input results in an increased pitch when the blade passes over the nose of the helicopter.

A defining aspect of rotorcraft is the dissymmetry of lift on the rotor disk in forward flight. The airspeed of the helicopter causes the advancing blade to experience a higher flow velocity than the retreating blade. When unaccounted for, this induces rolling motion due to force imbalance. To deal with this rotor blades flap as they rotate. When the blade flaps upward, the effective angle of attack decreases, resulting in a reduction of lift. When the blade flaps downwards, the lift is increased. To deal with the dissymmetry of lift on the rotor disk, the blade flaps upwards in the advancing phase and flaps back down in the retreating phase. As a result of the flapping motion however, the center of gravity moves inboard towards the center of the rotor disk when the blade flaps up. According to the law of conservation of momentum, objects spin faster when more of the mass is concentrated close to the axis of rotation. Consequently, the blade will try to 'lag' during downwards flapping and will try to 'lead' during the upwards flapping. In order to alleviate loads associated with this effect, a lead-lag hinge is included in the rotor assembly to act as a damper for the lead-lag motion. A fully articulated rotor system is a rotor that includes hinges for pitch, lead-lag and flapping motion. The diagram of an articulated rotor presented in Figure 2.2 shows these rotor hinges and their axis of rotation in an arbitrary order.

Another aspect of rotorcraft that makes their modeling more complicated than fixed wing aircraft is the concept of induced flow distribution also known as inflow. Induced flow is the vertical component of the flow that results from the air being forced through the rotor disk. This vertical component changes the local effective angle of attack distribution over the rotor disk. A representation of this effect is shown in Figure 2.3. In addition, the vortices in wake also influence the inflow distribution. The lift on lifting bodies results from bounded vortices that are attached to the surface. When these vortices separate from the surface they become free vortices that are located in the wake. For a rotorcraft in forward flight these free vortices move along with the flow. There exist multiple modeling methods for representing this effect and can be very computationally expensive if a high fidelity is required.

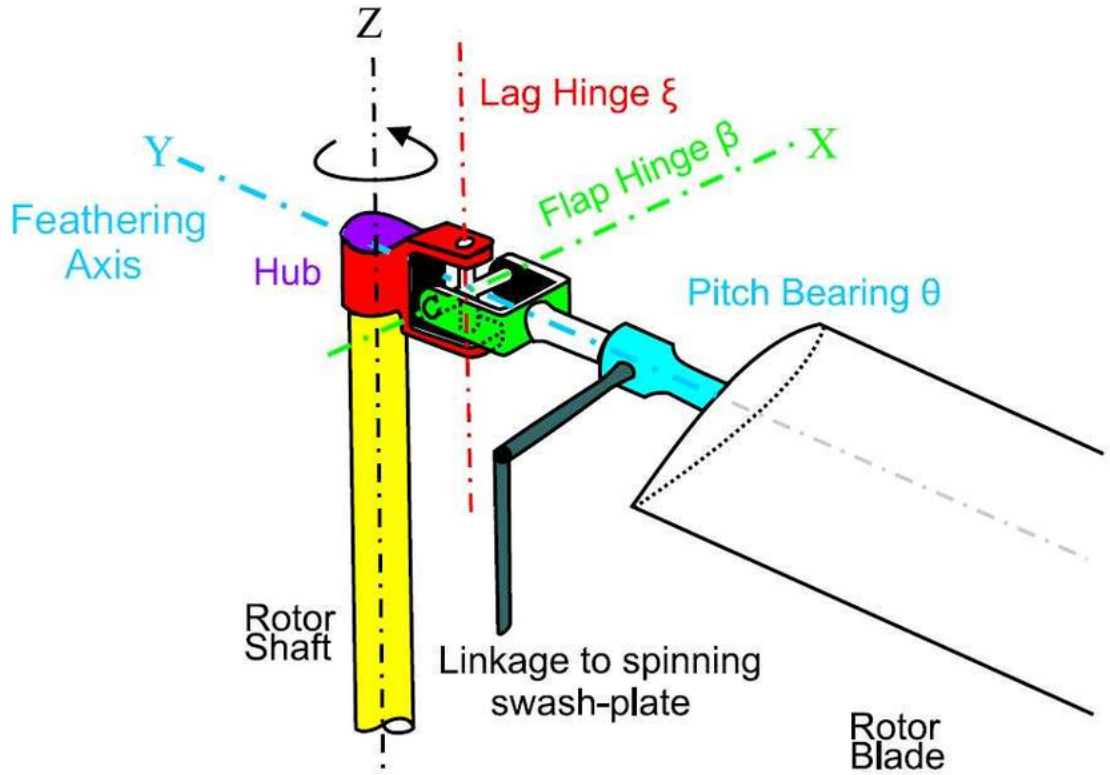

Figure 2.2: Definition of the rotor hinges that control blade dynamics (Marichal et al. (2013)).

2.2. Origin of rotor vibrations

A short background on the underlying physics on rotorcraft vibration follows from Nguyen (1994), which is summarized in this paragraph. The dominant source of excessive vibration is usually the main rotor of the helicopter. Even with perfectly identical blades the blades can experience harmonic aerodynamic effects such as dynamic stall, reversed flow and transonic effects in forward flight. Additionally, the blade airload distribution is affected by wake effects disturbing the inflow distribution. The effect is especially relevant in this case, since for a tandem rotor helicopter mutual wake interference is inherent to the rotorcraft's design. Moreover, rotor blades are rather slender and flexible beams connected to a set of torsional spring-damper hinges resulting in large periodic angular and bending deflections. These deflections are coupled to the aerodynamic loading on the blade, which makes the issue of rotor vibrations fundamentally an aeroelastics problem. The vibration addressed in this research revolves around what would be measured on a set of accelerometers, one located in each of the rotor pylons. During RTB the measurements from these accelerometers are used for the assessment of whether the vibration falls within acceptable parameters.

There are a number of distinctions that can be made between different types of vibration. Firstly there is the distinction between vibrations with a frequency equal to the blade revolution frequency, so called "1-per-rev" or 1/rev vibrations and the n/rev vibrations (n = nr. of blades). The 1/rev vibrations are associated with aerodynamic and inertial dissimilarities between blades. Both these dissimilarities are addressed during RTB. This process will be elaborated on in Section 2.3. The n/rev vibrations result from higher harmonic loading of the rotor and are mainly caused by aerodynamic effects. These include compressibility effects, stall, and wake interactions. These typically occur in high speed forward flight due to aerodynamic asymmetry or at very low speed, where the blade-wake and airframe interaction are the main causes. This type of vibration typically cannot be directly adjusted with the standard RTB procedure, as stated by Johnson (1980) and Robinson (1999), although the procedure for minimizing n/rev vibrations is often carried out in conjunction with RTB smoothing. Since RTB only deals with the 1/rev vibrations the n/rev will be considered out of the project scope.

There is an additional distinction to be made within the 1/rev vibration. Namely, lateral and vertical vibration. According to a study on RTB procedures by Renzi (2004), Vertical vibrations predominantly occur

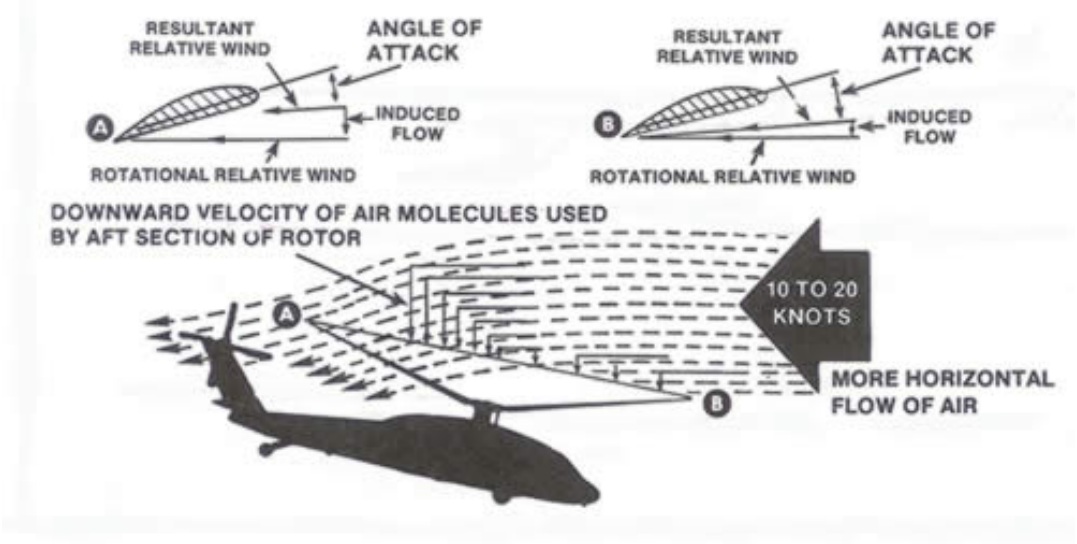

Figure 2.3: A visual representation for the effect of induced flow (ierw (2004)). In this case the induced flow component increases the effective angle of attack on the aft half of the rotor disk.

due to a difference in aerodynamic performance between the blades. When one blade produces a different amount of lift compared to the other blades at a specific azimuth location the result will be a vertical bouncing motion. In the case of pure vertical vibration an outside observer would notice the pilots going up and down at the same time. The aerodynamic imbalance that causes vertical vibration results from dissimilar blades. This dissimilarity is the result of manufacturing imperfections and blade or rotorhead wear. During the RTB procedure, adjustments to the trim tab and the pitch link are made to account for the vertical imbalance. Some specific types of defects are: damage/repairs, blade erosion from abrasive flight conditions, uneven twist distribution and wear of the rotor hinges. This research however, not so much considers specific defects themselves but only the effects of changes in blade properties i.e, a repair may cause a change in both flapwise stiffness distribution and CG location, but this work studies only the decoupled effects of a change in either property. This allows for further research to quantify the impact on vibrations of specific blade defects and repairs.

Lateral vibration is mainly caused by dissimilarities in mass distribution between the blades. To be more precise, the blade span moment is the main concern when it comes to lateral imbalance. When the helicopter experiences pure lateral vibration an outside observer would notice one pilot bouncing up and while the other pilot bounces in opposite phase. Another cause for lateral vibration is a variation in the lead-lag behaviour between the blades, due to for example a worn lag damper, since the lead-lag motion controls the CG arm. Furthermore, water absorption into the honeycomb structure of the blade due to capillary action can lead to lateral vibration. This problem appears to solve itself sometimes after a number of ground runs though, according to the RNLAF bladeshop. This is likely due to the centrifugal force of the spinning rotor acting on the water molecules. The main way to account for lateral vibration is by adjusting the tip balancing weights.

In order to limit the scope of this work to what is possible within the time frame for a thesis, only dissimilarities on the blade will be investigated. The effects of dissimilarities within the rotorhead, such as lag dampers and the pitch link remain for future research. Other sources of vibrations that are not part of the main rotor assembly such as the engines, oil cooler fans and drive shaft assembly will not be considered in this research, since they are also not addressed during RTB.

2.3. The Rotor Track and Balance Process

The RTB procedure is applied to the a helicopter rotor system in order to ensure that the vibrations of the system are within limits during flight. The procedure is required every time a set of blades is attached onto the hub. It is also carried out when pilots report having experienced excessive vibrations in flight. Vibrations in helicopters can lead to shortened component lifespan and crew fatigue and therefore need to be mitigated as much as possible according to Ferrer et al. (2001).

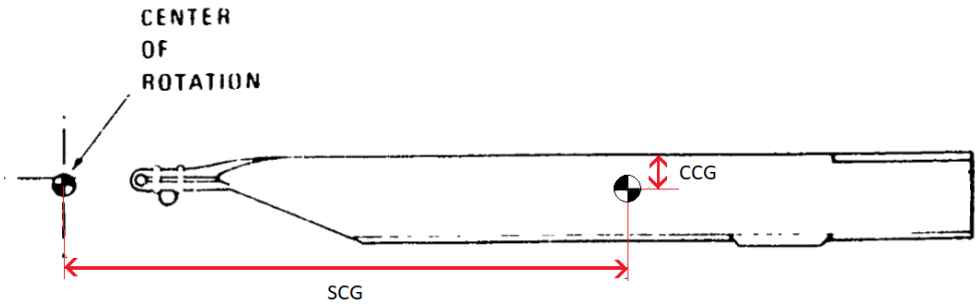

Figure 2.4: Definition of the spanwise and chordwise center of gravity location.

Even though the procedure is called tracking and balancing, perfect track has become less of a strict requirement. Excessive vibrations can still exist with perfect track and the inverse of that statement is also true, although perfect track is correlated with low vibration levels. This conclusion is supported by multiple publications such as: Wroblewski et al. (2000) and Rosen and Ben-Ari (1997a).

In order to balance for lateral and vertical vibrations, some adjustments are made to the individual blades. The helicopter that is treated in this report has two main rotors with three blades each. as discussed in Section 2.2, adjustments to the trim tab and pitch link are mainly to address vertical vibrations, while the dynamic balance weights are used to account for lateral vibrations, although each of these adjustments has a non-negligible effect on both directions of vibrations. The process consists of static balancing, which concerns the blade mass moment and dynamic balancing which concerns the blade dynamic behavior such as the flap and lag motion and the aerodynamic loads. Dynamic balancing is always performed after static balance has been achieved.

2.3.1. Static Balancing

The goal of rotor static balancing is to end up with a set of blades that requires a minimal amount of dynamic adjustments. Static balancing has the widest tuning range and therefore is performed prior dynamic balancing to provide a higher RTB success chance. Static balancing mainly addresses dissimilar spanwise mass distributions between the blades. Fortunately, this imbalance is also relatively straightforward to solve by adjusting the amount of blade tip weights, although the blades do have to be removed from the rotor hub for measurements. The actual total blade mass or CG location does not have to be identical for each blade, instead the blade span moment is of critical importance for low rotor vibrations (imagine balancing a seesaw with the fulcrum off-center). The span moment in this case represents the blade weight multiplied with the distance between the center of the rotor hub and the current blade center of gravity location. This is indicated in Figure 2.4.

The role of static balancing in the RTB process was investigated by Buckel (2003) for multiple US Army helicopters. From measurements it was concluded that there was much variance in the span moment between different blades. Many blade sets had span moment differences greater than the maximum span moment authority provided by dynamic balancing weights. This leads to a non-existent balancing solution if only dynamic balancing is performed. This is addressed by performing static balancing. Static balancing entails measuring the span moment and adjusting the amount of weights at the blade tip to meet a specific target span moment before initiating dynamic balancing. The static balance weights are different from the dynamic balance weights, such that the full dynamic weight adjustment range can be utilized during dynamic balancing. The Universal Static Balance Fixture (USBF) shown in Figure 2.5 is an example of span moment measuring equipment. Each of the blades will be adjusted until their span moments are as close to the manufacturer prescribed value as possible.

The chordwise moment is currently not being used for static balancing. Part of this research will be to investigate whether measuring chordwise moment could be used in order find matching blade sets. It is known from aeroelastics theory that the location of the center of gravity plays a significant role in the blade dynamic response.

Figure 2.5: The USBF span moment measuring system used for static balancing developed by Avion services (Buckel (2003)).

2.3.2. Dynamic Balancing

Dynamic balancing can be performed while the blades are mounted on the hub and after static balancing has been completed. Although the blades themselves do not have to be removed, making the adjustments to the blades is still a time consuming process. Dynamic balancing is an iterative process that starts with making adjustments to the blades, followed by ground runs and concluded by flight tests, during which vibration measurements are collected. The types of adjustments will be further elaborated on in 2.3.3. The measurements following each cycle are used to make further adjustments to the blades, after which a new iteration is initiated. The Health and Usage Monitoring System (HUMS) is an integrated system that is used to measure the vibrations. It consists of a set of accelerometers located under each rotor hub and a central processing unit. The test pilot is supposed to fly a specific flight condition for some time, such that HUMS can collect vertical and lateral vibration data for each flight condition. These airspeeds are: hover, 100 knots and 130 knots. The system provides vibration amplitudes based on the measured accelerations in inch per second (ips). When the helicopter returns to base the measured data is loaded into a computing program. The sensitivity coefficients of the pitch link, tab and tip weights are known from flight tests and are integrated in this software. Based on both the measured vibration during the flight and the known sensitivities of the blade adjustments the algorithm is able to suggest blade adjustments that should mitigate vibrations. It is hard to eliminate vibrations completely since an optimal solution for one condition might be unfavorable at another, as stated by Rosen and Ben-Ari (1997a). Therefore, measurements from all flight conditions are used to obtain a single solution. Specialized algorithms are required to solve this optimization problem.

2.3.3. Dynamic Balancing Blade Adjustments

As has previously been mentioned, there are three adjustment methods to balance the blade, tip weights, pitch link and trim tab. Each of these have different sensitivities when it comes to lateral and vertical vibrations. The pitch link and the trim tab are mainly used to tune for vertical vibrations, while the balance weights are mainly used for lateral vibration.

Dynamic Balance Weights

The tip of the blade can be removed to allow for the placement of balancing weights. Figure 2.6 shows the schematic representation of the blade tip. Note that the dynamic balance weights that are treated in this research are indicated as balance weights in the schematic. It can be observed that the other types of weights have a forward and a corresponding aft variant. These are mainly used for offsetting spanwise and chordwise mass distribution changes due to repairs to the internal blade structure and skin patches. The figure shows that the weights are located almost at the very tip of the blade.

After static balancing has been completed the span moments of the blades should be roughly identical. In flight however, aerodynamic effects could still cause lateral imbalance. During dynamic balancing the distribution of the weights is further adjusted in order to account for the dynamic effects experienced in flight. Just as was the case for static balancing, the dynamic balance weights are located in the blade tip.

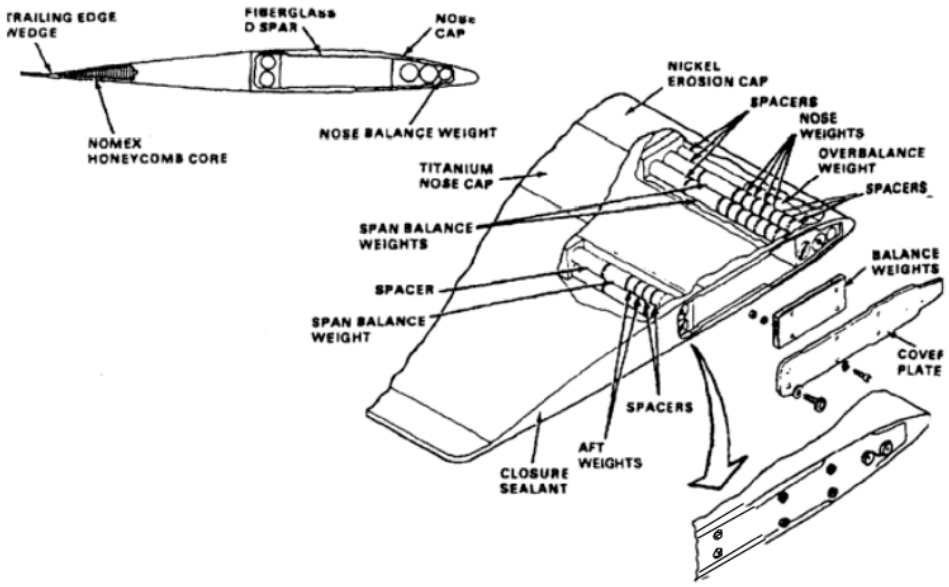

Figure 2.6: Rotor blade tip and tip mass assembly. (Renzi (2004))

Pitch Link
The second adjustment type is the pitch link. The pitch link is a rod that connects the blade pitch varying housing to the rotating part of swashplate. The swashplate position and tilt infer translational motion on the pitch link which is transformed into pitch rotation of the blade by the pitch varying housing. The pitch varying housing is the hinge that allows pitch rotation of the blade (see Figure 2.2). The pitch link can be extended and retracted in fixed increments, called 'notches' to create a pitch angle offset for individual blades. By adjusting the pitch the lift generated by a particular blade can be increased and decreased. The effect of a pitch link adjustment does not vary greatly with increasing airspeed. Maintenance personnel use a tool to adjust a turnbuckle by the amount of notches that are suggested by the RTB software. The pitch link location is indicated in Figure 2.1. In the image it can be seen where the pitch link connects to the pitch horn, which is part of the pitch varying housing. For the Chinook the pitch horn extends forward from the leading edge of the blade. Worn out pitch link assemblies could have reduced stiffness or a slack in the hinge causing in-flight vibration. During this work however the hinge and pitch link will be assumed as ideal.
Trim tab
the last adjustment type is the trailing edge tab. Using a bending tool this tab is deflected in increments of half degrees. The effectiveness of the trim tab increases as the airspeed increases. Therefore, the adjustment of the trim tab and pitch link depend on the airspeed dependent behavior of the measured vibrations. The deflection is performed by clamping the tab with a bending tool. The location of the tab on the blade is shown in Figure 2.10. A downside of the trim tabs is the fact that after repeated bending, the tab might become loose and will spring back towards neutral deflection slightly. This could be a cause for poor RTB results, although this research will not take this effect into account.

There could be other sources of inaccuracies during the RTB process, such as: noise in the accelerometer data, aerodynamic non-uniformity during test flights such as gusts and turbulence, imperfect trim tab deflection and measurement errors from the USBF. A study by Wang et al. (2005) created a stochastic model to account for these uncertainties. For this research the accelerometer, aerodynamic and tab/pitch deflection inaccuracies will not be included. However, this might be an interesting opportunity for future research.

2.4. Mathematical Description of Rotor Blade Vibrations

The general definition for vibration of an object is defined as shown in Equation 2.1 (Meirovitch and Parker (2001)).

$$x(t) = A \cdot \cos(\omega t - \psi) \tag{2.1}$$

Here, A equals the amplitude, ω the frequency, t time and ψ the phase shift. In the case of the 1/rev vibrations the frequency is equal to the rotor system main frequency. In this research the rotor frequency will be equal

to 3.75 Hz, following Bender et al. (1985). The phase shift is an indication of the location of imbalance on the rotor disk and is therefore vital in determining the right blade adjustments. The measured peak vibration is displayed in a vibration map. Such a map is shown in Figure 2.7.

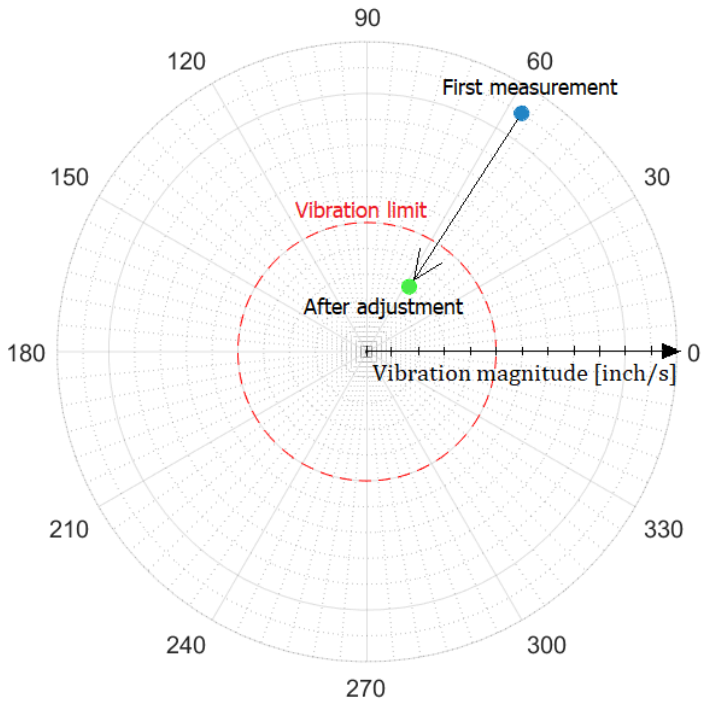

Figure 2.7: Example of a vibration map for either vertical or lateral vibration for a single flight condition. In this hypothetical only one iteration was required to reach a solution.

These polar plots from RTB software indicate the measured peak vibration amplitude and its azimuth angle. In the example from Figure 2.7 the initial measurement (blue) indicated a maximum vibration level of ρ inch per second at an azimuth angle of 57 degrees for a specific flight condition. A hypothetical adjustment to the blade is applied that has a sensitivity of $\Delta\rho$ inch per second at an azimuth angle of 237 degrees. This adjustment has ensured that the vibrations for this category are now within limits. In the actual situation the RTB software algorithm aims to provide a solution that works for all airspeeds and both vibration orientations. The allowed vibration limit varies between these conditions.

A complete theory on helicopter rotor system vibrations was first presented by Rosen and Ben-Ari (1997b). The applications of their research were discussed in their followup paper of the same year, Rosen and Ben-Ari (1997a). Their model closely resembles blade physics by using the forces exerted by the blades on the hub as the basis of their mathematical model. This approach allows for the inclusion of the effects of separate corrective measures, stored in a sensitivity coefficient matrix. This research provided the basis for many later works and its description of the rotor system is useful in this research. This section will shortly describe their mathematical description of rotor system vibrations. The coordinate systems definitions are shown below. Figure 2.8 shows the definition of the coordinate system with respect to the hub, denoted with subscript "H" and the rotating coordinate system that follows the blades, denoted with subscript "R". ϕ describes the rotor azimuth angle. Figure 2.9 describes the coordinate system with respect to the k^{th} blade. Here θ indicates the blade pitch, ζ the lead-lag angle and β the flapping angle.

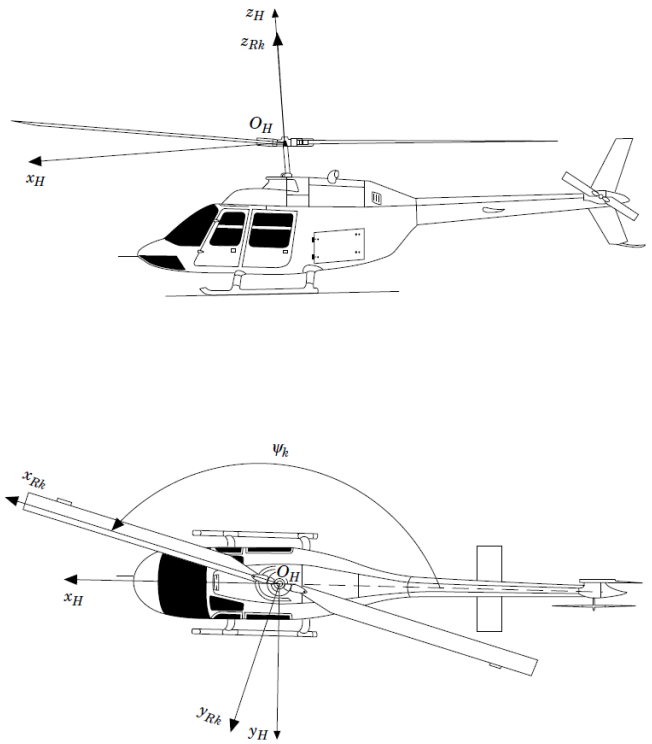

Figure 2.8: General definition of the hub (top) and rotating (bottom) coordinate systems. (Rosen and Ben-Ari (1997b))

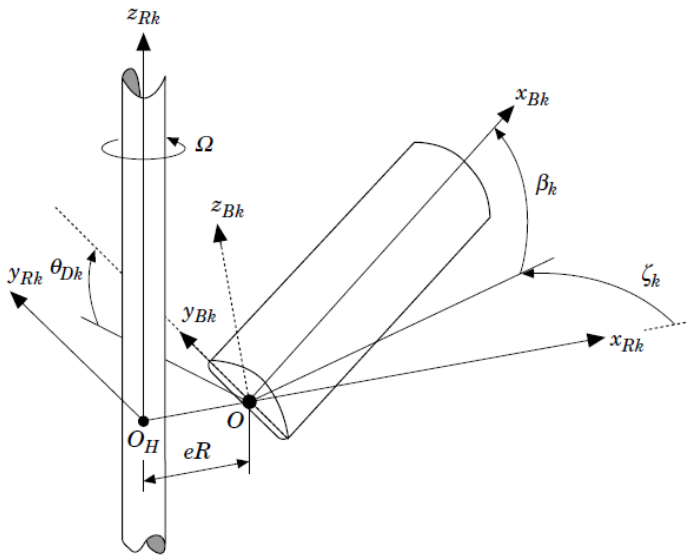

Figure 2.9: Coordinate system definition for the kth blade. (Rosen and Ben-Ari (1997b))

In the rotating axis system the research uses a truncated Fourier series, ignoring harmonics over the order of five to describe the forces on the hub (Equations 2.2 to 2.5 Rosen and Ben-Ari (1997b)):

$$F^R_{\alpha k} = F^{R0}_{\alpha k} + \sum_{n=1}^{5} \left[F^{Rns}_{\alpha k} \sin(n\psi_k) + F^{Rnc}_{\alpha k} \cos(n\psi_k) \right], \qquad \alpha \equiv x, y, z \tag{2.2}$$

Here α indicates the axis direction, R indicates the rotating axis system, k the blade number, n the harmonic order, s and c indicate the sine or cosine contribution and ϕ the azimuth angle. This results in a force vector consisting of one base term, five sine terms and five cosine terms for each blade, per axis direction $\mathbf{f}^R_k$ (order

33). Subsequently, the vector of perturbations relative to a nominal blade can be defined as the summation of the effects of natural perturbations (D) and the effects of corrective measures (E):

$$\Delta \mathbf{f}_{\mathbf{k}}^{\mathbf{R}} = \Delta \mathbf{f}_{\mathbf{k}}^{\mathbf{R,D}} + \Delta \mathbf{f}_{\mathbf{k}}^{\mathbf{R,E}} \tag{2.3}$$

The force and moment vectors per axis direction, per blade can be transformed from rotating coordinate system to hub (H) and can be collected in a single vector of order 55 that expresses the load on the rotor hub:

$$\Delta \boldsymbol{\ell}^H = \{\Delta \mathbf{f}_x^H, \Delta \mathbf{f}_y^H, \Delta \mathbf{f}_z^H, \Delta \mathbf{m}_x^H, \Delta \mathbf{m}_y^H\} \tag{2.4}$$

$\Delta \mathbf{m}_{\mathbf{z}}^{\mathbf{H}}$ is not included, since it mainly affects the drive train dynamics and is not a main source of rotor vibrations according to the authors. This resultant load vector can be defined as:

$$\Delta \boldsymbol{\ell}^H = \mathbf{S}^{LH,D}\mathbf{d} + \mathbf{S}^{LH,E}\mathbf{e} \tag{2.5}$$

In this equation $\mathbf{S}^{FR,D}$ and $\mathbf{S}^{FR,E}$ represent the sensitivity coefficient matrices, order $55 \times nN_d$ and $55 \times nN_e$, where n equals the number of blades. $\mathbf{d}_k$ and $\mathbf{e}_k$ are the perturbance and correction vectors of order nN_d and nN_e respectively. In the perturbance vector all the natural perturbations on blade parameters are quantified. These values need to be determined experimentally. Each deviation is then multiplied by the corresponding sensitivity coefficient, which can be based on mathematical models or flight tests. The model assumes small differences and therefore linear relations. The same applies for the correction vector. Currently the corrective parameters are: mass moment, trailing edge tab deflection and pitch link setting. Using a least squares approach, a solution for $\mathbf{e}$ is found that minimizes the absolute value of $\Delta \boldsymbol{\ell}^H$. This least squares method can be expanded to optimize over a range of different airspeeds, at the cost of increased computation time.

A disadvantage of the method is that in order to achieve an accurate result, an accurate representation of the blade is required, as concluded by De Bruin (2010). During RTB many blade parameters are unknowns, therefore the current procedures still rely on adjustments based on measurements. Additionally, there are other improvements to the method can be made to increase its fidelity. Firstly, the model assumed rigid blades. Including rotor aeroelastic effects will provide more accurate results and might be required to be able to model the behavior of the large blades. Secondly, a fairly simple aerodynamic model had been used.

RTB procedures in practice are based on vibration measurements. The balancing adjustments are based on a linear model and experimental data. The linear adjustment sensitivity coefficients a_{ijk} can be defined as (Hasty et al. (2008)):

$$a_{ijk} = \frac{\Delta v_{jk}}{A_i} \tag{2.6}$$

Here Δv_{jk} is the change in vibrations measured in flight condition j for sensor k. A_i is the change in magnitude of adjustment i, where the adjustments consist of: change in mass moment, pitch link setting and trim tab deflection. A similar equation can be presented for dealing with track spread coefficients b_{ijk} (Hasty et al. (2008)):

$$b_{ijm} = \frac{\Delta t_{jm}}{A_i} \tag{2.7}$$

Where Δt_{jm} is the change in track height for flight condition j, rotor m. Again A_i is the change in magnitude of adjustment i.

2.5. Description of the Rotor System

This research investigates a tandem rotor configuration with two counter rotating three-bladed rotor systems. The forward rotor rotates counterclockwise, while the aft rotor rotates clockwise. The following information on the blade structure has been published by the United States Army Aviation Engineering Flight Activity (Spring et al. (1979)): the blade internal structure consist of a D-shaped fiberglass spar assembly, a nomex honeycomb internal structure, covered by fiberglass skin and a titanium leading edge cap. A nickel erosion cap protects most vulnerable outermost 54 inches of the leading edge. The chord of the blades equals 32 inches and the rotor radius equals 30 feet. The airfoil for the rotor for the majority of the span is the Boeing Vertol VR-7, from 85% span to tip the VR-8 airfoil is used. The chord thickness for the inner section is 12% and tapers from 85% span to 8% at the tip. The rotor system operates at 225 rpm, or 3.75 Hz. The blade layout including twist distribution is visualized in Figure 2.10.

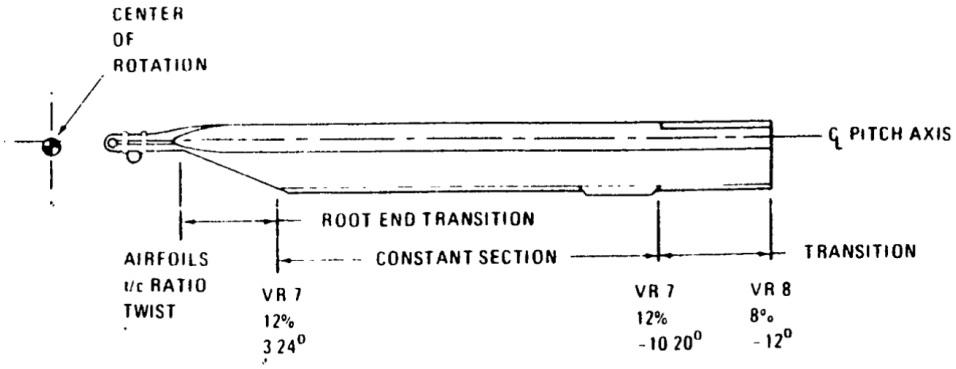

Figure 2.10: Rotor blade dimensions and description. (Bender et al. (1985))

There is a vertical spacing of $0.16R$ and a longitudinal spacing of $1.3R$ between the rotor systems. Without control inputs the rotor disks are angled slightly forward. The forward rotor is angled at 9° forward while the aft is canted 4°. The geometry of the tandem rotor system is presented in Figure 2.11.

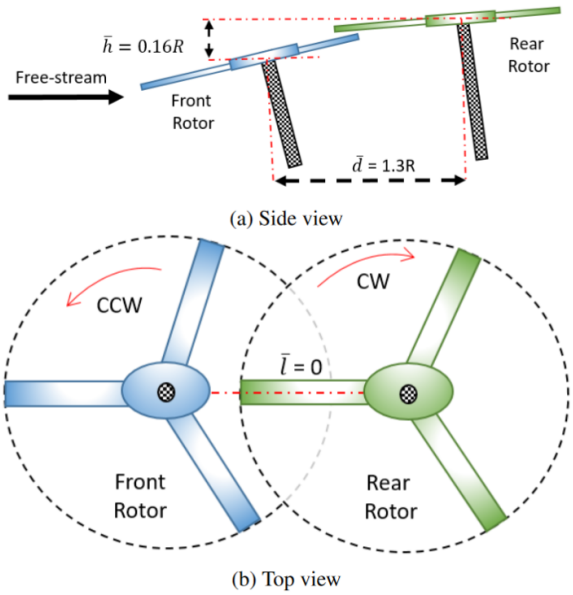

Figure 2.11: Tandem rotor system arrangement. (Guner et al. (2019))

2.6. Representation of Blade Dissimilarity

As has been discussed previously, blade dissimilarity is a cause of force and moment imbalance on the rotor hub. There exist three main causes of the inertial and aerodynamic blade dissimilarities, namely: manufacturing variance, operational wear and ballistic damage. In this research however the focus lies on the actual effect of variance in blade parameters on vibrations due to manufacturing variance and wear. The most occurring examples of such deficiencies are: moisture absorption, mass imbalance, damages and repairs. Further research into the causes of specific blade parameter deviations might pose an opportunity for future research. It might even become possible to detect certain blade damages using vibration data in future. For this research the implementation of these effects into the simulation model can be based on the way other studies have incorporated blade dissimilarities.

Kim (1999) studied the effects of ballistic damage on rotor blade vibrations. The modeling approach represented physical blade damage such as holes and delaminations by reducing the blade mass and stiffness parameters (m, E_1, E_2 and G_{12}) for impacted sections. The coefficients used to represent the effect of damage were estimations based on empirical data. The aerodynamic parameter degradation was based on damage

type dependent sensitivity coefficients (β_l, β_d and β_m), their values based on wind tunnel test data from Leishman (1993) and Leishman (1996).

Other researchers have modelled blade parameters as stochastic variables in order to account for wear and production defects. Hyun You et al. (2010) assess the effects of variance in blade material properties by running Monte Carlo simulation. Cross-sectional properties E_1, E_2, G_{12}, Poisson ratio ν_{12}, ply thickness t_i, elastic axis offset e_d and ply angle θ_{ply} for each node were based on a normal distribution with a certain mean value and standard deviation based on experimental data. Each of the blades was then assigned randomized properties independently. In contrast to Kim (1999) the reference mass and aerodynamic parameters were not included. A similar approach was taken by Murugan et al. (2011), which leaves out the influence of t_i, e_d and θ_i.

According to Kim (1999), the elastic axis offset considerably affects the aeroelastic response of the blade. It is considered to be worthwhile to include this property in the investigation. Additionally, the aerodynamic coefficient variation due to blade profile deformation is of interest. In the case of this research only the sensitivity values are of interest. It may be possible that a blade parameter proves to have high sensitivity, however that certain parameter does not show much variance in the set of operational blades. This should be investigated in the future.

3

Aerodynamics and Structural Dynamics in FLIGHTLAB

This section will discuss the theoretical concepts that play a role in this research. For this research FLIGHTLAB, developed by Advanced Rotorcraft Technologies, Inc (ART) will be used to perform the simulations. This specific software has been selected since it provides a high fidelity rotorcraft solver and has been used by the Royal NLR for many years. More importantly it includes the state-of-the-art Viscous Vortex Particle Method (VPM) for solving inflow distribution and rotor to rotor aerodynamic interference. Furthermore, the program allows the user to make changes to the internal module coding and the simulation runs can be set up using external scripts. FLIGHTLAB provides state-of-the-art aerodynamic, finite element, control and propulsion simulation for rotorcraft research and makes use of so-called selective fidelity modeling. Based on the purposes of the investigation the modeling methodologies can be adjusted to fit the specific requirements, while minimizing the computational cost. Some of the key features embedded in the software are the implementation of nonlinear unsteady aerodynamics, aeroelastic response modeling, loads and vibration prediction and finite element structural modeling.

In this case of this research, a large part of the governing theory is incorporated in the FLIGHTLAB software that will be used. The fundamental theory concerning vibratory forces on the rotor hub have been presented by Rosen and Ben-Ari and has previously been discussed in Section 2.4. The modeling approach and governing equations that will be presented in this section follow from the two theory manuals for FLIGHTLAB, Advanced Rotorcraft Technology, Inc. (2011a), Advanced Rotorcraft Technology, Inc. (2011b).

The structural representation of the blade will be presented in Section 3.1. This section will treat the discretization of the blade and how the forces, moments and deformations are computed. The computation of the local and total aerodynamic loads will be presented in Section 3.2. In Section 3.3 the choice of inflow model is explained. Furthermore the mathematical principles behind the Viscous Vortex Particle Method will be treated.

3.1. Structural Representation of the Rotor Blade

To properly compute the vibratory response of the blades it is required that the structural dynamics are modeled using a finite element approach with nonlinear beam elements (Du Val and He (2018)). The rotor blades are represented as slender, flexible beams with varying section properties in a moving frame of reference. Each of the blade elements consists of two nodes, both with six degrees of freedom. Additionally there are one torsion and two axial displacement degrees of freedom in between the nodes. This is represented in Figure 3.1. The equations of motion are defined in reference to the blade typical section. The elastic axis, the line connecting the points along the span where an applied load produces pure bending is used as a reference to which all the other section points of interest are defined. The resultant aerodynamic forces and moments act on the line connecting all the chord centers. A representation of the typical section as it is defined by ART is shown in 3.2.

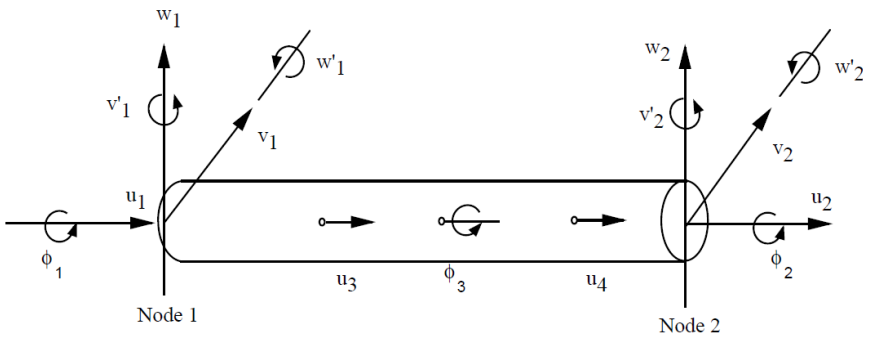

Figure 3.1: Nodal degrees of freedom for a beam element. (Advanced Rotorcraft Technology, Inc. (2011b))

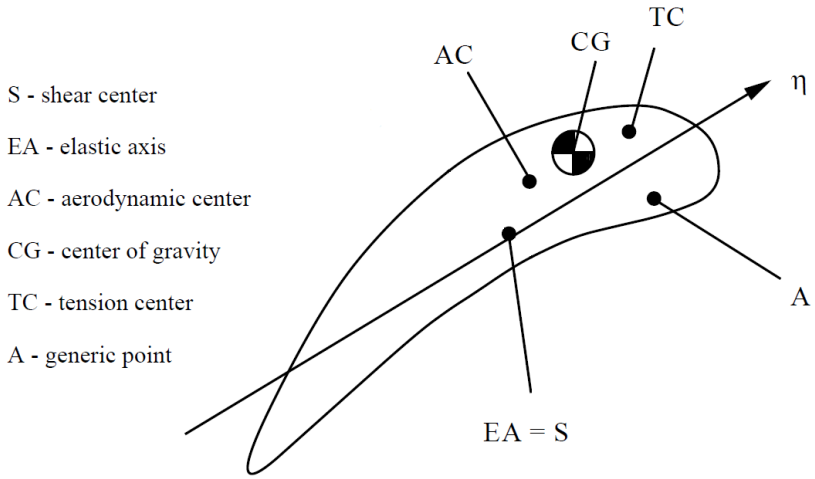

Figure 3.2: The typical section, as it is formulated in the FLIGHTLAB software. (Advanced Rotorcraft Technology, Inc. (2011b))

There are a couple of assumptions in the derivation of the equations of motion for the blade deformation. First of all, it is assumed that the strain is small enough to say Hooke's law is valid and a linear stress strain relation can be applied. Secondly, the effects of warping of the cross-section are included in the computation of the cross-sectional elastic constants, however the warping is ignored when it comes to inertial and applied loads. Thirdly, it is assumed that the blade is sufficiently slender and the blade dynamics are of low enough frequency such that transverse shear deformation is not required for computation of 1-D strain energy. The equations of motion for the blade elements are based on the principle of virtual work and the resulting element matrices are evaluated using Gaussian quadrature (Equations 3.1 to 3.6 from Advanced Rotorcraft Technology, Inc. (2011b)).

$$\sum_{i=1}^{N_e} \left(\delta U^{(i)} - \delta W_b^{(i)} - \delta W_a^{(i)} \right) = 0 \tag{3.1}$$

Here δU represents the strain energy, δW_b the work done by body forces and δW_a the work done by the applied loads. The definition of the contribution of strain energy is defined as follows:

$$\delta U = \int_0^l \delta \mathbf{z}^T \mathbf{f} dx \tag{3.2}$$

Here $\mathbf{z^T}$ is the transpose a the column vector of order 12, containing the deformations u_e, v, w, ϕ and their first and second derivatives. $\mathbf{f}$ is the column matrix of generalized forces corresponding to $\mathbf{z}$ and is defined as:

$$\mathbf{f} = R^T \mathbf{F} \tag{3.3}$$

here **F** is the column vector containing the axial section force V_x, the twisting moment M_x and bending moments M_η and M_ζ. While R^T represents a transformation from the displacement variables to the 1-D strain measures $\epsilon_x, \kappa_x, \kappa_\eta$ and κ_ζ. The virtual work of body forces δW_b can be described as the summation of the zeroth through to the second mass moment terms:

$$\delta W_b = \delta W_{b0} + \delta W_{b1} + \delta W_{b2} \tag{3.4}$$

The virtual work due to applied loads δW_a consists of the externally applied loads and static loads in the undeformed element coordinate system E, P_E and S_E and the applied moments in the deformed element coordinate system $Q_{S'}$. From Hodges (1985) the definition of δW_a is defined as:

$$\delta W_a = \int_0^l \left[\left(\mathbf{P}_E + \mathbf{S}_E \right) \cdot \left(\delta u \mathbf{b}_1^E + \delta v \mathbf{b}_2^E + \delta w \mathbf{b}_3^E \right) + \mathbf{Q}_{S'} \cdot \overline{\delta\theta}_{S'}^{S'E} \right] dx \tag{3.5}$$

Here u, v and w are the displacements, shown in Figure 3.1 and $\mathbf{b}_1^E$, $\mathbf{b}_2^E$ and $\mathbf{b}_3^E$ are the associated unit vectors. $\overline{\delta\theta}_{S'}^{S'E}$ represents the rotation matrix from S' to E.

The displacements in the virtual work are defined using shape functions and can be expressed as:

$$\begin{Bmatrix} u_e \\ v \\ w \\ \phi \end{Bmatrix} = \begin{bmatrix} \phi_u^T & 0 & 0 & 0 \\ 0 & \phi_v^T & 0 & 0 \\ 0 & 0 & \phi_w^T & 0 \\ 0 & 0 & 0 & \phi_\phi^T \end{bmatrix} \begin{Bmatrix} \mathbf{q}_{u_e} \\ \mathbf{q}_v \\ \mathbf{q}_w \\ \mathbf{q}_\phi \end{Bmatrix} \tag{3.6}$$

Here ϕ^T are column matrices containing the shape functions for each displacement (these shape functions are defined in Advanced Rotorcraft Technology, Inc. (2011b)) and $\mathbf{q}_{u_e}$ contains the degrees of freedom of the node as a function of time. These expressions for the displacements and their variations are substituted into Equation 3.1 in order to obtain the element matrix equations.

3.2. Modeling of Aerodynamic Loads

The computation of the airloads in FLIGHTLAB is performed by an integrated blade element theory approach. In blade element theory the blade is discretized into elements each representing a specific section of the blade. These aerodynamic segments can be defined independently from the finite element sections. The blade varies along the span in a couple of ways as is visualized in Figure 2.10. Blade element theory determines the rotor performance by the summation of the contributions of all n elements along the span. The flow velocities and the forces acting on the section for hovering flight are visualized in Figure 3.3.

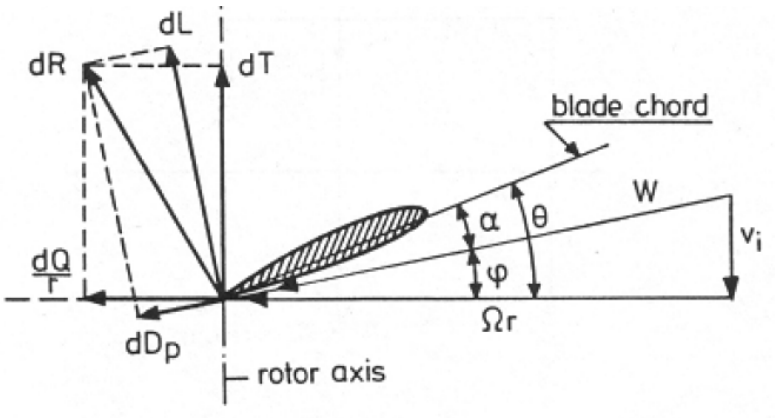

Figure 3.3: Overview of the velocities and forces acting on a blade element (Marrant and Pavel (2002))

Here an element is considered, located at radius r from the hub centre with no forward airspeed. In that case only two velocity components are involved: the velocity due to rotation Ωr and the induced velocity v_i, together forming the blade flow velocity W. The angles of interest are angle of attack α and pitch angle θ.

The Lift contribution dL is by definition perpendicular to W, while the contribution to thrust dT is defined perpendicular to the rotor disk.

The thrust T of a blade is defined by the summation of all n element contributions across the span (Marrant and Pavel (2002)):

$$T = \sum_{i=1}^{n} \int_{R_{in_i}}^{R_{out_i}} c_{l_i} \frac{1}{2} \rho (\Omega r)^2 c_i \, dr \tag{3.7}$$

Here the small angles assumption is made, such that the element thrust contribution is equal to the lift contribution. In this equation c_{l_i} is the local section lift coefficient, ρ the air density, n the total number of elements, c_i the local chord. The integration is taken between the radius of the inner node R_{in_i} and the outer node R_{out_i}. The equation for drag is similar, instead including the drag coefficient c_{d_i}. In forward flight, the asymmetric velocity distribution also needs to be integrated into the method.

FLIGHTLAB offers a number of aerodynamic models for computing the section airloads. For this research the quasi-unsteady airloads model has been used. The quasi-unsteady model differs from the fully unsteady method by assuming the stall acts in a quasi-steady manner and does not include noncirculatory airloads. It does however include all the other factors that the unsteady method accounts for such as pitch rate, reverse flow and yawed flow. Quasi-unsteady aerodynamics was the most complex method available, since the two fully unsteady methods (Onera and Leishman) require dynamic stall parameter input, which is currently not available for the VR-7 and VR-8 airfoil. These parameters would follow from windtunnel measurements, which for this research cannot be performed. Not being able to include noncirculatory airloads and the delay effects could reduce the accuracy of the measured vibrations in the simulations, although it is not clear to what extent in this case.

The quasi-unsteady airloads consist of two components, the circulatory airloads and the profile drag. The circulatory airloads follow from unsteady thin airfoil theory and an independent wake model. The results from the thin airfoil method are enhanced by accessing an airfoil data file that contains the Mach/angle of attack dependent behavior of the aerodynamic coefficients. This data file contains information from windtunnel measurements that provide stall and compressibility effects, which would be absent from a basic thin airfoil theory approach. The effective angle of attack for a section is determined by combining the results from wake interaction, the inflow distribution, blade pitch rate and reversed and yawed flow effects. The aerodynamic coefficients are based on the look-up table values together with the effective angle of attack and the local Mach number (Equations 3.8 through 3.24 from Advanced Rotorcraft Technology, Inc. (2011a)). The three orthogonal airflow directions are denoted by u, v and w.

$$\alpha_e = \tan^{-1} \frac{w_{e3qc}}{-v} \tag{3.8}$$

$$w_{e3qc} = w + \frac{1}{4} c \omega_x \frac{v}{|v|} \tag{3.9}$$

$$\beta = \tan^{-1} \left(\frac{-u}{v_{2d}} \right) \tag{3.10}$$

$$c_l = \frac{c_{l2D}(\alpha_e \cos^2 \beta, M)}{\cos^2 \beta} \tag{3.11}$$

$$c_d = \frac{c_{d2D}(\alpha_e \cos \beta, M)}{\cos \beta} \tag{3.12}$$

$$c_m = \frac{c_{m2D}(\alpha_e \cos^2 \beta, M)}{\cos^2 \beta} \tag{3.13}$$

Here β represents the yawed flow angle, w_{e3qc} the normal airflow computed at the three quarter chord point and α_e the effective angle of attack. The circulatory airloads on the individual sections can then be obtained from:

$$L_{yc} = \frac{1}{2} \rho c v_{2d} w |c_l| \frac{v}{|v|} \tag{3.14}$$

$$L_{zc} = \frac{1}{2} \rho c v_{2d} v c_l \tag{3.15}$$

$$M_{xc} = \left(\frac{1}{2}\rho c^2 v_{2d}^2 c_m + \frac{1}{4} c L_{zc}\right)\frac{v}{|v|} \tag{3.16}$$

Here M_{xc} represents the pitching moment acting on the section midchord and v_{2d} the resultant 2-D airflow. The section profile drag can be obtained by applying the following:

$$L_{xpd} = -\frac{1}{2}\rho c v_{3d} u c_d \tag{3.17}$$

$$L_{ypd} = -\frac{1}{2}\rho c v_{3d} v c_d \tag{3.18}$$

$$L_{zpd} = -\frac{1}{2}\rho c v_{3d} w c_d \tag{3.19}$$

Where v_{3d} represents the 3-D resultant airflow. The total quasi-unsteady airloads in the local coordinate system then become:

$$F_x^p = l L_{xpd} \tag{3.20}$$

$$F_y^p = l\left(L_{yc} + L_{ypd}\right) \tag{3.21}$$

$$F_z^p = l\left(L_{zc} + L_{zpd}\right) \tag{3.22}$$

$$M_x^p = l M_{xc} \tag{3.23}$$

$$M_y^p = M_z^p = 0 \tag{3.24}$$

3.3. Inflow Model

In recent years the most widely applied inflow models were the finite state models, such as the Pitt-Peters model (Pitt and Peters (1981)) and the Peters-He (Peters and He (1995)). These are dynamic models, as they are able to account for rotor flap, lag and unsteady aerodynamic effects. A separate wake model however is required to account for the effects of the bound, trailing and shed vortices on the inflow distribution. These models have proved to work very well for most rotorcraft simulation purposes. A shortcoming of these modeling types however is a poor performance when dealing with mutual aerodynamic interaction (Gladfelter et al. (2020)). In the case of this research concerning a tandem rotor system this drawback is deemed quite relevant. Moreover, dynamic inflow has a significant influence on the rotor dynamic modes, since the inflow dynamics fall within a comparable order of magnitude as the blade flapping mode and the lead-lag mode, according to Chen and Hindson (1986). In a recent effort to investigate the feasibility for condition based maintenance for the US Army CH-47D by Terpening et al. (2016) a simulation model of the tandem rotor helicopter was built using the RCAS software. The researchers used two inflow modeling approaches: a uniform inflow model and a prescribed wake model. It was not made clear from their report why precisely these two inflow models have been selected from numerous options, although the authors indicated that the uniform inflow model was included to assess whether complex inflow modeling was required at all. Unfortunately the researches had to conclude that the model did not compare well enough to validation data to be useful. Although, it was concluded that the prescribed inflow method was more accurate than the uniform model. This is to be expected as the uniform inflow model does not take any of the rotor dynamics into account. A possible cause for them not to obtain accurate enough results could be the simplicity of the chosen inflow method.

A recent inclusion into the FLIGHTLAB software is the Viscous Vortex Particle Method (VPM or VVPM) inflow solver which has been developed in house by ART, He et al. (2017) specifically for handling multi rotor wake interaction. As this method was specifically created to account for rotor wake interaction it has been selected for the purposes of this research. The basic working principles behind this method will be presented in this section.

3.3.1. Vorticity Particle Modeling

The VPM method uses the Lagrangian formulation of Navier-Stokes equations to solve the rotor vorticity field. The vorticity dynamics are then defined as:

$$\frac{d\boldsymbol{\omega_v}}{dt} = \boldsymbol{\omega_v} \cdot \nabla \mathbf{u} + \nu \nabla^2 \boldsymbol{\omega_v} \tag{3.25}$$

Here $\omega_\mathbf{v}$ is the vorticity, ν the kinematic viscosity and $\mathbf{u}$ the velocity field. Defining the vorticity using the Lagrangian approach helps solve the problem of wake vorticity transport, He and Zhao (2009). This method requires no grid generation and the computation of the vortex particles can run fully parallel to the rotor computations. By not making use of a grid problems occurring due to numerical diffusion or dissipation are not an issue and it greatly reduces computational cost. Instead, vortex particles are created and shed along the blade length which are tracked along their paths throughout the rotor wake for a specified amount of time. A visualization of the particles at a specific time step in hover conditions is shown in Figure 3.4.

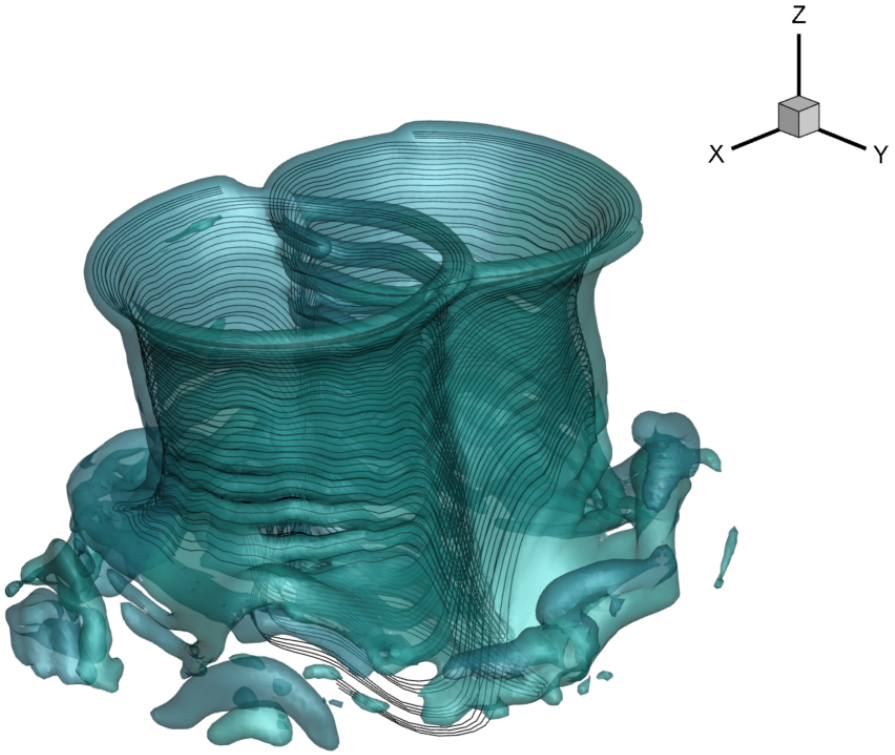

Figure 3.4: FLIGHTLAB VPM generated wake visualized using vorticity isosurfaces in Tecplot. Particle tracing for particles created near the blade tip, shown by the black streamlines has also been visualized.

The rotor wake field is discretized into N vector valued vortex particles. The distributed vorticity is then defined as (Equations 3.26 to 3.29 from He et al. (2017)):

$$\boldsymbol{\omega}_v(\mathbf{x}, t) = \sum_{i=1}^{N} \xi_\sigma(\mathbf{x} - \mathbf{x}_i)\boldsymbol{\alpha}_i \tag{3.26}$$

Here $\mathbf{x_i}$ is the position vector, $\alpha_\mathbf{i}$ vector-valued total vorticity Vector of particle i and ξ_σ the vorticity distribution function. He et al. (2017) suggested a Super Gaussian distribution for ξ_σ. The vortex particle dynamics based on incompressible Navier Stokes equations are then modeled as a convection-diffusion process:

$$\frac{\boldsymbol{\omega_v}}{dt} = \boldsymbol{\omega_v} \cdot \nabla \mathbf{u}_{tot} + \nu \Delta \boldsymbol{\omega_v} + \boldsymbol{\gamma_{src}} \tag{3.27}$$

$$\frac{\mathbf{x}}{dt} = \mathbf{u}_{tot} = \mathbf{u}_\infty + \mathbf{u}_{vpm} + \mathbf{u}_{src} \tag{3.28}$$

In this equation $\gamma_{\mathbf{src}}$ represents the source vorticity from the aerodynamic element surfaces and ν represents the kinematic viscosity of air. The total resultant air velocity $\mathbf{u}_{tot}$ is the summation of the free stream velocity, the wake induced velocity $\mathbf{u}_{vpm}$ and the source induced velocity $\mathbf{u}_{src}$. The source vorticity in this method is based on a lifting line blade element method. The circulation is related to the vorticity generation in the following way:

$$\boldsymbol{\gamma_{src}} = -\frac{d\boldsymbol{\Gamma_b}}{dt} + \mathbf{v_b}\nabla\cdot\boldsymbol{\Gamma_b} \tag{3.29}$$

The first term in this equation represents the shed vorticity while the second term represents the trailed vorticity from the blade elements. $\mathbf{v_b}$ is the resultant air velocity relative to the element.

A disadvantage of this solver method may be the incompressibility assumption. Compressibility effects are known to cause vibration in rotor systems. These vibrations fall within the higher order harmonics though, for which RTB is not an effective remedy as discussed in Section 2.2.

3.3.2. Rotor Wake Modeling

While in flight the rotor blades create shed and trailed vortices which affect the blades aerodynamic performance. As defined by Johnson (1990), in relation to rotorcraft: shed vortices are created by azimuthal variation of the circulation and detach from the blade in radial direction. The trailed vortices are caused by a spanwise variation of the circulation and are oriented parallel to the flow when they leave the blade. These phenomena are also included in the VPM method and the vorticity strengths are incorporated into the VPM tracker particles. These particles are tracked along their path through the wake, instead of computing the vorticities at grid coordinates. When lifting line theory is used for the blade section airloads the blade bound ciculation is obtained from the Kutta-Joukowski theorem:

$$\mathbf{L} = \rho\mathbf{v}x\boldsymbol{\Gamma}_b \tag{3.30}$$

Here $\mathbf{L}$ represents the blade circulation per unit length, $\mathbf{v_b}$ the resultant relative air velocity and $\boldsymbol{\Gamma}_b$ represents the blade-bound circulation. The assumption is made that the number of airload segments is large enough such that the bound circulation for a single segment can be assumed constant. The vorticity source shed into the wake by a blade airload segment can then be defined as (He and Zhao (2009)):

$$\boldsymbol{\gamma}_w = -\frac{d\boldsymbol{\Gamma}_b}{dt} + \mathbf{v}_b\nabla\cdot\boldsymbol{\Gamma}_b \tag{3.31}$$

In this equation the first term denotes the shed vorticity and the second term denotes the trailed vorticity for a specific blade airload segment. At every time step in the simulation new particles are created along the blade trailing edge to take into account changes in the bound circulation, while particles that reach the specified maximum age are deleted. All contribution of the particles are included in the determination of the local angle of attack and the dynamic pressure for the lifting line section, therefore creating a closed loop between the section airloads and wake effects.

4

Modeling Setup

In this section the implementation of the experiment in FLIGHTLAB will be discussed. There are a number of different simulations set-ups that will be performed. These can be divided into three main groups. The first being the baseline run, where all blades are exact copies of each other. From this approach the baseline vibration values for each flight condition can be obtained. The second group pertains the simulation of RTB adjustments. These are of importance to be able to properly replicate the effects of blade adjustments performed during RTB. Additionally the effect of these adjustments is known and can be used as a way of validating the model. The third group exists of the blade structural and aerodynamic imperfections. These will be modeled both as occurring in 10% span section increments and for occurring along the entire span.

First the general model settings for the main rotor system will be treated in Section 4.1. In Section 4.2 it will be discussed how an adjustment to the pitch link, trim tab and tip weights is implemented in the computations. Furthermore it elaborates on how adjustments were made to the blade structural and aerodynamic properties within the FLIGHTLAB framework. The trimming process and collection of the results will be treated in Section 4.3.

4.1. Rotor Model

The environmental conditions follow the definitions of the International Standard Atmosphere (ISA) and the rotorcraft will be flying at 500 feet. First the model of the rotorcraft is loaded into FLIGHTLAB. Then, for a single blade, either on the forward or rear rotor the blade properties are redefined as desired. This is performed on the blade that is designated 'blade 1' in the FLIGHTLAB model editor and is by default located at an azimuth angle of 0 °, which is in the direction of the rear of the rotorcraft. The model is then trimmed to the desired flight condition.

One of the questions this research investigates is what the effect is of the tandem rotor configuration on rotor vibrations and whether the VPM modeling approach is required to capture this effect. It needs to be investigated how the baseline vibrations change due to the rotor wake interference and whether there are changes in the sensitivities for variance of a blade property. Therefore there will be two separate models which will have their results compared. A finite element rotor model within FLIGHTLAB consists of four main modules, namely: blade structure, airloads, induced velocity (inflow) and rotor interference. The blade structure module in this case indicates the representation of the rotor hinges. For both models these are specified in Table 4.1.

Table 4.1: Overview of module selection for both simulation approaches.

Module	Model without interference	Model with interference
Blade Structure	Articulated Rotor	Articulated Rotor
Airloads	Quasi-Unsteady	Quasi-Unsteady
Induced Velocity	Peters-He Finite State	VPM
Rotor Interference	None	VPM

The model without interference will be used to compare the VPM model to. For the model without interfer-

ence a Peters-He finite state inflow model was selected, as it is a widely used high fidelity method. The model without interference will be further referred to as the finite state inflow model. The model with interference effects will be referred to as the VPM model.

A numerical investigation into the effects of overlap in a tandem rotor system has been performed by Lee et al. (2009). The researchers used a hypothetical tandem rotor helicopter and varied the geometrical dimensions to study the effects. In the paper it is stated that in forward flight the wake of the forward rotor passes under the rear rotor, influencing its aerodynamic properties. The rear rotor however has nearly no effect on the forward rotor. The effect of this wake influence is an increase in induced power required by the rear rotor. This effect is visualized in Figure 4.1. The tandem front rotor induced power coefficient c_{P_i} is nearly identical to an isolated single rotor system, while the rear tandem rotor c_{P_i} is higher. The influence on the rear rotor is reduced with increasing advance ratio μ, which is defined as the free stream velocity divided by the rotor tip speed. Even though it is not included in this figure, the author notes that the influence on rear rotor also decreases in the direction to $\mu = 0$ (hover). On the right the definition of stagger d and gap H are defined. D is the rotor diameter.

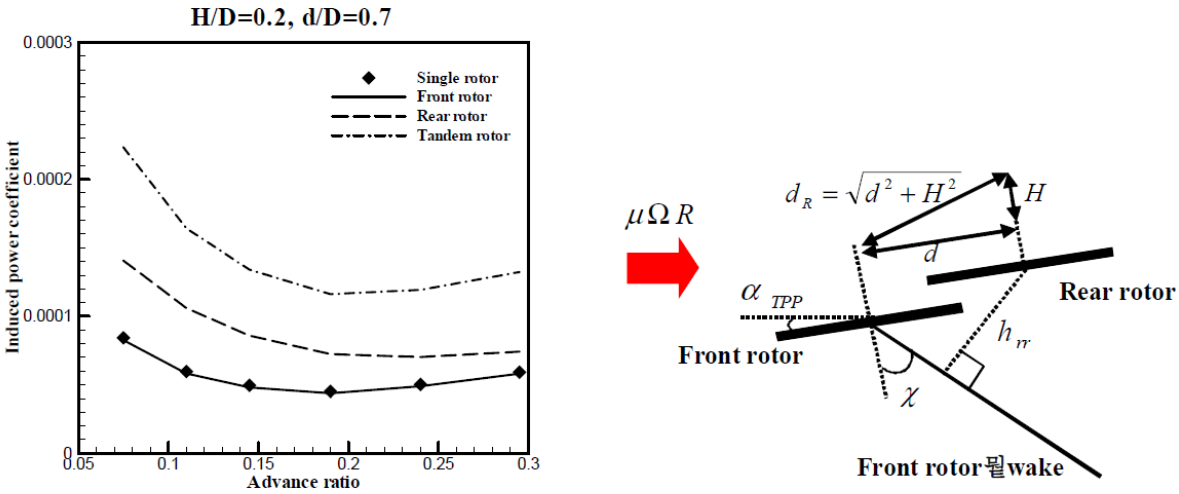

Figure 4.1: Effect of Tandem Rotor Configuration on Rotor Power Coefficient. (Lee et al. (2009))

The relation between the increased c_{P_i} on the rear rotor and the 1/rev vibrations not something that has received much attention through research at this point in time. Based on the research by Lee, it is expected that vibratory responses for the forward rotor will be similar for both the model with and without aerodynamic interference modeling.

The blades of both rotors are all identical to each other in the baseline version of the model. The discretization of the blades is done separately for aerodynamic sections and nonlinear beam segments. In this case the blade is divided into 39 aerodynamic sections and 24 nonlinear beam elements.

The take-off weight of the rotorcraft is set at 44,262 lbs. The fuselage is modeled as a point mass. The fuselage airloads follow from look-up tables containing experimental data. These airloads act on the single point of the fuselage. As has been stated by Lee et al. (2009) though, the inclusion of an elastic fuselage may alter the vibratory response of the aircraft. Therefore, there will also be a couple of simulations with a modal fuselage representation. The effects will only be investigated for a few blade parameters however, due to the increased computational cost. A representation of the rotorcraft in FLIGHTLAB is shown in 4.2.

4.2. Representation of Blade Adjustments and Properties

The modeling of the three blade adjustment types is important mainly for answering the research question that asks whether the results from FLIGHTLAB will match with flight test data. The representation of adding a tip mass is the most straightforward and only requires changing the blade's mass distribution. Modeling a pitch link adjustment required a deeper dive into the source code of FLIGHTLAB before it could be successfully adjusted as required. Including blade tab deflection required some aerodynamic analysis, as coefficient data was only available for an undeflected tab. Most of structural properties were adjustable using their finite element distributions, while the aerodynamic performance was be changed by creating a table of offset values that could be imposed on the standard coefficient tables.

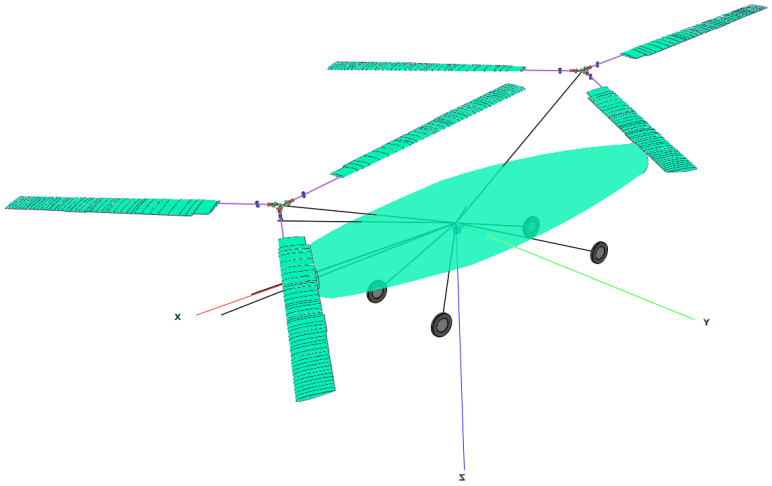

Figure 4.2: Representation of the model elements in the FLIGHTLAB xanalysis environment.

4.2.1. Dynamic Balance Weights

The vibrex dynamic balance weights (vibrex referring to a line of RTB products by Chadwick Helmuth, a Honeywell subsidiary) are used during dynamic balancing of the rotor and affect both the rotor track and vibrations. These weights are inserted at the very tip of the blade. Multiple of these weights can be placed in the blade tip, however only the change in vibration per weight is of interest. Weights can either be added or removed. In this investigation however, only the effect of adding a weight is considered since this action can be compared to reference data. To represent an added balance weight, the weight distribution of the outermost nonlinear beam element (located 0.98-1.0 span) is adjusted.

4.2.2. Pitch Link Adjustment

The pitch link is the connecting element between the swashplate and the rotorblade and transforms the collective and cyclic stick inputs into blade pitch changes. Each pitch link however, can be adjusted to create an offset. By lengthening or shortening the pitch link the blade pitch for an individual blade can be adjusted to track and balance the rotor. A diagram of the pitch input is shown below in Figure 4.3.

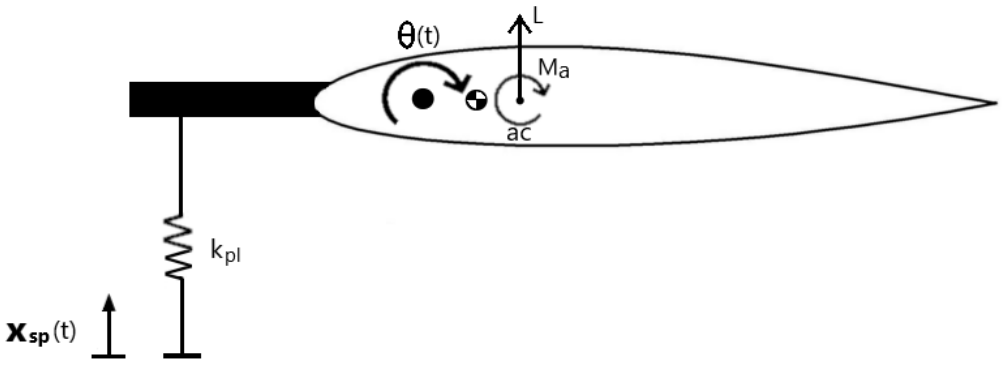

Figure 4.3: Schematic representation of the rotor blade pitch input. Note that the rotation center, CG and aerodynamic center are not placed in their actual locations and vary based on radial position of the blade section.

The blade pitch angle θ is determined from the swashplate input vector $\mathbf{x}_{sp}$, taking into account the aerodynamic forces and moments that act on the pitch link, which has a stiffness k_{pl}. The pitch link is represented by the linear spring element that connects to the pitch horn, which is the element extending forward from the leading edge. In FLIGHTLAB three methods of representing this system are available: no pitch link model, a simplified pitch link and advanced pitch link model. When the 'no pitch link' model is selected the pitch link assembly is replaced with a controlled torsional spring system. The linear spring and the corresponding arm

are incorporated into an equivalent torsion spring that is positioned at the center of rotation and the swashplate input is transformed accordingly. This simplifies the model and reduces the computational cost and is sufficient for most use cases. The simplified model allows the user to more accurately represent the pitch link assembly. Using this setting the length, radial location and the cant angle of the pitch horn can be specified. This setting becomes required when one is interested in the loads acting on the pitch link. The advanced pitch link model allows for a more exact representation of the pitch link. Here the shape of the pitch horn and the location of the pitch link can be expressed in 3-D space.

For this investigation it was chosen to apply the 'no pitch link' model, since the loads acting on the pitch link are not of interest. Replacing the linear spring system with an equivalent torsional spring system should still produce a similar dynamic response. In this case the vertical extension of the pitch link due to an adjustment of one notch can be translated into a rotational displacement. This rotation offset is then applied to the controlled torsion spring element in the model tree.

4.2.3. Blade Tab Deflection

The blade tab is located at between 67% and 75% of the span and is deflected to a required setting during the RTB process. The deflection of the tab adjusts the pressure distribution of the blade section and subsequently changes the aerodynamic performance in a comparable way to how ailerons work on fixed wing aircraft. The effect of tab deflection has been investigated using the 2-D flow solver XFOIL. The airfoil profile with and without tab is published in the US Army Helicopter Design Datcom (Dadone (1976)). The profile including the trim tab is shown in Figure 4.4. For the tab a positive deflection is defined as upwards.

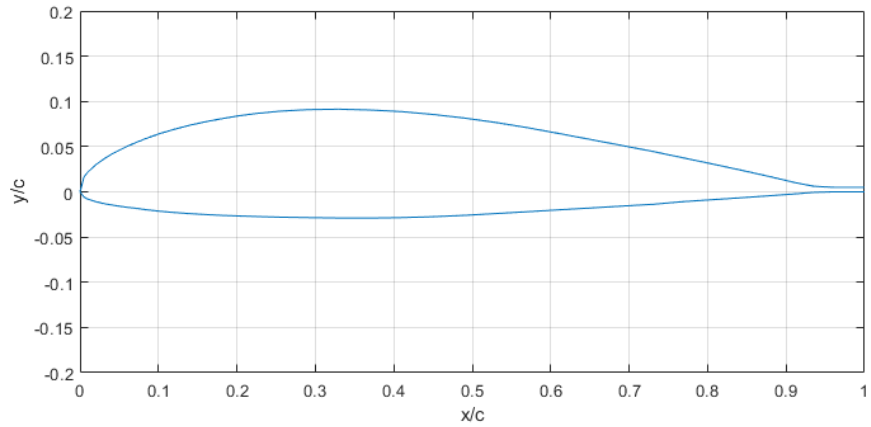

Figure 4.4: VR-7 airfoil shape, with the trailing edge trim tab attached.

Even though a CFD analysis would provide more accurate results, in this case the extra time required to perform such an analysis is not available. XFOIL is a solver for incompressible viscous flows (Mach < 0.3), particularly well suited for low Reynold's number airfoils (Re < $0.5e^6$) as specified by Drela (1989). This may not be ideal for this research, since the Reynolds number on the blades will be greater than half a million and the blade is influenced by compressibility effects. At the fastest RTB test flight regime of 130 kts under sea level ISA conditions and with a nominal rotor RPM of 225 the Reynolds number at location of the trim tab is approximately $1e^7$ with a Mach number of 0.67. Maughmer and Coder (2010) however, showed that XFOIL for a Reynold's number of two million matched very well with the linear part of lift curve for airfoils, as shown in Figure 4.5. The drag coefficient however was underpredicted. In the region of $0.3 < C_l < 1.0$ the drag coefficient predicted by XFOIL was lower by approximately 10%.

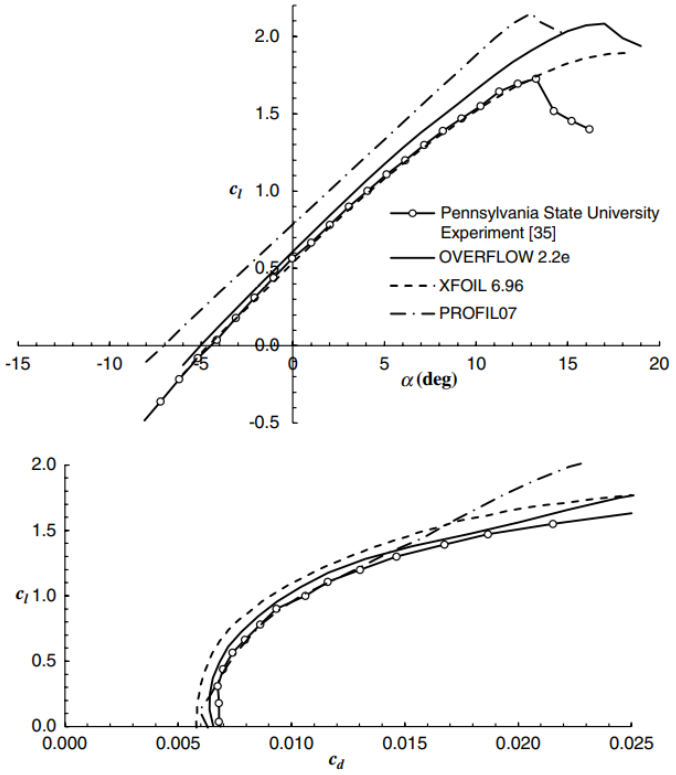

Figure 4.5: Comparison between flow solvers and experimental data for the HTR 1555 Heavy-Lift Military Tiltrotor inboard section, Re = 2.0 e^6 (Maughmer and Coder (2010).

In this analysis the 2D airfoil coefficient data follows from CFD data on the VR-7 and VR-8 blade sections. So, for the basic airfoils and for the airfoil with an undeflected tab the aerodynamic coefficients are known between 0.0 < Mach < 1.0. The only missing information is the ΔC_l, ΔC_d and ΔC_m per degree of tab deflection in either direction. These delta values are small compared to the airfoil base values. Therefore, a small error in the drag polar of the deflected tab is expected to have a relatively low impact. A more significant drawback of using XFOIL is its inability to predict airfoil performance at medium to transonic Mach numbers. Moreover, at Mach numbers over 0.4 the solver is unable to converge.

In order to still try and represent the Mach dependent behavior of the aerodynamic coefficients it was chosen to take the XFOIL results at $M = 0.2$ and extrapolate to $M = 1.0$ using CFD data from a different helicopter type. In this case aero coefficient data was available from a different, smaller helicopter (unnamed due to restriction of data). A Matlab script was set up that would express the percentage difference between a data point at a certain Mach number and the data point at $M = 0.2$. This Mach dependency was then imposed on the trim tab deflection coefficients for the VR-7 airfoil. It is realized that this is a very crude approach and the behavior of both tabs is not identical, since they are not of equal dimensions. However, it was decided that it would be better to include it, rather than having the aerodynamic coefficients stay constant with increasing Mach number. Also, the results for the trim tab only play a part in the validation of the model and will not influence the conclusions on which blade parameter has a greater effect on rotor vibration. In Figure 4.6, 4.7 and 4.8 the aerodynamic performance of the trim tab is shown for a zero and ten degrees angle of attack.

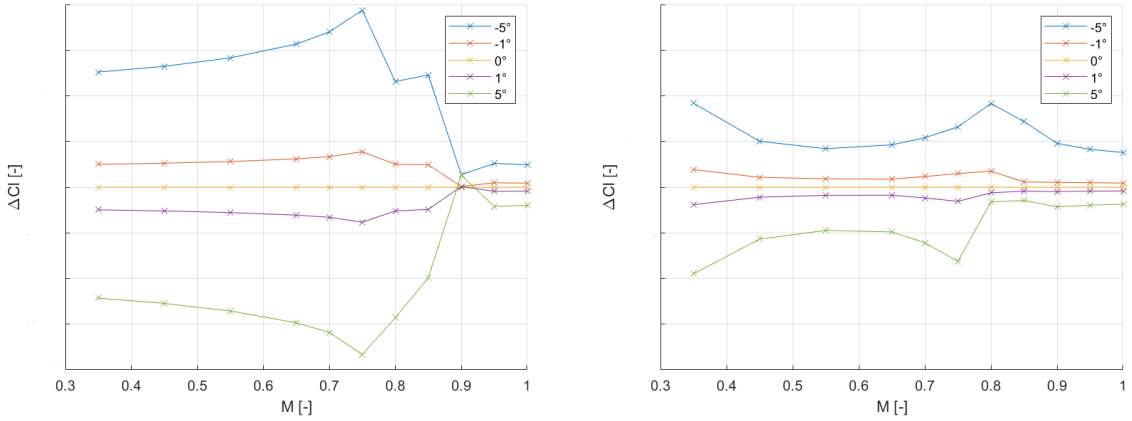

(a) $\alpha = 0$. (b) $\alpha = 10$.

Figure 4.6: Effect of trim tab deflection on section lift coefficient, extrapolated from M = 0.2 to M = 1.

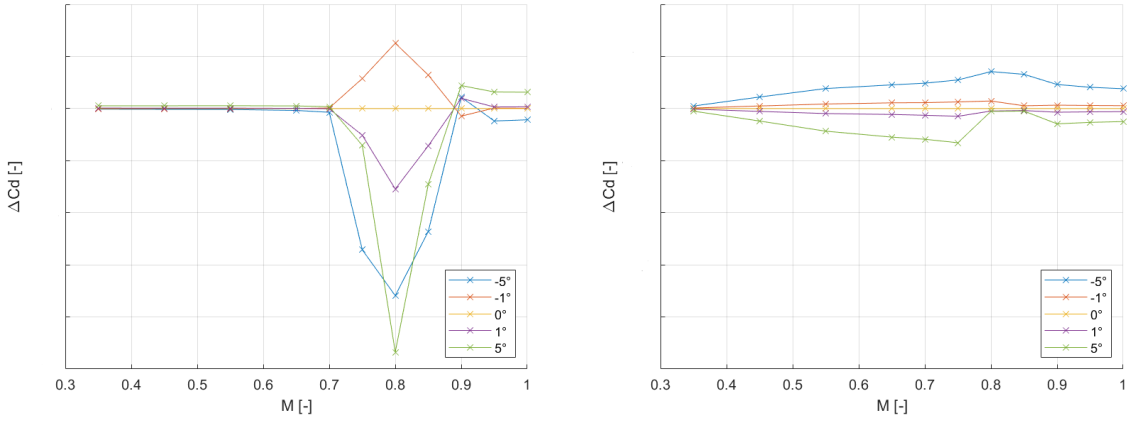

(a) $\alpha = 0$. (b) $\alpha = 10$.

Figure 4.7: Effect of trim tab deflection on section drag coefficient, extrapolated from M = 0.2 to M = 1.

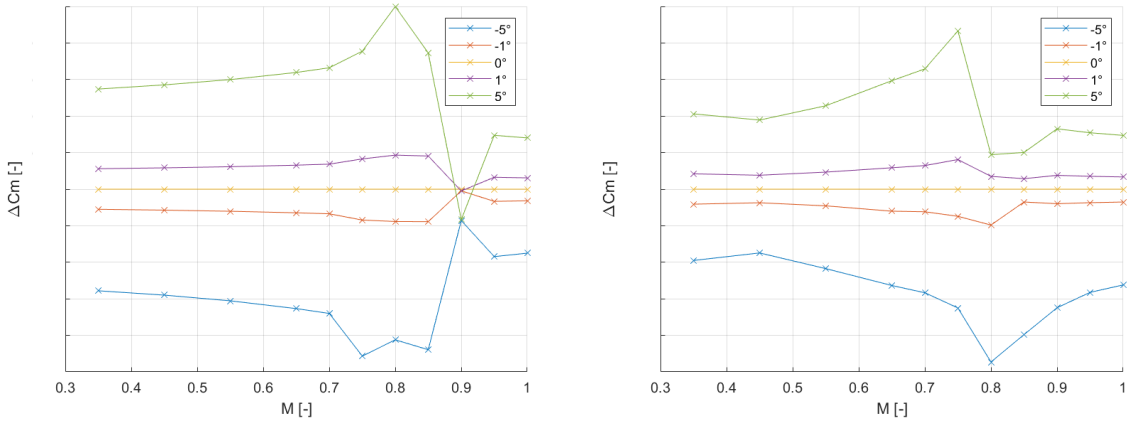

(a) $\alpha = 0$. (b) $\alpha = 10$.

Figure 4.8: Effect of trim tab deflection on section moment coefficient, extrapolated from M = 0.2 to M = 1.

It can be observed at lower angles of attack that up from $M = 0.7$ the coefficients are most significantly af-

fected by compressibility effects, evident from the jumps occurring in the curves. Also, at smaller tab deflection angles these jumps are relatively much more moderate compared to those from higher deflection angles. On top of that, with increasing angle of attack the region between $0 < M < 1$ is not as constant as when $\alpha = 0$. To investigate to what extent the compressibility plays a role, the maximum expected Mach number the tab will experience can be predicted. At the most outboard point of the trim tab at a forward speed of 130 knots this leads to a Mach number of about 0.65. This means that the trim tab will not experience the conditions where the jumps in the aerodynamic coefficient curves start appearing. This means that if during the validation of the trim tab effectiveness, the tab proves to be too (in)effective, that the reason is most likely due to an error in the prediction of the tab aerodynamic performance by XFOIL at $M = 0.2$. From these curves in Figures 4.6 through 4.8 the ΔC_l, ΔC_d and ΔC_m values were taken and stored in a look-up table file. In FLIGHTLAB a custom component representing the tab and its deflection has been created as it is not possible to add trim tab elements in the basic version of the software. This tab component is embedded as a subcomponent into the component tree of the quasi-unsteady aerodynamic span sections that correspond to the spanwise location of the tab. This component acts as a lookup table that adds Δ values based on the tab deflection angle, angle of attack and Mach number to the section lift, drag and moment coefficients at every time step. Since validation data is only available for a one degree deflection, only that tab setting will be investigated.

4.2.4. Section Structural Property Variation

Damage, repairs, wear and manufacturing imperfections change the structural properties of the blades in a certain way. In actual cases it is not likely that only one parameter would be impacted by an imperfection. In this case however the property variations will be investigated individually in order to try and find the most significant contributors to in flight vibrations. In Section 2.6 previous research into the effects of blade dissimilarity has been discussed. Based on the parameters selected by those researchers and the ones mentioned in their recommendations the following have been selected for this work: E_1, E_2, G_{12}, the twist distribution η_t, the chordwise mass moment M_c and the elastic axis offset e_d.

The finite element, nonlinear elastic beam rotor model in FLIGHTLAB is constructed from an input table data file. This file specifies the section structural properties at each specific span station. The finite element data file which FLIGHTLAB imports consists of 10.000 nodes. The model used for this analysis consists of 24 nonlinear beam elements. These are dimensioned from the input file using interpolation. The stiffness parameters stored in the input file that are relevant to this investigation are stored as the multiplication of the elastic modulus with the area moments of inertia $E_1 \cdot I_{yy}$ and $E_2 \cdot I_{zz}$ and shear modulus multiplied with the torsional constant $G_{12} \cdot J$. These will be referred to as $EIYY$, $EIZZ$ and GJ from this point. To study the effects of property variance in specific span sections an edited input file was created to represent each of the cases of interest. In this case that implies that for example for $EIYY$ there are eight separate sets of data to represent adjustments in the individual span sections $0.3R - 0.4R$, $0.4R - 0.5R$ ... $0.9R - 1.0R$ and across the entire span, which defined as $0.3R - 1.0R$. Only 30% span and further outboard are considered, since the rotor hinges are located inboard of this radial location. The adjusted input files are created using a script that reads the information stored in this file. The script is able to scale a specific property for a specific span range. In this investigation it was chosen to scale with 10% as it seemed to be a factor that would be impactful, without being completely implausible. For the shift in e_d and CG a shift of $0.05c$ was proposed. A change in chordwise mass moment will be represented by a shift of section centers of gravity. An offset in spanwise mass moment will not be considered as it is assumed to have been balanced during static balancing.

The basic FLIGHTLAB software itself does not include the ability to add dissimilar blades to a rotor system. In fact, FLIGHTLAB only allows the user to specify one set of blade properties per rotor. When the model is loaded into the analysis tool the other blades are constructed as copies of the original and given a phase shift. To include a single dissimilar blade a script was created that reconstructs the base blade after the model has been loaded. This reconstruction is then based on the adapted input file. These new blade properties are then not transferred to the other blades on the rotor. This approach works for the adjustments to the stiffnesses and the chordwise CG location. Adjusting the elastic axis location is more complicated, since the section CG and aerodynamic center are defined in relation to the elastic axis location. Therefore, to create a pure shift in elastic axis, the CG and ac need to be shifted in the opposite direction. Therefore the input file for this case needed to be adjusted for both the e_d and CG tables. The location of the aerodynamic center is not represented in the input file and is placed during the construction of the model. Therefore it is also required to adjust the ac location parameter, stored in the blade model tree. To adjust the blade twist angle the blade does not have to be reconstructed. The twist angle property stored in the blade model tree can be multiplied with the required percentage using a short script.

4.2.5. Section Aerodynamic Performance Variation

Due to ageing, repairs or manufacturing tolerances each blade will show slightly different aerodynamic performance. This non-uniformity in aerodynamic performance can result from for example variance in surface roughness and leading edge bluntness due to operating in abrasive environments such as sandy deserts and changes in profile shape due to skin repairs. The relation between the defects and the change in aerodynamic performance will not be investigated in this research, instead a performance penalty will be imposed on the blade based on an engineering guess. This is done in order to conclude whether it would be of interest to further investigate the effects of blade profile imperfections on the aerodynamic coefficients. In this case, just as for the variance in many of the investigated structural parameters a property alteration of 10% was chosen, as is it assumed to represent an upper limit of realistic variation. Only a depreciation in aerodynamic performance is investigated, since it is expected that the performance of a blade rarely improves over time, if ever. A change in moment coefficient was not included in this research.

This can be implemented in the model by using the approach that was used to represent a deflection of the blade tab. The span sections of interest can be designated as having a tab element, however instead of adjusting the section aerodynamic coefficients using the lookup table created for the tab, the component refers to a different lookup table representing a 10% change in lift or drag corresponding to the specific Mach number and angle of attack.

4.3. Solver Process

Once the model has been loaded into the analysis tool the rotorcraft model will be trimmed to the flight specified flight conditions. The atmospheric conditions for the analysis are set to ISA standard day with zero wind velocity. Before starting the trim algorithm the test conditions need to be set. The test conditions for the runs are defined in Table 4.2.

Table 4.2: Test conditions for the FLIGHTLAB analysis.

Property	Value
Altitude	500 ft
Airspeed	0/100/130 kts
Vehicle mass	44,262.0 lbs
Azimuth steps per rotation	100

The number of azimuth steps per rotation determines the amount of computations that are performed per revolution. This is an important variable as it has a large impact on the computation time. It can not be too low however, since it determines the amount of accelerometer measurements per revolution, thus controlling the accuracy of the prediction of the vibration magnitude and azimuth angle. Once the test conditions have been set the trim procedure can be initiated. There are three choices of trim algorithm included in FLIGHTLAB: the Newton-Raphson Method, the Newton-Hooke method and the Hooke-Jeeves method. From a first couple of trial runs it was observed that the Newton-Raphson method was the fastest algorithm when the initial conditions were quite close to the solution. This makes sense as the Newton method is one of the fastest ways of solving an optimization problem. A disadvantage of the Newton method is poor convergence chance when the initial point is relatively far from the solution, following from Burden and Faires (1989). This issue can be solved by first finding the trimmed solution for each airspeed for the helicopter with perfect rotor blades. This can be done by using one of the slower methods with a higher convergence chance such as the Hooke-Jeeves algorithm. The trim solution for the models with dissimilar blades will still be close to the solution for the base model. Therefore the Newton method can be used for all subsequent trim operations with the solution for the base model as initial condition. This initial condition specifies the input for the states, used to trim the model. For this analysis the trim variables are: lateral and longitudinal cyclic, collective setting, pedal input and pitch and roll attitudes. The trim targets are steady states of linear and angular accelerations. The required steady states and their tolerances are shown in Table 4.3.

Table 4.3: Trim target for the FLIGHTLAB analysis.

Property	Steady State	Tolerance
$\ddot{x}_b$, $\ddot{y}_b$, $\ddot{z}_b$	0 ft/sec^2	0.04 ft/sec^2
$\dot{p}_b$, $\dot{q}_b$, $\dot{r}_b$	0 rad/sec^2	0.01 rad/sec^2

Once the helicopter model has been trimmed the simulation is run for ten full rotations. During these cycles one hundred accelerometer measurements are gathered per rotation. This results in a sinusoid of ten periods containing all the vibration responses for all frequencies of interest. To obtain the 1/rev vibrations from this data the Fast Fourier Transform (FFT) can be applied (see Appendix A). Applying this the FFT gives the vibration magnitude per frequency. An FFT plot will show the peaks at the frequencies where the vibration magnitude is large. In the case of Rotorcraft vibration, this will usually be the natural frequency at 1/rev, at 3/rev and at « 1/rev (i.e. occurring from the engines). To obtain the 1/rev vibrations the value at 3.75 Hz needs to be selected.

5
Results

In this chapter the results from the FLIGHTLAB analyses will be presented and compared. As has been stated in the preceding chapters, three distinct modeling approaches have been applied. First, to create a baseline for the investigation into the effects of mutual rotor wake interference a model was created where the rotor interference module has been disabled. The second version of the model includes the VPM approach to modeling the rotor infow and wake interference. The third model, with a modal elastic fuselage module will be discussed in the validation part of this report. Each parameter change has been investigated for three different airspeeds, for seven separate 10% span sections and on full span adjustment. These will be presented in bar graphs with each set of three bars representing adjustment for a section at the three velocities. A set of base values will also be included. This set indicates the measured vibrations without any blade dissimilarities. All the other points of data in the graph represent the magnitude difference between the base value and the result from a dissimilarity case.

The graphs indicate the result from adjusting specific 10% span sections and an adjustment of the property along the entire span. This allows for conclusion to be drawn on the most crucial defect locations. By including results from editing both short span sections and along the full span a preliminary conclusion can be drawn on whether the vibration levels increase linearly with a larger affected span section. If the measurement for a full span adjustment equates to the summation of all span section contributions, the relation is likely to be linear. All the presented vibration magnitudes due to rotor adjustments are relative to the baseline, i.e. if the baseline measurement would indicate 0.1 ips at an azimuth angle of 180° and the measurement for an adjusted blade indicated 0.1 ips at 90°, the presented result would be a magnitude of 0.2 ips at azimuth 90°. In this chapter, first the results from the analyses will be presented, followed by a discussion of the results in the final section.

It is important to note that for this report all of the vibration values that will be presented have been normalized, as the actual values have been restricted. Normalization has been applied separately for both lateral and vertical orientations. What this means is that a measurement of 1.0 represents the maximum measured vibration level across both the non-VPM and the VPM model for either lateral or vertical orientation. Both modeling approaches can be compared however, as they have been normalized with the same value. Keep in mind also, that the 1.0 value may correspond to an outlier and might make some results look small in comparison, while those could still represent excessive vibration. Whether a parameter is considered significant or not has been based on whether it exceeds the limit set for that flight condition, although unfortunately the actual limits could not be disclosed as they have been restricted.

First all the results gathered from the model without VPM inflow modeling will be presented in Section 5.1. This is then followed by the presentation of the results gathered from the model with VPM enabled in Section 5.2. Since it is not easy to compare both sets of data when they are presented this way Section 5.3 has been created that shows results from both models side by side. This is only done for changes along the complete span in order to keep the figures clear, however measurements on both rotors are now included. After presenting all the results an investigation was performed to try and find the causing principle that leads to increased vibration. Firstly in Section 5.4 it was investigated whether blade property changes alter the blade eigenmodes and frequencies in such a way that it may cause the increased vibrations. Secondly in Section 5.5 it was investigated whether the changes in the parameters cause a change in aerodynamics loads in such a way that it causes the vibration. In Section 5.6 all the results from previous sections within this chapter will

be more extensively discussed.

5.1. Without Aerodynamic Rotor Interference

Part of the investigation aims to look at the effect of the tandem rotor system and the modeling approach required to represent such a system. Therefore first a set of simulations was run where rotor to rotor interference was not modeled. In this case the VPM inflow model was replaced with the Peters Finite State inflow model that does not take the wake of the other rotor into consideration. By comparing the results between the model with and without rotor wake interference conclusions could be drawn on the effect of rotor interference on rotor vibrations and whether VPM modeling is required to accurately represent the tandem rotor system. As was discussed in Section 4.1, the rear rotor loses some power due to wake interaction, while the forward rotor is less affected. Due to these losses the rear rotor requires more rotor power, possibly leading to higher vibration levels. First these results with no interference will be presented, which can then be compared to the results in the next section. All the following data is for an adjustment to a blade on the forward rotor and all the measurements follow from the forward accelerometer. The first set of results has been plotted in Figures 5.1 to 5.8.

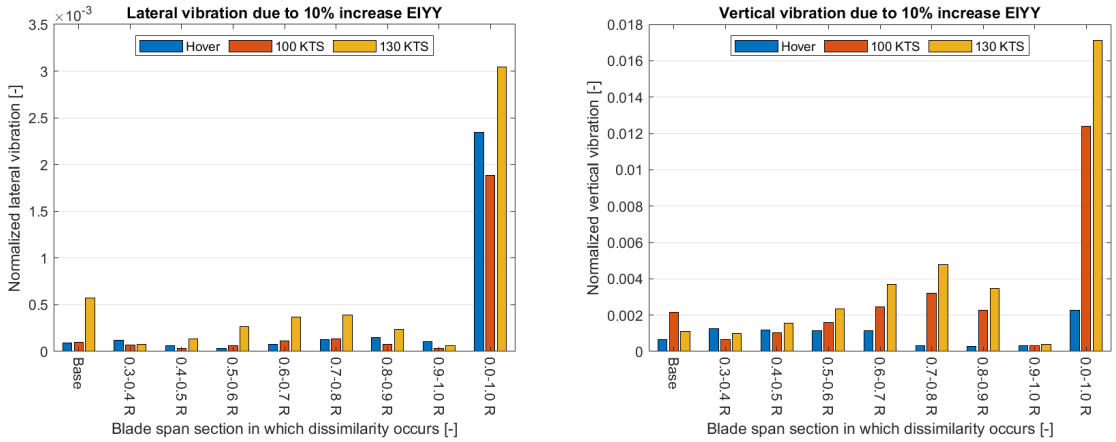

Figure 5.1: Lateral and vertical vibrations due to a 10% increase in flapwise stiffness.

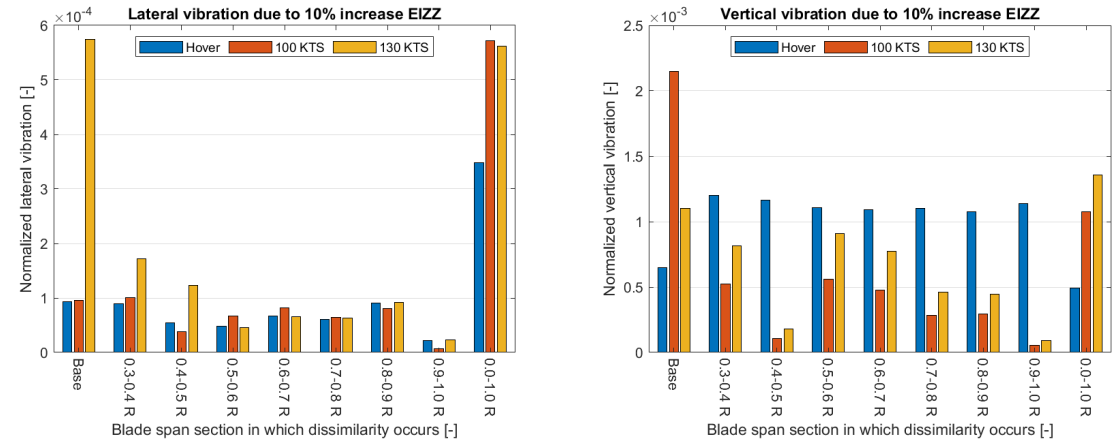

Figure 5.2: Lateral and vertical vibrations due to a 10% increase in lag stiffness.

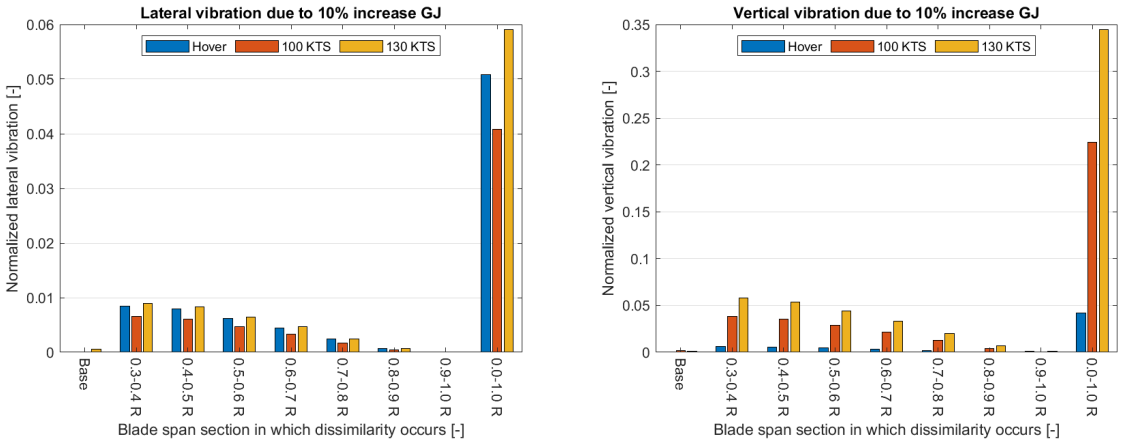

Figure 5.3: Lateral and vertical vibrations due to a 10% increase in torsional stiffness.

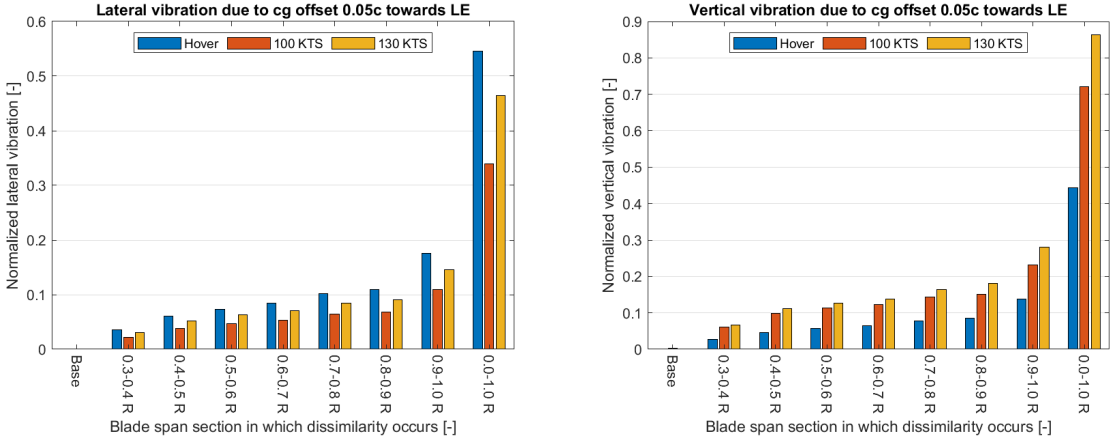

Figure 5.4: Lateral and vertical vibrations due to a shift in chordwise CG location of 0.05c towards the leading edge.

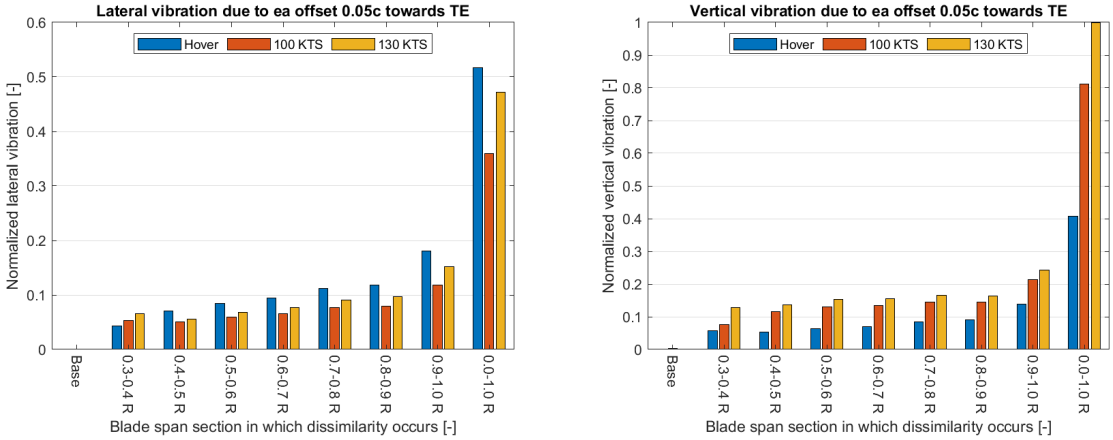

Figure 5.5: Lateral and vertical vibrations due to a shift in chordwise elastic axis location of 0.05c towards the trailing edge.

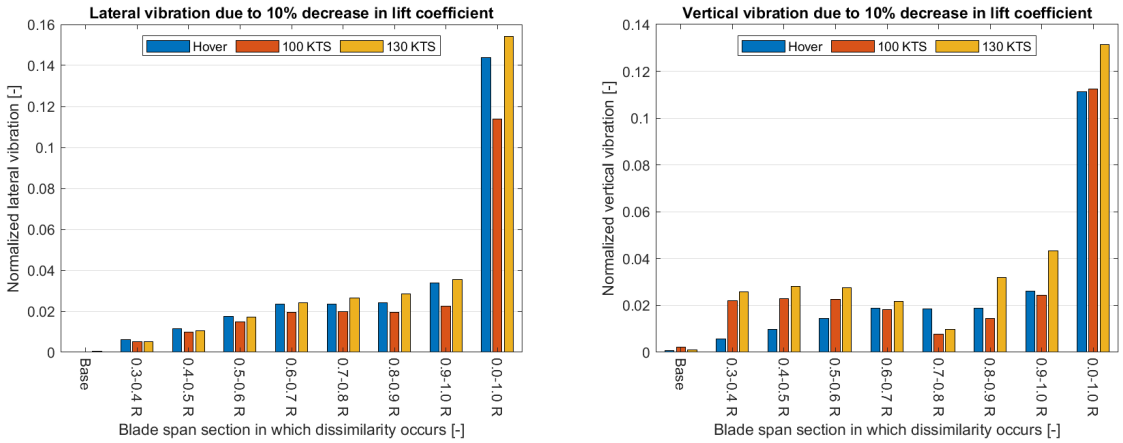

Figure 5.6: Lateral and vertical vibrations due to a 10% reduction in section lift coefficient.

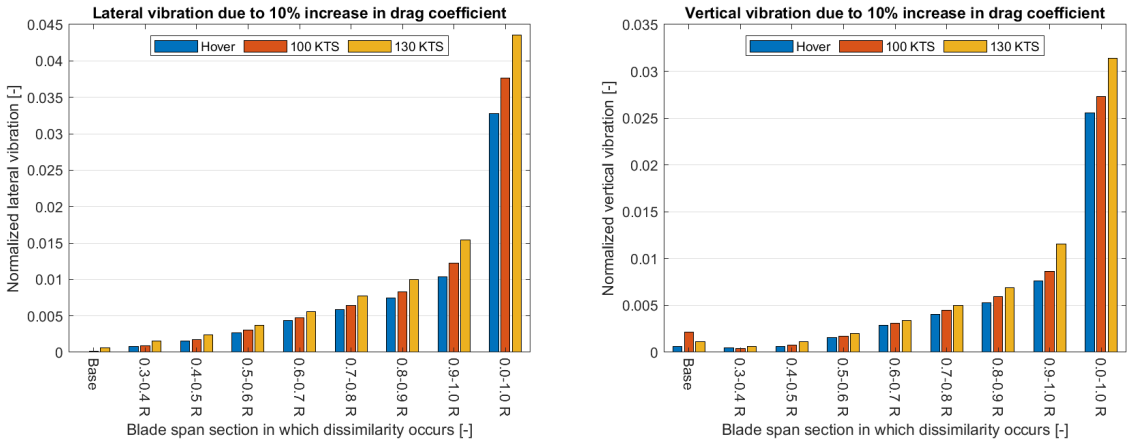

Figure 5.7: Lateral and vertical vibrations due to a 10% increase in section drag coefficient.

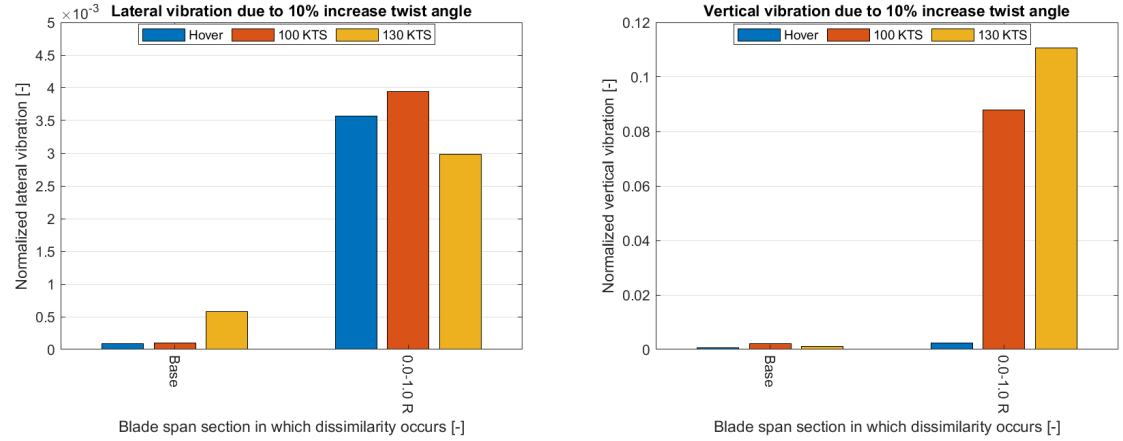

Figure 5.8: Lateral and vertical vibrations due to a 10% increase in section twist angle.

From these sets of bar plots it can be observed that concerning the blade stiffness properties, that the effects of adjusting flapwise bending stiffness $EIYY$ and the chordwise bending stiffness $EIZZ$ are insignificant compared to the torsional stiffness GJ. For the adjusted GJ it can be observed that the most significant span section is near the root of the blade. This seems logical, as a torsional displacement near the root would affect

the blade pitch angle along the remaining span, resulting in a greater change in lift distribution compared to when only the tip is affected. When it comes to the chordwise relocation of the typical section points CG and e_d, it seems that both are of a similar significance. When it comes to the aerodynamic properties of the blade, it seems that the section lift coefficient has a greater effect on vibrations than the drag coefficient. An increase in twist distribution mainly influences the vertical vibrations, however only at higher airspeeds. The twist distribution has only a minor impact on the lateral vibrations.

5.2. With Rotor Interference

For the model with a VPM the same investigation is repeated and the data collected. So in the following sets the same model and adjustments are used, but with the inflow model changed to the VPM, including rotor to rotor interference. Again, this set of results only considers an adjustment to a blade on the forward rotor and the measurement again is taken from the forward accelerometer.

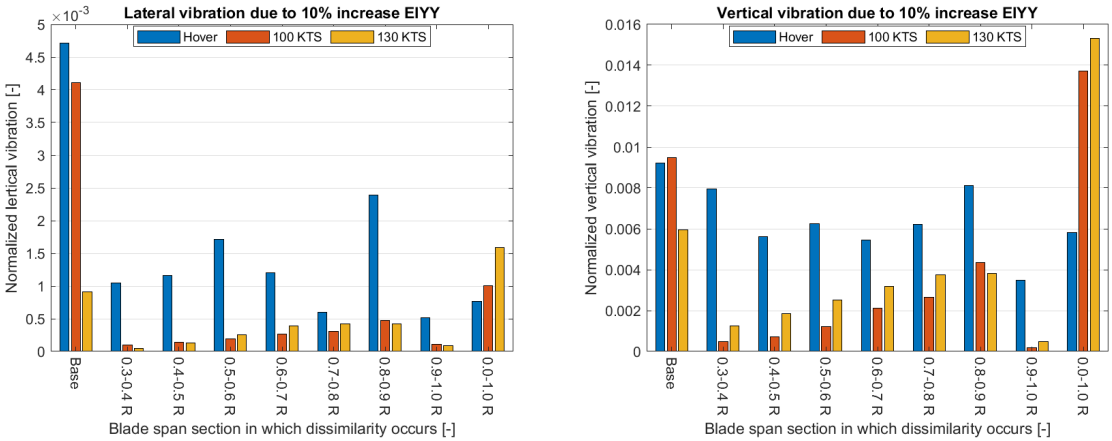

Figure 5.9: Lateral and vertical vibrations due to a 10% increase in flapwise stiffness.

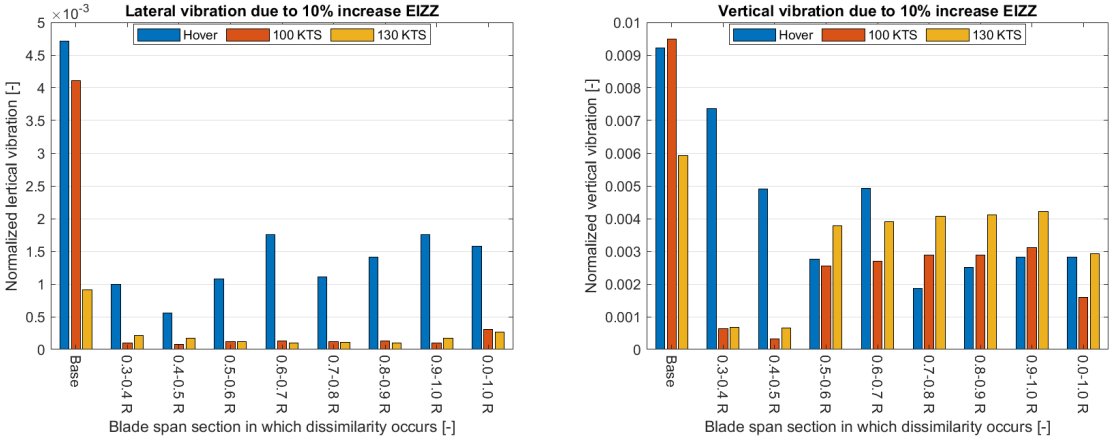

Figure 5.10: Lateral and vertical vibrations due to a 10% increase in lag stiffness.

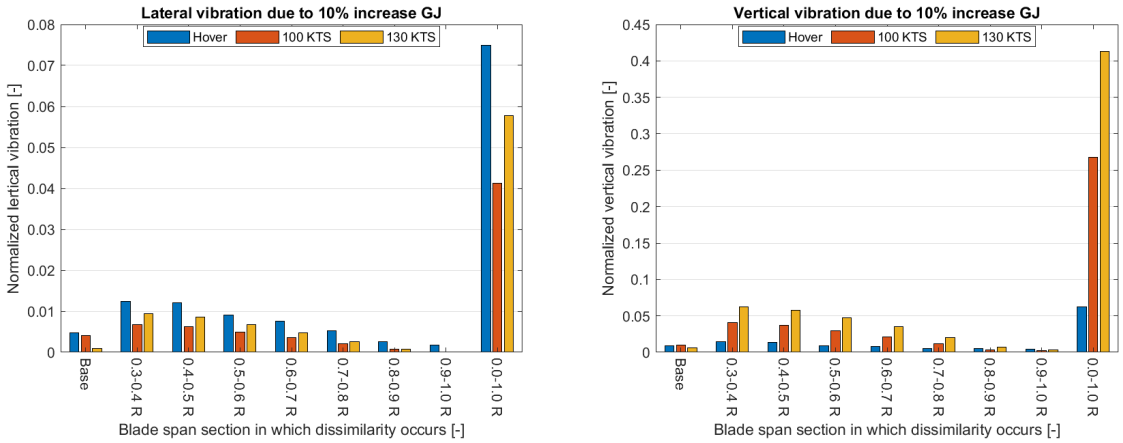

Figure 5.11: Lateral and vertical vibrations due to a 10% increase in torsional stiffness.

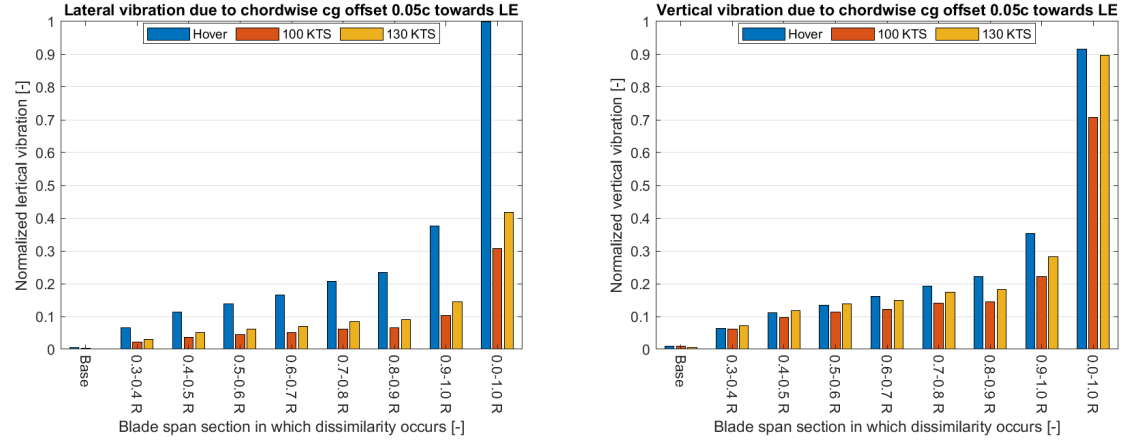

Figure 5.12: Lateral and vertical vibrations due to a shift in chordwise CG location of 0.05c towards the leading edge.

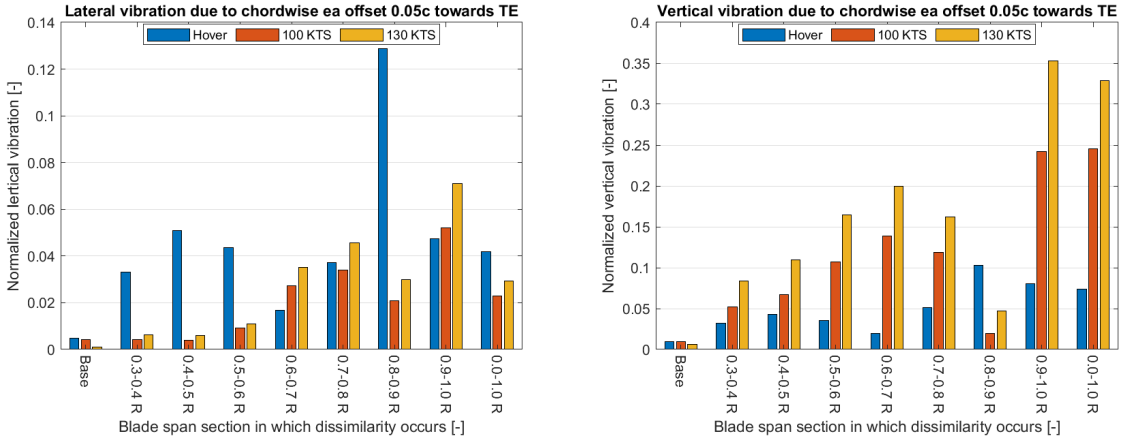

Figure 5.13: Lateral and vertical vibrations due to a shift in chordwise elastic axis location of 0.05c towards the trailing edge.

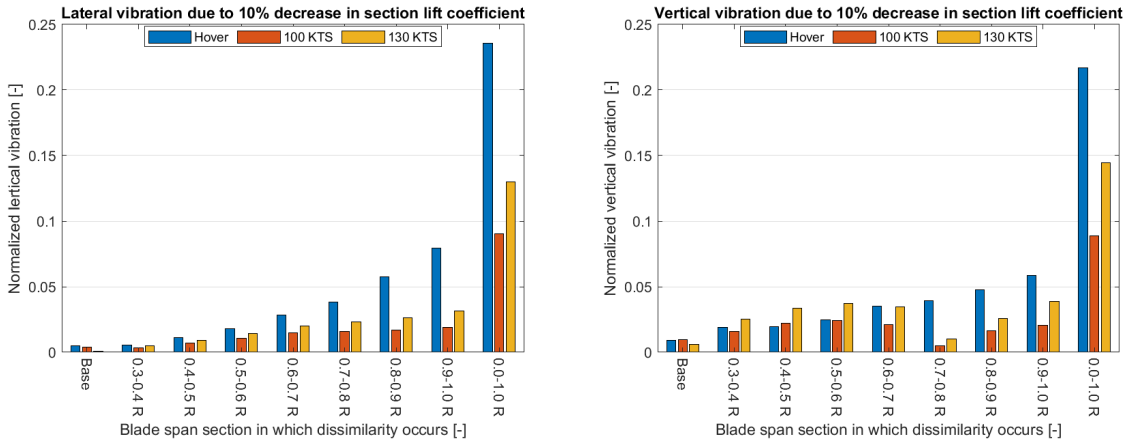

Figure 5.14: Lateral and vertical vibrations due to a 10% reduction in section lift coefficient.

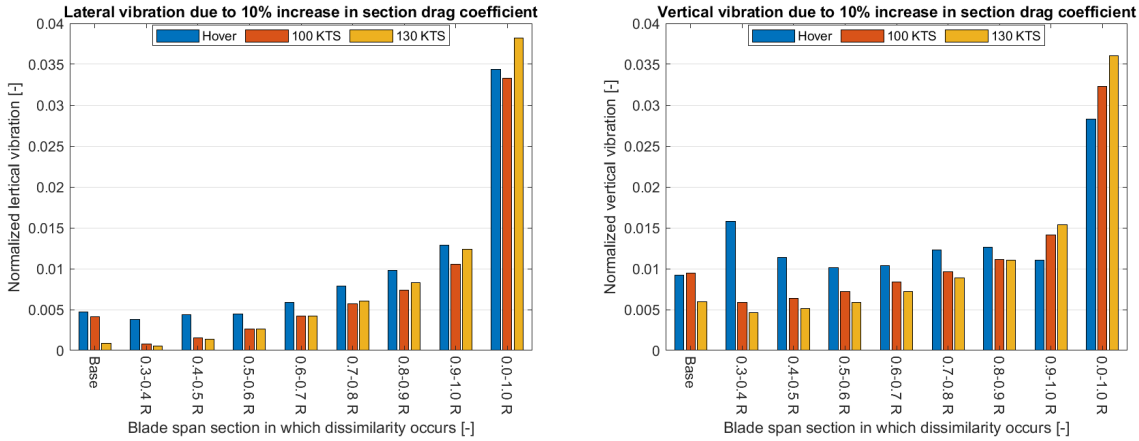

Figure 5.15: Lateral and vertical vibrations due to a 10% increase in section drag coefficient.

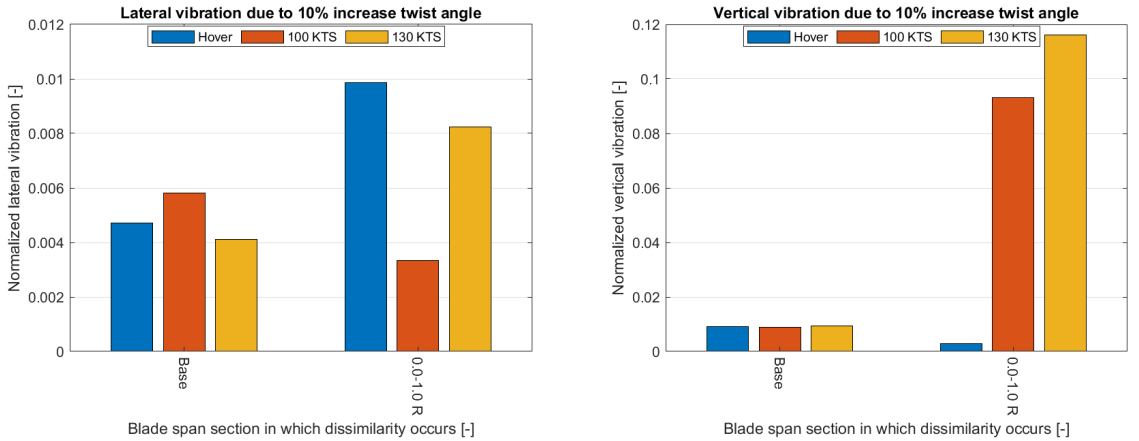

Figure 5.16: Lateral and vertical vibrations due to a 10% increase in section twist angle.

One thing that becomes clear by comparing these results to ones from the finite state inflow model is that the baseline vibrations are quite a bit higher for the VPM model. As the base model has identical rotors it is likely that this results from the rotor wake interactions that were not captured before. Also it can be noticed that the measured vibration in hover are quite a bit higher for the VPM model. As will be shown in Section 6 on the validation, it seems that for the vibration in hover, that the VPM model provides an overestimation, compared to the finite state inflow model. Assuming that the vibration in hover is overestimated, the trend in the figures is comparable to what is shown in the previous section. Again, the torsional stiffness appears to be the only one of the stiffness parameters that has a significant influence on the vibration, as an adjustment to $EIYY$ and $EIZZ$ does not surpass the baseline vibration level. When it comes to shifting the center of gravity, the results are also comparable to the finite state model, accounting for the overestimation for the hover case. The behavior of shifting the elastic axis has changed a lot compared to the previous section however. Somehow the measurement for an adjustment to the full span has a lower or equal effect than adjusting the 90% - 100% span section. it is assumed that these results are erroneous, rather than a true representation of such blade defects. When it comes to the aerodynamic performance, again the results closely resemble those from the finite state model, except these seem to be of a lower magnitude.

5.3. Comparison Between Both Models

One of the goals of this investigation is the effect of the tandem rotor system on the vibration levels, and whether the VPM model is able to accurately capture this. The second part of that statement will be further investigated in chapter 6. For now, the difference between the finite state and VPM models can be examined by presenting them side by side. In the upcoming set of figures the results for adjustments along the full span for both the forward and the rear rotor are presented for both modeling approaches. As was stated in Section 4.1, the effectiveness of the tab, tip weight and pitch link was lower on the rear rotor due to rotor wake interaction. It is likely therefore that an inertial or aerodynamic dissimilarity would have a lower sensitivity on the rear rotor. This effect would then be more apparent in the results for the rear rotor of the VPM model. The bending stiffnesses for either direction are left out, as they are so small that the comparison will not be able to show any clear pattern. Also the elastic axis shift was left out, as the series behaved so differently between the two inflow models.

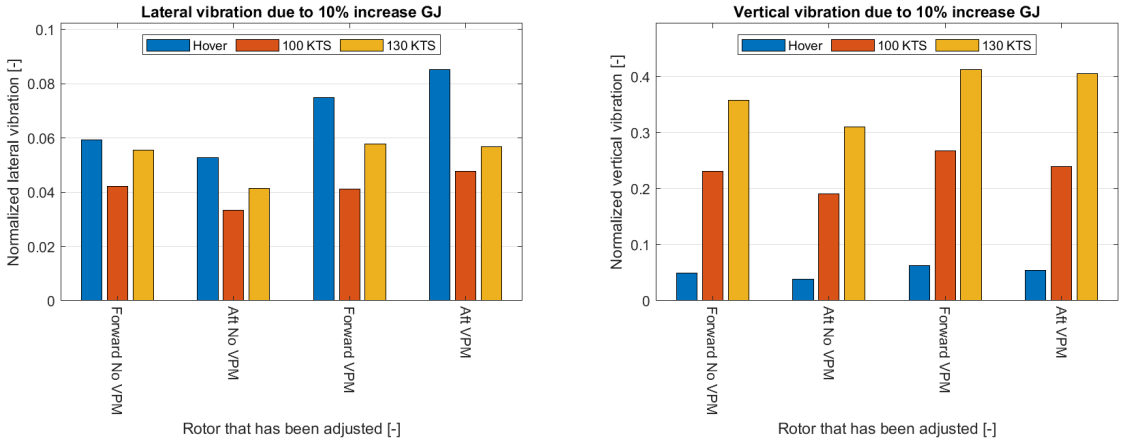

Figure 5.17: Lateral and vertical vibrations due to a 10% increase in torsional stiffness.

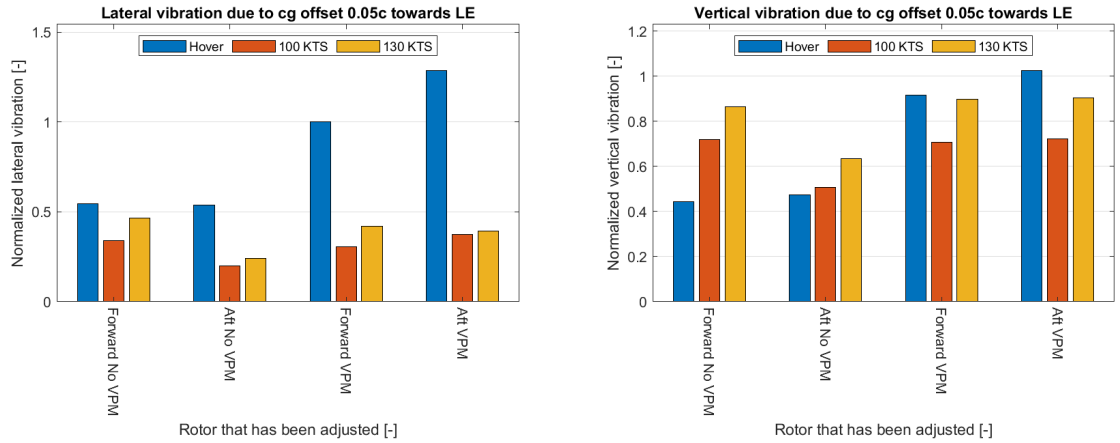

Figure 5.18: Lateral and vertical vibrations due to a shift in chordwise CG location of 0.05c towards the leading edge.

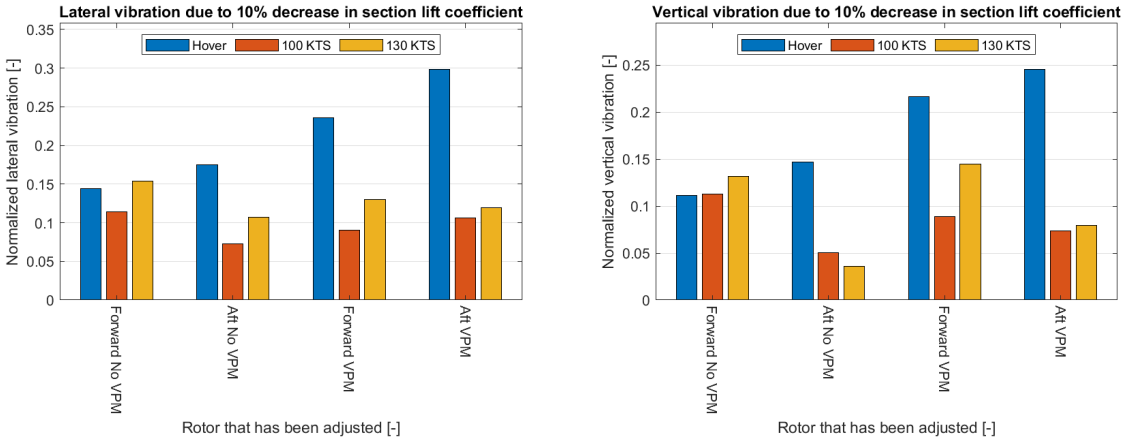

Figure 5.19: Lateral and vertical vibrations due to a 10% reduction in section lift coefficient.

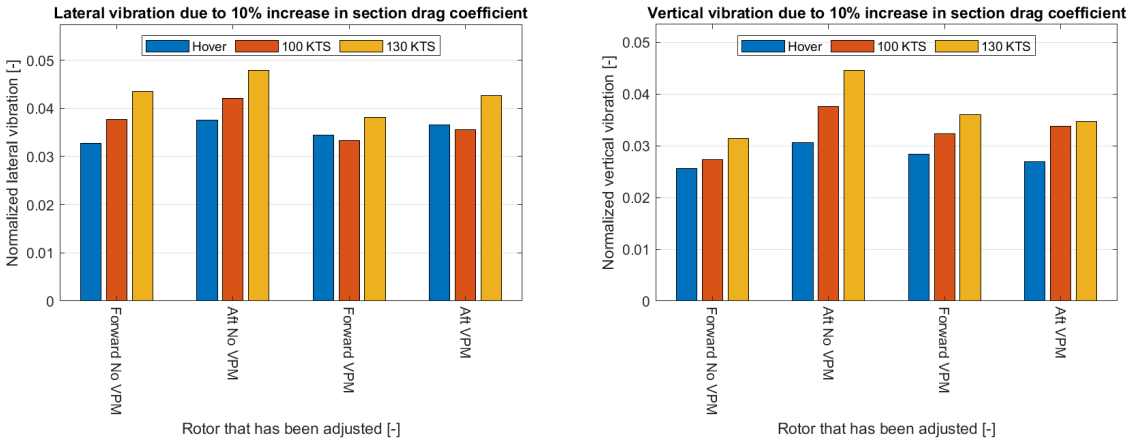

Figure 5.20: Lateral and vertical vibrations due to a 10% increase in section drag coefficient.

Again, when looking at the results for hover, it needs to be taken into account that for the VPM model the vibration magnitude is quite a bit higher compared to the finite state model. This is especially relevant for the case of adjusting the CG, where the VPM model predicts double the vibration level. In general the VPM model shows slightly higher vibrations. One exception to this is a change in drag coefficient.

When it comes to the difference between adjustments made to the forward and rear rotor there is not a clear relation that stands out. For the finite state model in general the results are slightly lower on the rear rotor, with the exceptions of the vertical vibration for the lift coefficient and for both orientations for the drag coefficient. For the VPM model there exists a lot of variation in the difference between forward and aft. When considering only the 100 kts and 130 kts cases the results for both rotors are quite similar. In hover though, the vibration increases on the rear rotor. It is currently unclear what is the cause for this effect.

5.4. Modal Analysis

In order to investigate the fundamental principles behind the 1/rev vibration and the causal relationship with defects, a modal analysis into the rotor blade modes was initiated. The eigenmodes of a structure represent the natural deformation behavior due to some excitation. The most relevant modes are the bending modes in either direction and the torsion mode. The modes are characterized by a eigenfrequency and mode shape. These modes are usually visualized using grid points in a 3-D system or for 2-D systems by just a curve.

The mode shape, eigenfrequency and order of the eigenmodes are dependent on the structural and geometrical properties of the structure. For rotor blades the spanwise and chordwise bending are often renamed flapwise and lead-lag bending respectively. As the mode shapes represent the dynamic response at specific eigenfrequencies, the set can also be called the frequency response of the blade. Since these eigenmodes correspond to specific frequencies it is of interest for this research to investigate whether the modes that approach the natural rotor frequency are influenced by changes in specific blade properties as this may indicate a causal mechanism for the resulting vibrations. This can be done by comparing the modes of altered blades to the baseline blade. Also, the modes for different types of adjustments can be compared to see whether the ones with a greater effect on the 1/rev vibrations show distinct behavior.

In the case of rotorcraft however, two additional characteristics make it more difficult to compare static measurements on the ground and finite element analysis to the real situation, namely the rotation speed and airloads. Due to the centrifugal force acting on the rotating blade, stresses are created that introduce a centrifugal stiffness matrix into the equations of motion (Hoa (1979)). Additionally, the airloads on the blade also act on its structural states, introducing an aerodynamic stiffness and damping matrix in addition to the centrifugal matrix Hulshoff (2012). This has an effect on the frequency response of the blade, that varies with the rotor speed and airspeed. In addition, in a single revolution the blade airloads will change depending on whether it is moving against or along with the flow. FLIGHTLAB allows for modal analysis both with and without airloads, at different rotor speeds. Both methods will be investigated in this section. Unfortunately the modes of the CH-47 rotor blades and computational recreations are subject to restriction and have been removed from the report that is made available for the committee and the public.

5.4.1. Modes of the Nonrotating Blade

Even though the static frequency response of the blades does not represent the situation under flight conditions, it is the only response that can be measured. A Ground Vibration Test (GVT) analyses the blade response to an excitation in order to measure the modes and accompanying frequencies. To execute the GVT the blade is mounted in a special fixture. This is another simplification of the actual situation as it excludes both the lag damper and the pitch link removing their stiffness and damping values from the system. Instead the blade is clamped at the root. The GVT tests can be compared to the FLIGHTLAB eigenmode analysis. If adding a defect on a blade shows an observable difference in the modes from computational methods, and if GVT would correlate poorly performing blades to a shift in mode shapes it would warrant further investigation to determine if a causal relationship can be established.

FLIGHTLAB is able to generate mode shapes based on the finite element representation of the blade. For the investigation into the static modes a separate model was generated that would closely resemble a GVT setup. That means airloads are excluded and the rotor hinges are given infinite stiffness and zero damping. The rotational speed at which the eigenmode is computed is non-zero, as at that point a singularity exists for an articulated rotor model due to the way FLIGHTLAB calculates, instead 5% rpm is used. Two of the stiffness parameters were chosen for comparison, the flapwise stiffness $EIYY$, which did not show a large influence on vibrations and the torsional stiffness GJ, which did have an impact on vibration levels. Also the chordwise

CG, a non-stiffness parameter shift was included. The changes were applied along the entire blade span, as it has the greatest impact. Three versions of the blade were tested, first a baseline version, second a change in stiffness of 10% and third a change of 20%. This was done to examine the behavior with increasing defect magnitude. The resulting eigenfrequencies are shown in Table 5.1. In order the modes are: first flapwise bending, first lag bending, second flapwise bending, third flapwise bending and first torsion.

Table 5.1: The frequency response and corresponding modes for a stationary blade, with infinite pitch link stiffness and no damping. Note: all frequencies are normalized with respect to the first eigenfrequency for the base blade and therefore have no units.

Adjustment	Mode 1 (F1) Frequency [-]	Mode 2 (L1) Frequency [-]	Mode 3 (F2) Frequency [-]	Mode 4 (F3) Frequency [-]	Mode 5 (T1) Frequency [-]
Base	1.000	2.398	5.365	14.325	17.307
$EIYY$ 110%	1.047	2.405	5.622	14.972	17.338
$EIYY$ 120%	1.091	2.410	5.868	15.566	17.387
GJ 110%	1.000	2.398	5.365	14.342	18.124
GJ 120%	1.000	2.398	5.366	14.352	18.905
CG 0.05c to TE	1.001	2.398	5.365	14.325	17.307
CG 0.05c to LE	1.001	2.398	5.364	14.289	17.338

From this table it can be observed that the bending modes are mostly affected by bending stiffness and the torsion mode mostly by the torsional stiffness which is to be expected. The change in frequency however is quite small. A general definition for the eigenfrequency of an object is given in Equation 5.1.

$$\omega = \sqrt{\frac{k}{m}} \tag{5.1}$$

From this equation it follows that for a 10% increase in stiffness k, or mass m the eigenfrequency is expected to only increase by 1%, which is approximately the case for the values from Table 5.1. It is difficult however to draw conclusions merely based on the static frequencies, as the frequencies increase with increasing rotational speed. The static modes shapes that are closest to the 1/rev are investigated further, since modes closest to the natural frequency are expected to have the greatest influence.

It was also investigated whether the modeshapes are influenced by altering the blade properties. This was only done for changes along the complete span of the blade, since these cases show the greatest vibration magnitudes. Since mode shapes represent normalized deflection it would be expected that a change along the entire blade would not change the shape of each mode. This was confirmed as it was found for the eigenmodes listed in the above table that the dominant mode shapes for blades with a parameter change are identical to those of the base blade. Some slight shifts in mode shapes were observed for the non-dominant modes however, these shifts were in the order of 10^{-3} so these are deemed insignificant.

5.4.2. Modes of the Rotating Blade

Due to the centrifugal and aerodynamic forces that act on the blade additional stiffness and damping matrices are introduced into the equations of motion. The modal frequencies increase with increased rotor rpm and the behavior of the modes changes. In fact, Peters et al. (1986) states that one of the more challenging aspects of rotor design is ensuring that the eigenfrequencies do not closely match the forcing frequencies, as the 1, 2, ... n/rev are not widely spaced and provide many possibilities for resonance. Also, modes are often coupled due to the relationship between blade pitch, elastic deformation and the airloads. This is complicated further by the fact that the aerodynamic loading of the blade depends on the azimuth angle and airspeed. For the rotating blade scenario the connection of the blade to the rotor hub differs from the way the blade is fixed in the GVT. For the rotating blade the pitch link stiffness and the lag damper are included. In order to check for the influence of defects the eigenfrequencies and modes were analyzed at the nominal rpm, the eigenfrequency results of this analysis for modes are presented in Figure 5.2.

Table 5.2: The frequency response and corresponding modes for the articulated rotor blade at nominal rpm. Note: all frequencies are normalized with respect to the first eigenfrequency for the base blade and therefore have no units.

Adjustment	Mode 1 (F1) Frequency [-]	Mode 2 (F2) Frequency [-]	Mode 3 (F3) Frequency [-]	Mode 4 (T1) Frequency [-]
Base	1.000	2.561	4.340	4.381
$EIYY$ 110%	1.005	2.598	4.226	4.529
$EIYY$ 120%	1.009	2.635	4.190	4.585
GJ 110%	0.995	2.560	4.486	4.486
GJ 120%	0.991	2.559	4.469	4.792
CG 0.05c to TE	1.011	2.561	3.818	4.435
CG 0.05c to LE	0.992	2.562	4.432	4.859

From this table it can again be concluded that for the rotating blades the defects do not change the eigenfrequencies by much. Note that the rotation frequency is lower than the first eigenfrequency in the above table. From this table it can be observed that the change in predicted frequency for the first eigenmode is at most 1%, even for blade defects that caused higher vibrations such as increased torsional stiffness and chordwise CG shift. This 1% difference is much smaller than the difference between the first eigenfrequency and the 1/rev frequency.

Again, the mode shapes were investigated, now for the rotating blade. Same as for the static blade however, it was found that the dominant mode shapes are unaltered by changes in blade parameters applied along the full span. Since such a modification shows no effect on mode shape while a complete spanwise change causes highest vibration magnitudes, and the fact that the eigenfrequencies do not approach the 1/rev frequency it is deemed that the frequency response of the blade is not likely the cause for in-flight vibration due to modified blade parameters.

5.5. Airload Distribution

Another possible cause for the increased vibration due to defects could be a change in airload distribution on the blade that has altered structural properties. The torsional stiffness and chordwise shifts for both CG and e_d influence the pitch deformation of the blade sections due to airloads acting on the blade. It is possible that this interaction is strong enough that the effective angle of attack distribution along the span of the altered blade is changed. A short analysis was performed to investigate this assumption. Due to time constraints only the chordwise change in CG was simulated again using the VPM model, as this parameter caused high vibration magnitudes, as shown previously. The spanwise lift coefficient distribution was collected for a few full rotations after achieving trimmed flight. From this data the distribution for 90 degrees azimuth angle was taken for all three blades. The lift coefficient distribution for both unaltered blades were basically identical to each other, while the blade with the applied CG shift to the leading edge showed a decrease in lift coefficient. The decrease in lift coefficient of the altered blade compared to the average between the two ideal blades is shown in Figure 5.21.

In this figure the high offset in lift coefficient for hover is apparent. This could be connected to the outliers that are seen for hover in the VPM model results. Note however that the figure shows local lift coefficient and not loads. Therefore, accounting for airspeed, the behavior shown above could be connected to the results from Figure 5.12. A forward shift in CG would decrease the pitch deflection since the distance between it and the aerodynamic center decreases or becomes more negative, leading to a lower effective angle of attack. This expectation is confirmed in the above figure. In order to definitely prove that a change in airload distribution due to a change in blade parameters is the cause for the excessive rotor vibrations more data needs to be collected in the future.

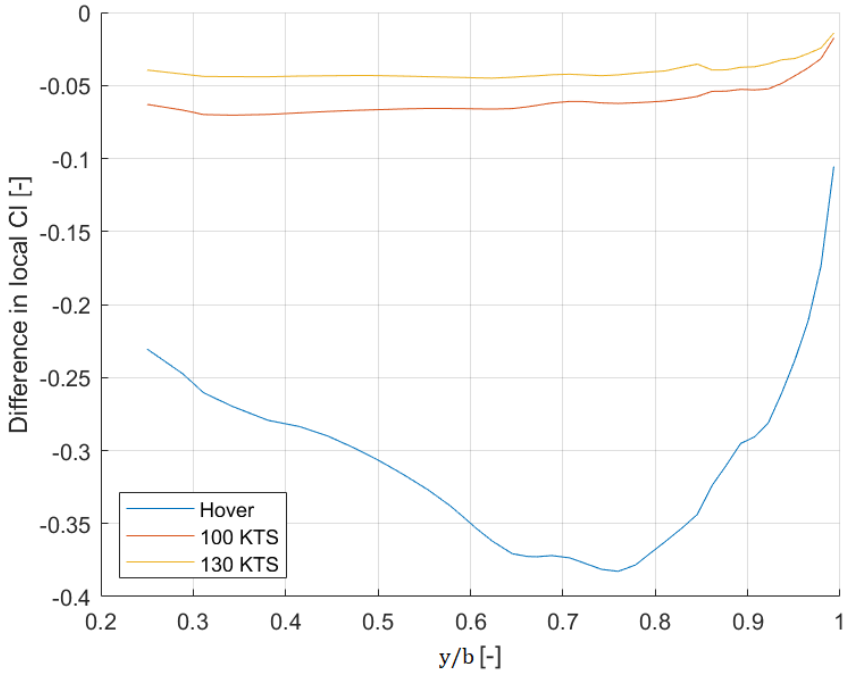

Figure 5.21: Loss in spanwise lift coefficient for a blade with CG shifted to the LE by 0.05c along the entire span, compared to ideal blades.

5.6. Discussion of Results

From the results that have been presented in this chapter a number of interesting observations can be made. When it comes to ranking the parameter sensitivities one of the interesting results is the fact that both flapwise and lag bending stiffness do not seem to have any significant influence on vibrations as their effects barely exceed the baseline measurement. Notably, a change in flapwise bending stiffness seems to have little effect on 1/rev vibration according to the FLIGHTLAB analysis. This is an interesting result, as a change in bending deflection would influence the loading of the blade and the resultant force on the hub. Moreover, the first bending mode frequency lies closest to the 1/rev frequency. A possible explanation for EIYY having nearly no effect could follow from Peters et al. (1986), which states that at the lower end of the frequency spectrum the centrifugal stiffness matrix dominates. Examining this effect for this specific blade would be an interesting opportunity for future research. For chordwise bending, it might be more in line with expectation that its sensitivity is lower. This deformation mode has a higher frequency, and the deflections in this plane are small compared to flapwise bending. Torsional stiffness does seem to have a large impact on the system vibrations. It is a possibility that the vibrations are mainly a result of a change in aerodynamic loading instead of a change in frequency response, as the torsion response of the blade is key parameter in the aeroelastic blade response. This conclusion is further strengthened by the fact that the adjustments that do not change the stiffness properties also cause vibrations equal to, or greater than a 10% change in torsional stiffness. Although it needs to be noted that these results are for arbitrary changes in blade properties. It cannot be concluded whether these changes are comparable to actual worst case scenarios for blades in the inventory.

When comparing a chordwise shift in center of gravity to a shift of the elastic axis, both seem to have a comparable effect, although the VPM model does seem to have trouble dealing with modeling the elastic axis offset. Both of these parameters influence the pitch deflection of the blade sections and it seems likely that this is the cause for the force imbalance on the hub, as the pitch changes the loading of the blade. It would be of interest to in future look at the actual effect on blade aeroelastic behavior and comparing the loading of each individual blade. A change of 10% directly applied to the section aerodynamic coefficients seems to have a similar effect as changing CG and e_d, although the sensitivity of the aerodynamic coefficients is lower compared to that of CG and e_d. It would be interesting to investigate whether these changes in CG, e_d therefore cause a greater than 10% difference in aerodynamic loading.

Another observation from these bar plots is the relation between airspeed and vibration magnitude. In

general, for the lateral orientation the highest vibrations are measured at hover and at high speed, while for the vertical vibration it is lowest in hover and increases with airspeed. It is possible for lateral vibrations that the rotor power is the driving factor, while for vertical vibration the velocity of the flow is the main cause. As for the overprediction of vibration levels in hover for the VPM model, it was hypothesized that the VPM model overestimates the required rotor power in hover. If the required rotor power predicted by the model would be greater than the real scenario, the vibration levels would also be overestimated. Especially in lateral direction. To investigate this, the trimmed collective settings for both approaches were obtained. If the VPM model introduces more power losses into the system it would require a higher trimmed collective setting to compensate. Unfortunately, there is no reference to compare the FLIGHTLAB results to. The predicted collective settings for both inflow modeling approaches are presented in Table 5.3.

Table 5.3: Trimmed collective settings compared for both modeling approaches. Results are normalized with respect to the collective setting in hover.

	Hover	100 KTS	130 KTS
Finite State Inflow	1.000	0.873	1.076
VPM Inflow	1.163	0.949	1.144
Increase	16.31%	8.74%	6.30%

The increase in collective setting for the VPM model in hover compared to the finite state model is 16.31% and decreases with increasing airspeed. This is to be expected, as with increasing airspeed, the rotorcraft spends less time within the wake's zone of influence. This is also in line with what was presented by Lee et al. (2009) in Figure 4.1. A collective setting increase of 16.31% does not seem likely to cause a near doubling of the predicted rotor vibrations between models, such as is the case for CG shift and c_l. Those two appear to be outliers, as the other parameters do not show a similar drastic increase.

To investigate the effects of shifting CG and e_d further an additional simulation was run where both parameters were shifted towards the leading edge by 0.05 of the chord. In this case the results for shifting only CG were used to normalize the results for shifting both. The results are shown in Table 5.4.

Table 5.4: Relative change in vibration when shifting only CG and both CG and e_d to the leading edge. Note that vibration magnitudes are normalized with respect to the vertical vibrations due to CG shift in hover.

Parameter	Orientation	Hover Vibration Coefficient [-]	100 KTS Vibration Coefficient [-]	130 KTS Vibration Coefficient [-]
CG to LE	Vert	1.000	1.627	1.950
	Lat	3.464	2.157	2.951
CG + e_d to LE	Vert	0.984	2.060	2.445
	Lat	3.001	2.032	2.714

From the simulation results it appears that shifting e_d along with the CG slightly increases the vibration in vertical direction and slightly decreases the vibration in lateral direction. The effects of shifting both therefore do not seem to stack. A possible explanation could be that when it comes to CG and e_d, that both the distance from the original point and the distance between the two points play a role in causing vibration. When shifting both it could be the case that the increased vibration due to a shift away from the initial point is compensated by not increasing the distance between CG and e_d. More research into this phenomenon is required to reach a definite conclusion.

When it comes to comparing the two modeling approaches, it seems that both give relatively similar results. To compare the two Section 5.3 offers the best figures for the best comparison. These figures were created to investigate the behavior between adjusting the forward and adjusting the rear rotor. It was expected to see an indication for the ability of the VPM model to capture the reduced effectiveness of adjusting the rear rotor. It was also assumed that the forward rotor is hardly influenced by the rear rotor, therefore the predicted vibrations on the forward rotor were expected equal for both models. It seems however that such conclusions cannot be drawn from these results, as for some parameters the vibrations on the forward rotor differ quite a bit between models. Furthermore, there does not seem to be a clear trend between modifying forward and rear rotors to base any conclusions on. Also, the VPM model overestimates the vibration in hover (which will be proven in chapter 6), which is an argument for just using the less complex finite state inflow

model. To argue which model is best suited for tandem rotor vibration modeling it would be better to look at validation data, which will be done in Section 6.

One of the possible causes for the vibrations due to a defect was suggested to be the frequency response of the blade. The results from the modal analysis from FLIGHTLAB however showed little variation in eigenfrequencies and mode shapes. It was expected to see more significant changes due to for example a 10% increase in bending stiffness. Also, both a parameter with a small effect on vibrations ($EIYY$) and one with a large effect (GJ) show little effect on the frequency response of the blade.

6

Validation and Sensitivity Analysis

In this section the validity of the FLIGHTLAB model will be assessed. This will be done by comparing the effectiveness of RTB adjustments on the trim tab, tip weights and the pitch link from the model to measurements from test flights that have been performed with the CH-47. Also, in this chapter it will be investigated whether replacing the rigid fuselage to generate all the results from chapter 5, with an elastic fuselage will significantly influence the results. This is done to assess the recommendation from previous works such as Terpening et al. (2016) to include an elastic fuselage. In Section 6.4 it will be analyzed whether the inclusion of an elastic fuselage changes the effectiveness of blade adjustments and whether the reference values are more closely approximated. Conclusions can then be drawn on whether the added complexity of an elastic fuselage would be justified. Since the conditions for the flight tests are not known it is of interest to determine whether changes in for example the take-off weight and overall CG location have a large influence on the measurements. A sensitivity analysis was carried out to investigate the effects of differences in test conditions and its results will be presented in Section 6.5.

The vibration data from the flight tests was gathered using multiple helicopters with varying flight hours. The flight testing consisted of first collecting data for three different flight regimes, followed by a single adjustment made to a single blade. The helicopter was then flown again and the vibration was measured again in the same flight regimes. This was repeated a number of times for each adjustment on both rotors. The sensitivity coefficient of each adjustment type on each blade on both rotors was taken by averaging the results from flight testing. The coefficients are expressed for pitch link as $ips/notch$, for the dynamic balance weights as $ips/weight$ and for trim tab as $ips/degree$.

The coefficients from flight testing have been plotted in polar coordinates in the following sections with the results from the FLIGHTLAB analysis overlayed for comparison. Each of the figures will include four polars representing the vertical and lateral vibration on both the forward and rear rotor. The zero azimuth angle in the polar axes points to the rear of the rotorcraft. Note that in the figures all the azimuth axes are ordered counter-clockwise, while the rear rotor spins in the clockwise direction. The radial axis of the plots represents the measured change in vibration in ips.

First the effects of making RTB adjustments to the blade will be presented. In Section 6.1 the results for adjusting the pitch link will be compared. This is followed by the deflection of the trim tab in Section 6.2. In Section 6.3 the addition of tip weights will be treated. In Section 6.4 the effects of including a modal fuselage will be analyzed. This is done by comparing the effectiveness of blade adjustment for the rigid and modal fuselage. In this case both models have the VPM applied. The sensitivity analysis will be treated in Section 6.5.

6.1. Effects of Pitch Link Extension

The first adjustment that will be looked at is an adjustment of the pitch link by one notch. First an adjustment on the forward rotor will be compared for both the finite state inflow model (fig. 6.1) and the VPM model (fig. 6.2). First the result will be presented with a short discussion of the results at the end of this section.

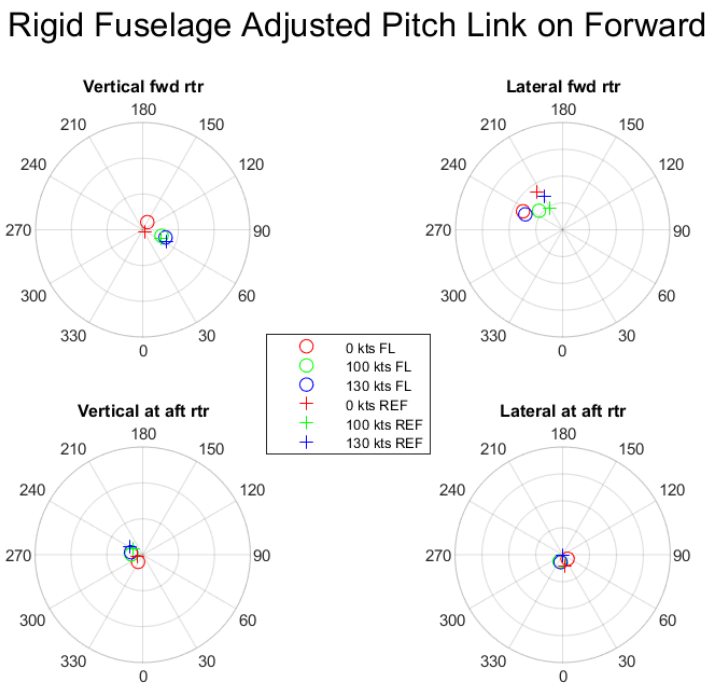

Figure 6.1: Predicted vibration magnitude and azimuth angle for the model without rotor interference due to adjustment of the pitch link by one notch on the forward rotor.

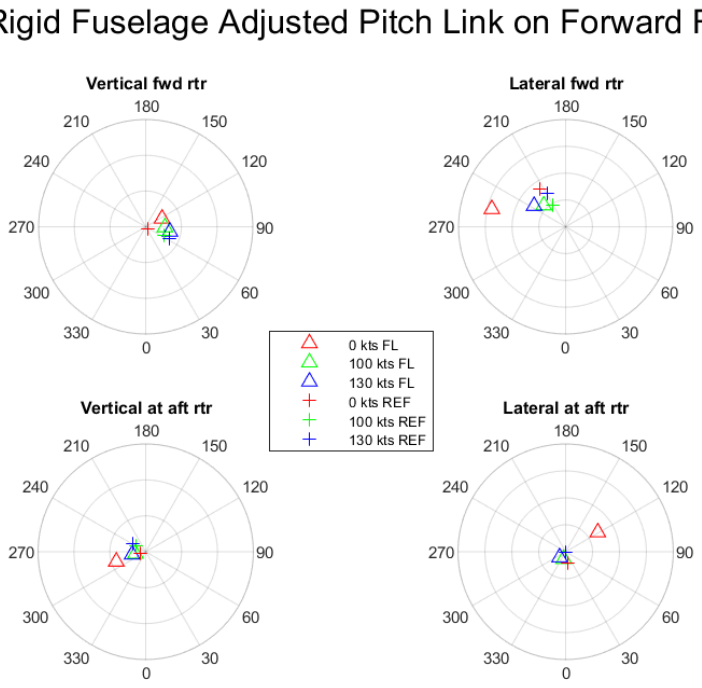

Figure 6.2: Predicted vibration magnitude and azimuth angle for the VPM model due to adjustment of the pitch link by one notch on the forward rotor.

The results for an adjustment on the rear rotor for the finite state inflow model are shown in Figures 6.3 and 6.4 respectively.

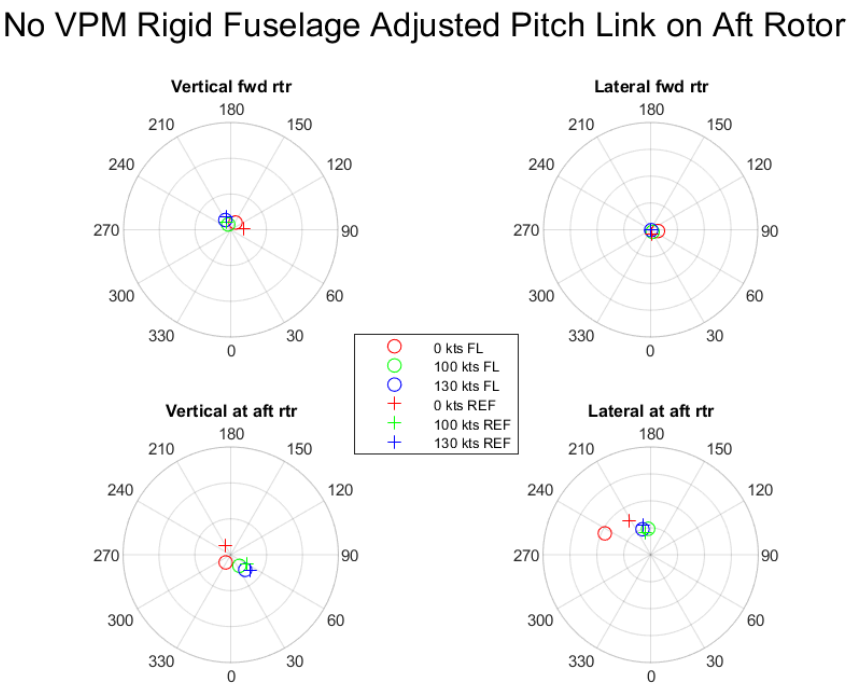

Figure 6.3: Predicted vibration magnitude and azimuth angle for the model without rotor interference due to adjustment of the pitch link by one notch on the rear rotor.

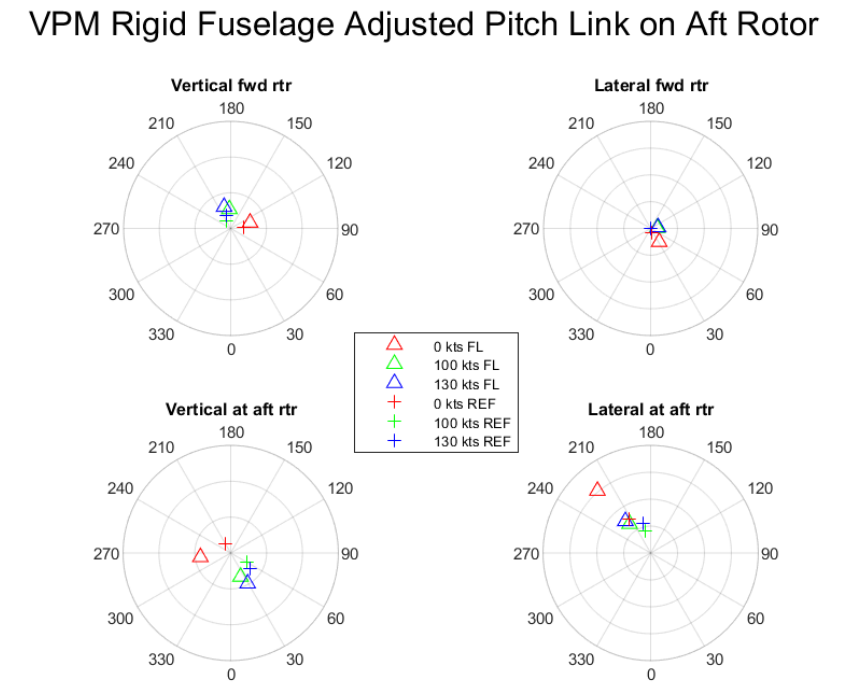

Figure 6.4: Predicted vibration magnitude and azimuth angle for the VPM model due to adjustment of the pitch link by one notch on the rear rotor.

From these figures it can be concluded that the modeling of the pitch link adjustment approximates the averaged measurements from the test flights quite well. When it comes to the distinguishing the two models the differences are small. One thing of note and which will return throughout the rest of these results is the fact that for the VPM model the vibration magnitudes in hover are too high. The azimuth angle is also not greatly affected by the choice of model. The effects of an adjustment on the opposite rotor are too close to zero to be able to conclude whether VPM is more able to capture the effect of one rotor on the other.

6.2. Effects of Trim tab Deflection

The trim tab deflection was based on the analysis performed in Section 4.2.3. There the aerodynamic performance of the trim tab was assessed using XFOIL. As was stated in that section the accuracy of that analysis was not as high as it could be, since XFOIL is not the ideal tool for an analysis at such Reynold's and Mach numbers. Now the effect of the chosen method can be analyzed by comparing the results for a trim tab deflection in FLIGHTLAB to the available measurements. First the results for the finite state and VPM inflow models are compared for a deflection of one degree of the tab on the forward rotor in Figures 6.5 and 6.6 respectively.

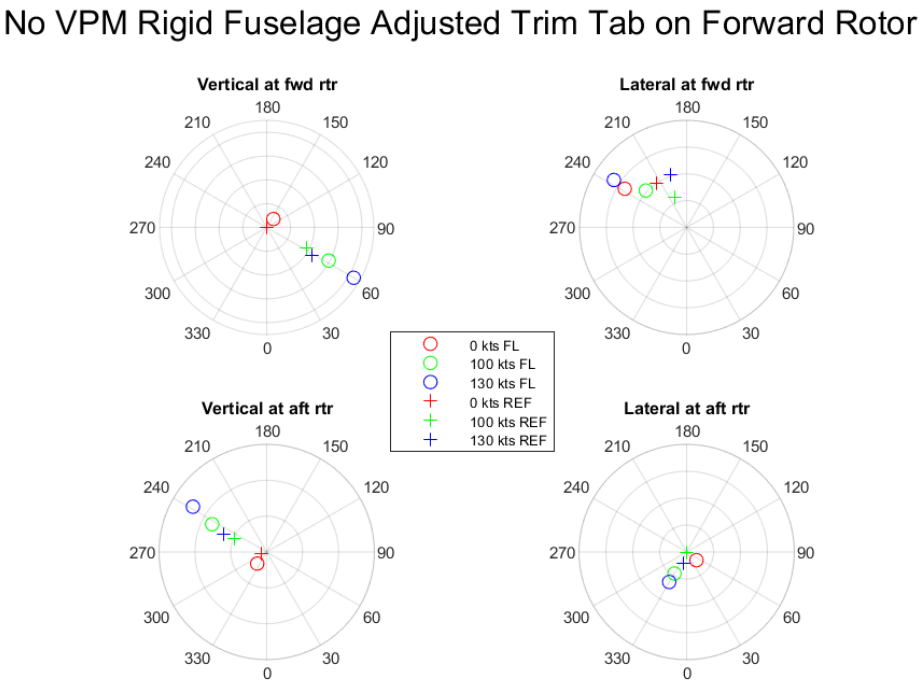

Figure 6.5: Predicted vibration magnitude and azimuth angle for the model without rotor interference due to adjustment of the trim tab by one degree on the forward rotor.

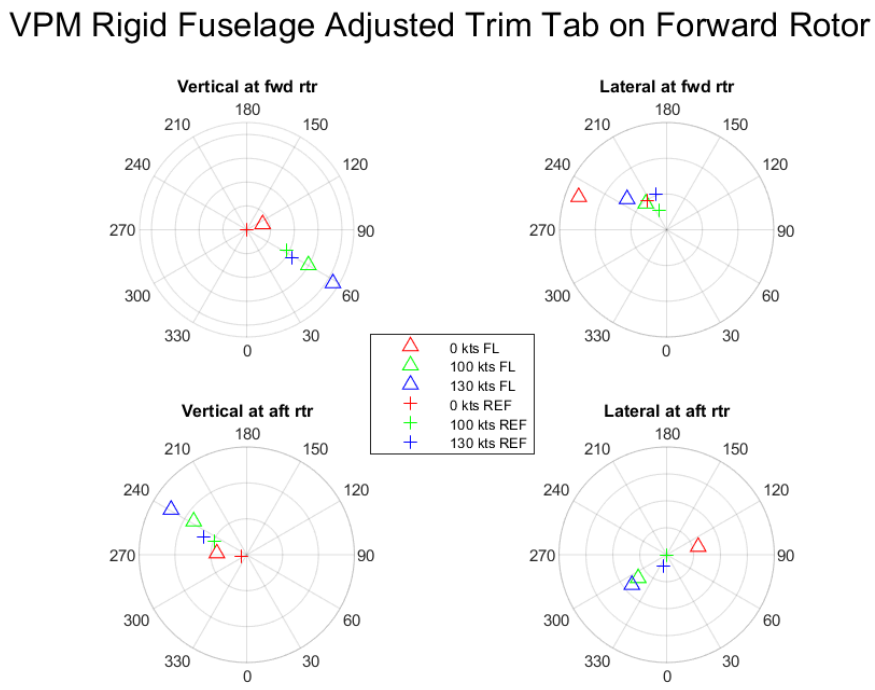

Figure 6.6: Predicted vibration magnitude and azimuth angle for the VPM model due to adjustment of the trim tab by one degree on the forward rotor.

The results for an adjustment on the rear rotor for the finite state inflow model are shown in Figures 6.7 and 6.8 respectively.

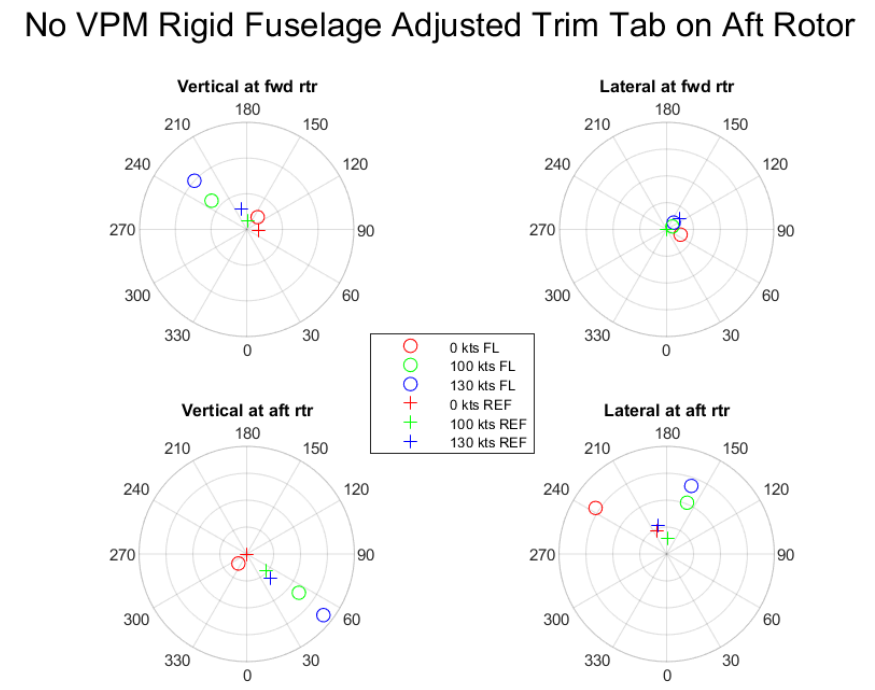

Figure 6.7: Predicted vibration magnitude and azimuth angle for the model without rotor interference due to adjustment of the trim tab by one degree on the rear rotor.

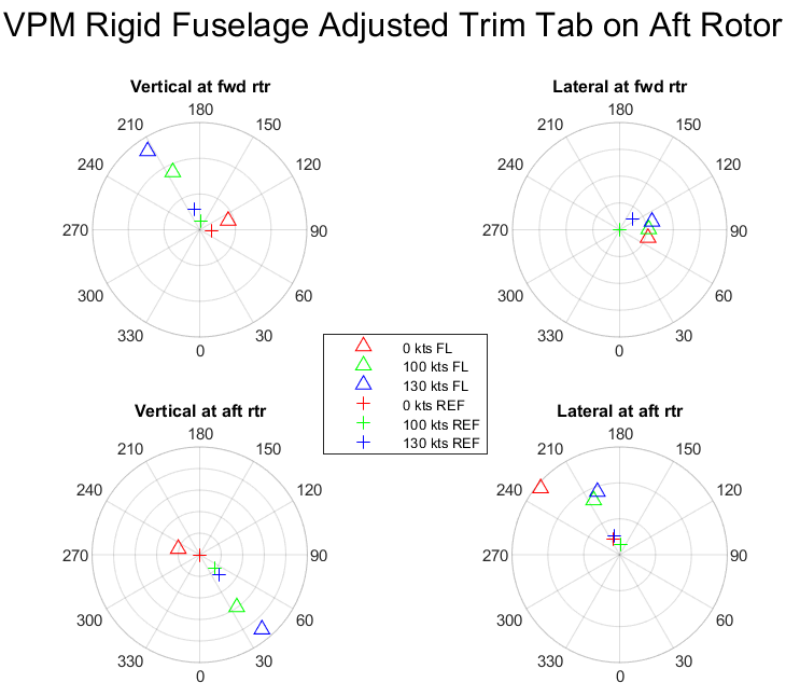

Figure 6.8: Predicted vibration magnitude and azimuth angle for the VPM model due to adjustment of the trim tab by one degree on the rear rotor.

From these figures it can be concluded that the predicted tab aerodynamic effectiveness is too high. The overestimation of the vertical vibrations indicates an over prediction of the section lift coefficient by XFOIL. The trend and azimuth angle of the results corresponds quite well to the reference values however. Therefore it would be of interest to in future model the trim tab deflection using CFD analysis. Again, by comparing the two different modeling approaches the overestimation of vibration magnitude in hover for the VPM model is apparent. When looking at an adjustment on the aft rotor there are some differences in azimuth angle between both models, where the VPM seems to more closely match the azimuth angle of the reference values. Although is difficult to base conclusions on these results, as it would be interesting to see how the results change based on higher fidelity aerodynamic analysis of the trim tab.

6.3. Effects of Adding Dynamic Balance Weight

Adding balance weights to the tip of a rotor blade is a way to balance lateral vibrations. This effect does not depend much on the airspeed of the rotorcraft. In this case the effect of adding a single balancing weight was investigated. This is shown for an adjustment to the forward rotor of the finite state inflow model in Figure 6.9 and in Figure 6.10 for the VPM model.

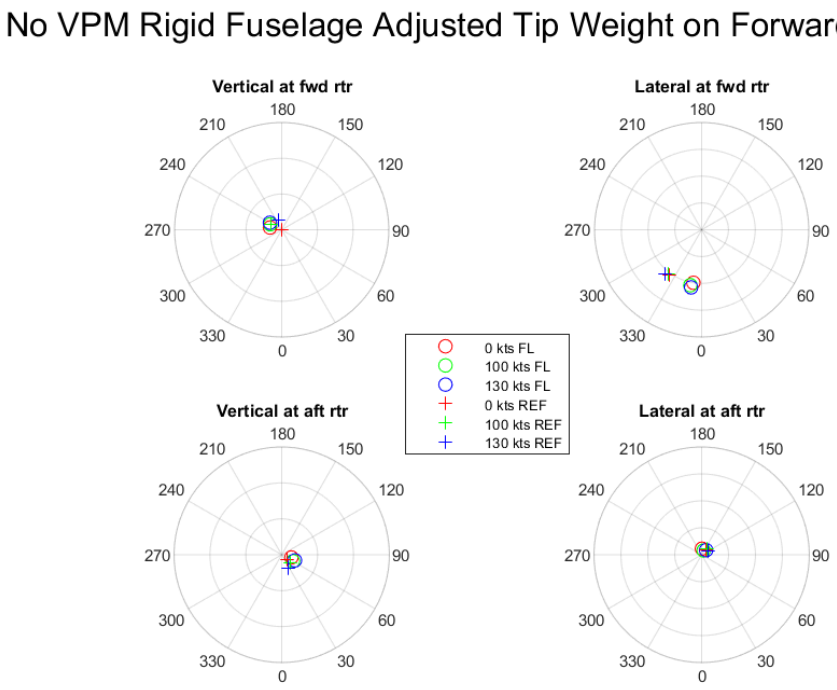

Figure 6.9: Predicted vibration magnitude and azimuth angle for the model without rotor interference due to addition of one balance weight on the forward rotor.

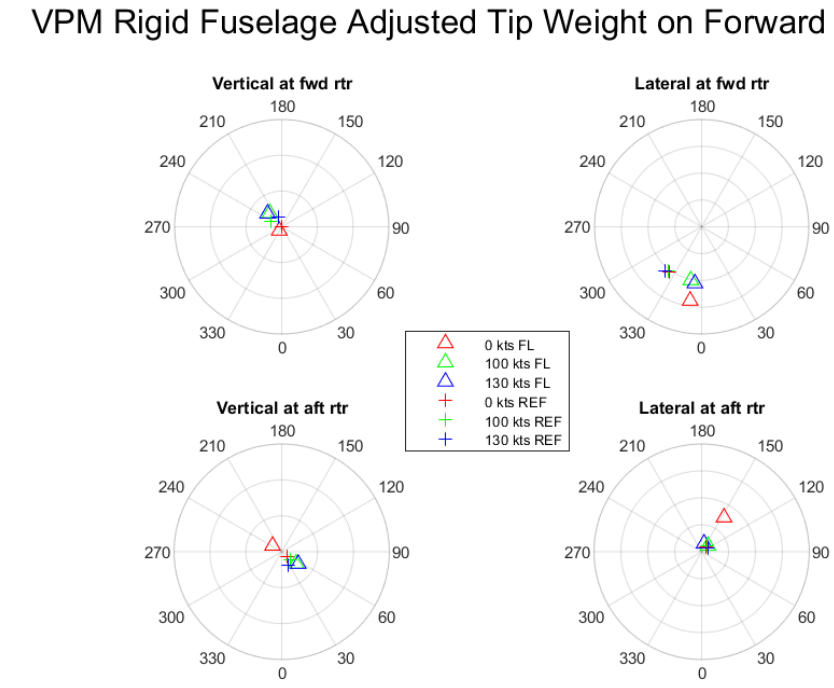

Figure 6.10: Predicted vibration magnitude and azimuth angle for the VPM model due to addition of one balance weight on the forward rotor.

The results for an adjustment on the rear rotor for the finite state inflow model are shown in Figures 6.11 and 6.12 respectively.

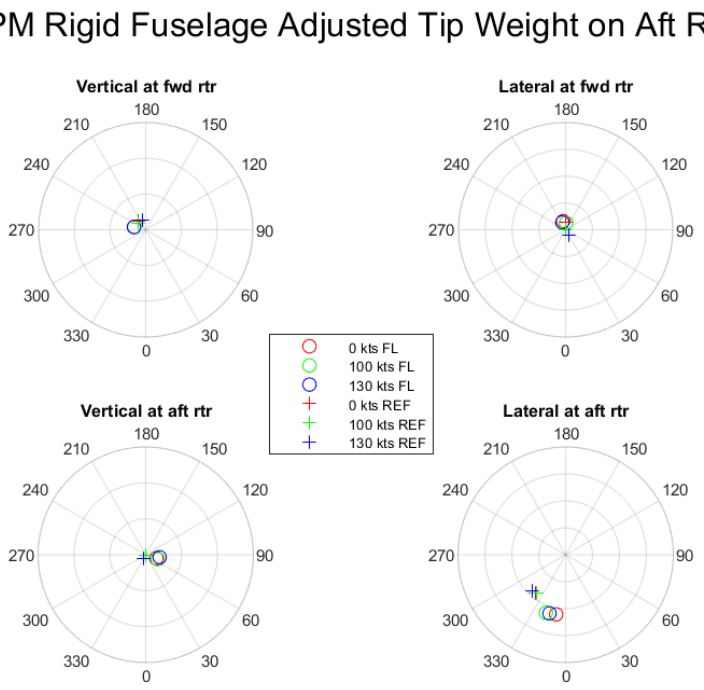

Figure 6.11: Predicted vibration magnitude and azimuth angle for the model without rotor interference due to addition of one balance weight on the rear rotor.

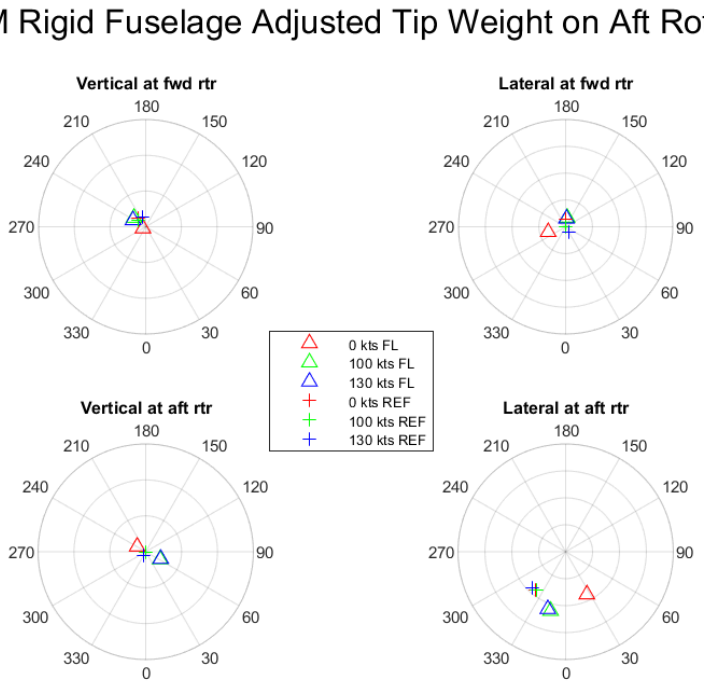

Figure 6.12: Predicted vibration magnitude and azimuth angle for the VPM model due to addition of one balance weight on the rear rotor.

The effect of the balance weights is approached quite well by the FLIGHTLAB models. The magnitude of the vibrations is similar to the results from the flight testing, although the azimuth angle is off slightly. The VPM

model azimuth angles are slightly closer to reference values, although not by much. In hover however the VPM model overestimates again compared to finite state inflow model.

6.4. Elastic Fuselage Comparison

It was recommended by previous works to analyze the effect of including an elastic fuselage to check whether this would allow for more accurate predictions of the rotor vibrations. It would require too much effort to actually construct a discretized 3-D elastic model of the fuselage. From previous investigations into the frequency response of the fuselage however there exists a modal representation of the fuselage that was tuned for the 3/rev frequency. Therefore this research also aimed to include a preliminary investigation into whether this recommendation actually would have merit and would warrant further research. This can be done by using the available modal fuselage representation and investigating what effects it has on the sensitivity coefficients and whether it could be expected that a more extensive analysis with a higher fidelity elastic model would give more accurate results. In this case the results for the rigid fuselage VPM model are compared to a VPM model with the modal fuselage. This is done for the pitch link in Figures 6.13 and 6.14, for the trim tab in Figures 6.15 and 6.16 and for the balance weights in Figures 6.17 and 6.18. Note that the vibration limits are no longer indicated for a closer view, which changes the scale compared to results shown in the previous sections.

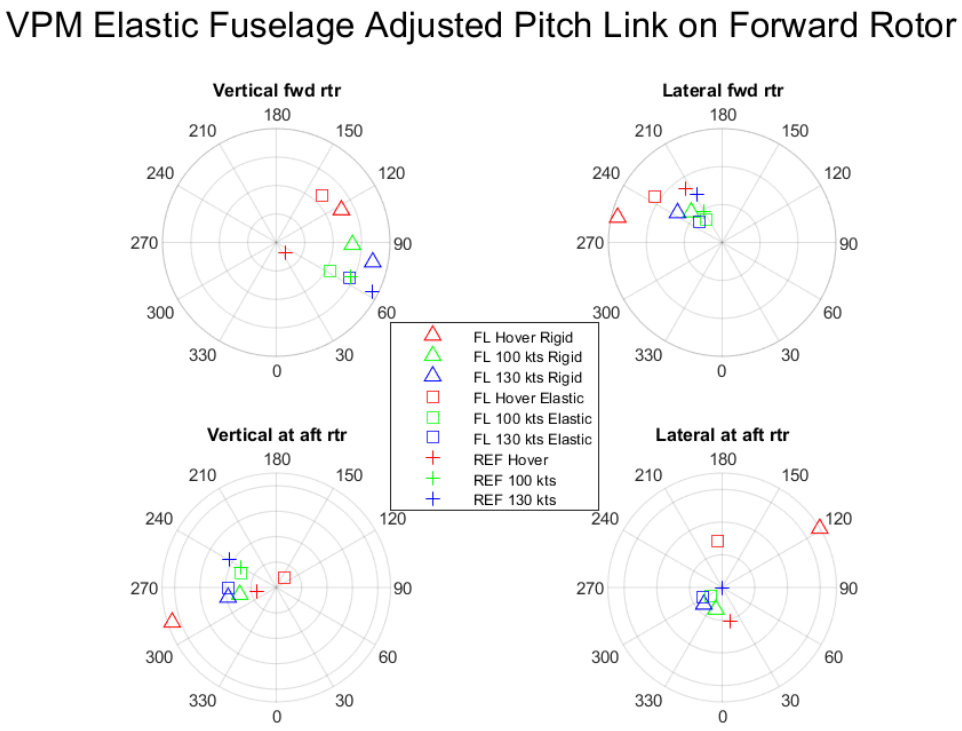

Figure 6.13: Predicted vibration magnitude and azimuth angle for the VPM model due to adjustment of the pitch link by one notch on the forward rotor.

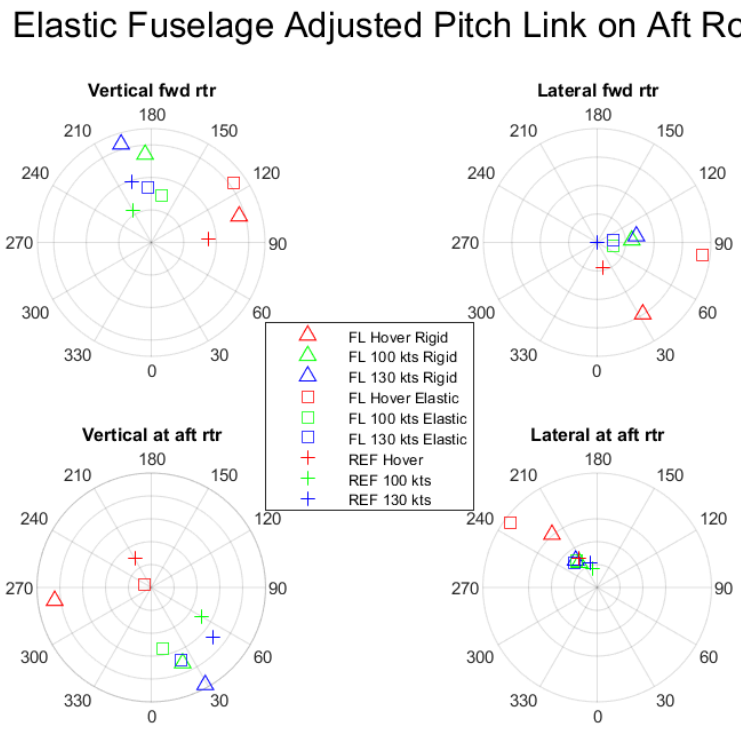

Figure 6.14: Predicted vibration magnitude and azimuth angle for the VPM model due to adjustment of the pitch link by one notch on the rear rotor.

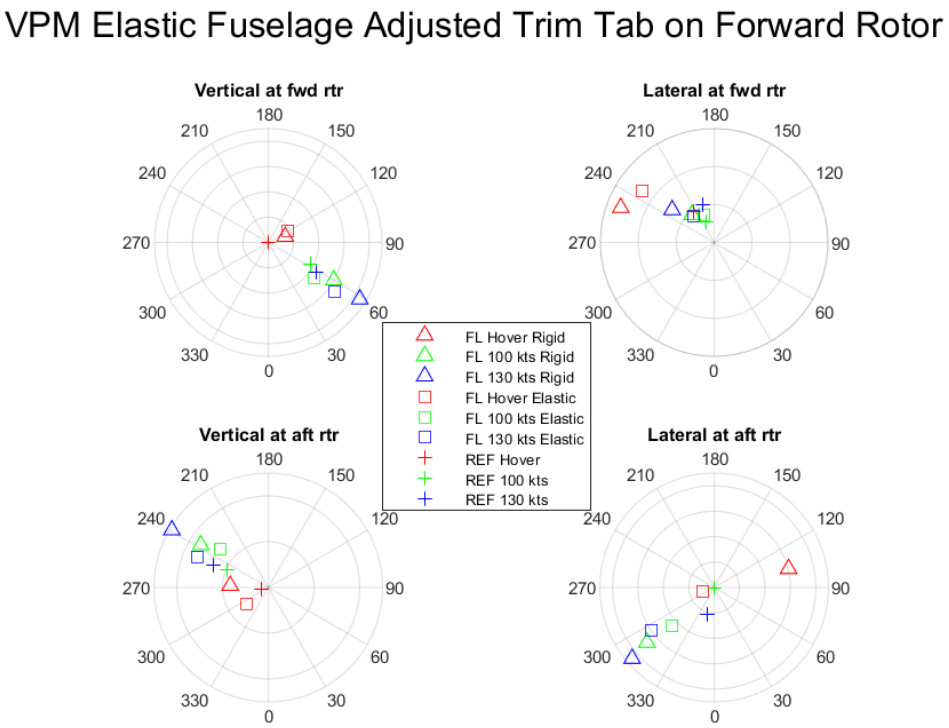

Figure 6.15: Predicted vibration magnitude and azimuth angle for the VPM model due to adjustment of the trim tab by one degree on the forward rotor.

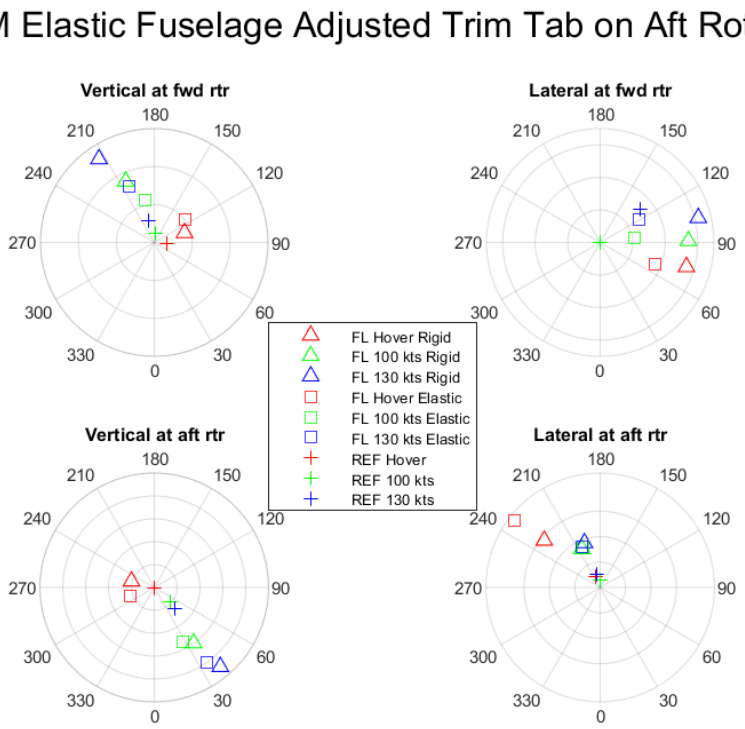

Figure 6.16: Predicted vibration magnitude and azimuth angle for the VPM model due to adjustment of the trim tab by one degree on the rear rotor.

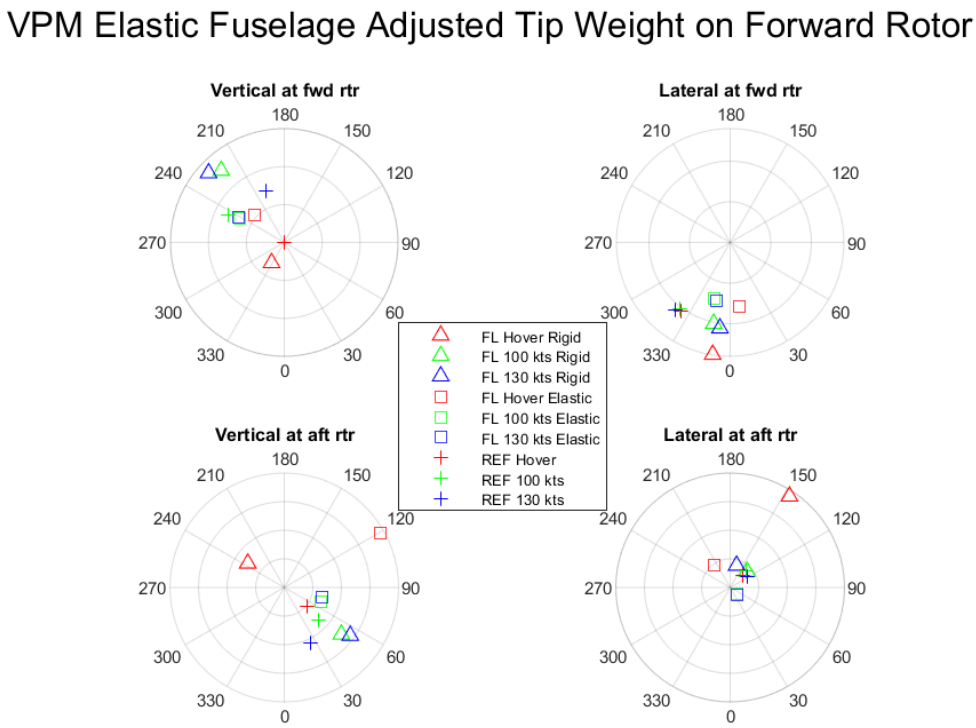

Figure 6.17: Predicted vibration magnitude and azimuth angle for the VPM model due to addition of one balance weight on the forward rotor.

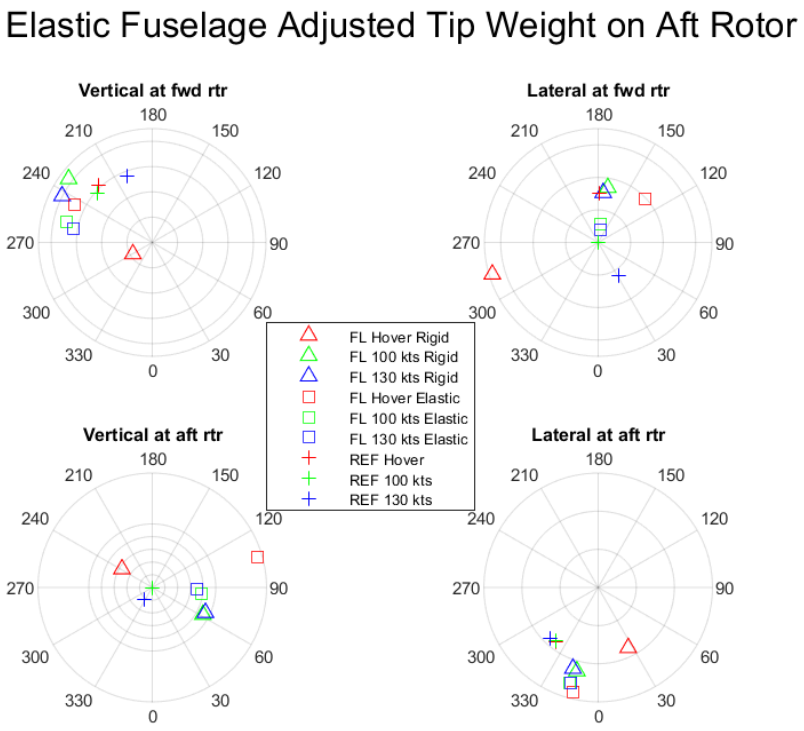

Figure 6.18: Predicted vibration magnitude and azimuth angle for the VPM model due to addition of one balance weight on the rear rotor.

One of the main observations that can be made from these comparisons is the fact that the elastic fuselage in general shows a lower vibration magnitude than the rigid fuselage model. In some cases the results from the elastic model therefore matches more closely to the reference data, as is the case for the pitch link adjustment and the trim tab. Also in a number of cases the azimuth angle is shifted more in the direction of the reference data. This can be seen for example in the results for the pitch link adjustment. The results for the balancing weight show a slightly more striking result, where the rigid model matched quite well to the measurements. In this case the elastic model lateral vibration magnitude decreases, away from the measurements for an adjustment on the forward rotor and increases, away from the measurements for an adjustment to the rear rotor (shown in the top right corner of fig. 6.17 and the bottom right corner of fig. 6.18).

It is hypothesized that the reduced vibration magnitudes for most elastic fuselage results is due to the fact that the fuselage now absorbs energy from the rotor vibrations as the fuselage natural frequency is much greater than the 1/rev frequency. The inclusion of the elastic fuselage leads to more accurate results in many cases, however also leads to worse results in other cases. Also it needs to be kept in mind that the reference values are only from one series of measurements and are averages of many different measurements, including measurement imperfections and variance between the different helicopters. It is therefore difficult to conclude without a doubt that one model is closer to the real situation, as in this case all FLIGHTLAB results match the reference values quite closely, only with minor differences between each model. Based on the additional effort required and the added computational cost for the elastic fuselage it is hard to justify its inclusion. It is definitely not required to create a ranking of parameters based on their influence on rotor vibrations. Possibly in the future, when defects can be very accurately measured and quantified for rotor blades in the inventory it might be of interest use an elastic fuselage model in order to find the most accurate sensitivity coefficients for balancing algorithms.

6.5. Sensitivity Analysis

Since the flight test data is an average of many different test flights, it would be interesting to look into the possible variation in results that could occur between different aircraft. A small number of parameters has been selected for which the simulations were run again to test for variance. There are many different param-

eters that could be changed on the aircraft, however there is no time to test all of them. It will already be possible to draw some conclusions from just a small sample. The first parameter that will be investigated is the aircraft CG location. As the CG shifts the rotor power will change for both rotors in order to stay in equilibrium. If the CG is shifted forward, the arm to the rear rotor is increased and the power on the forward rotor needs to increase in order to compensate. From the results chapter is was already proposed that the lateral vibrations scale with rotor power. Therefore this should become apparent when comparing results between the original model and one where the CG has been shifted. The same is true for an increase in aircraft take-off weight. Both of these theories were investigated, with one model including a shift in CG of 10% towards the nose and one model at MTOW. The system CG shift was chosen arbitrarily as the forward and aft CG limits were not available. In order to compare both of these versions to the baseline VPM model the balance weight sensitivity was analyzed again for both. The results for the simulations are shown in Figures 6.19 and 6.20 for the CG shift and the MTOW aircraft respectively.

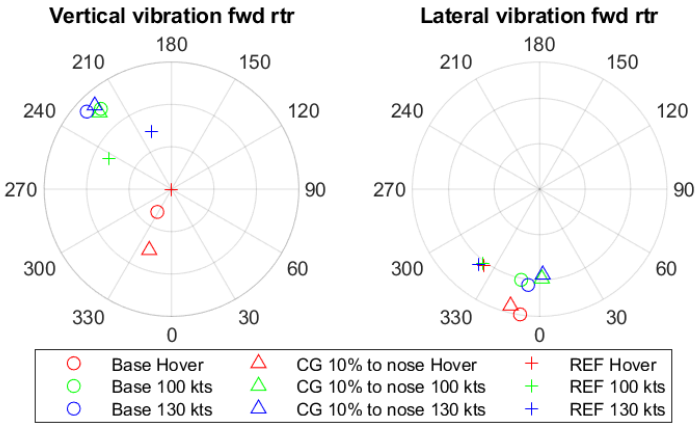

Figure 6.19: Comparison of the balance weight sensitivity for a shifted rotorcraft CG location.

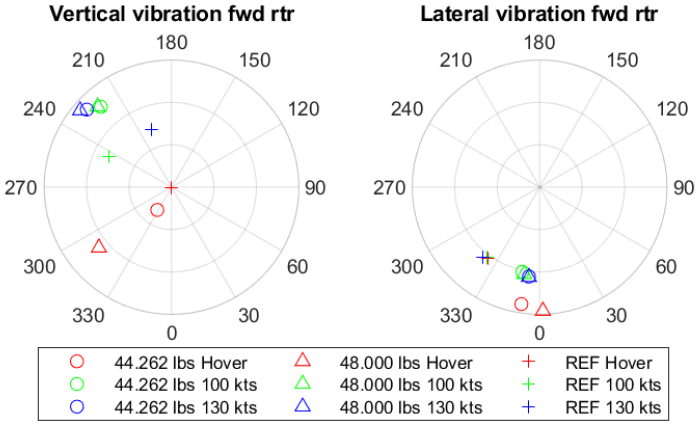

Figure 6.20: Comparison of the balance weight sensitivity for different rotorcraft weights.

It appears that the take-off weight of the helicopter has a negligible impact on the vibration magnitude. Oddly, it seems that the shifted CG caused the opposite effect of what was predicted, namely a slight decrease in lateral vibration on the forward rotor.

Another possible cause for the variance in the results could be different structural damping values between older and newer blades. To investigate this a version of the model was created with 10% increased structural damping in blade finite element properties. The same investigation as was executed for the previous two figures was repeated. The results of which are shown in Figure 6.21.

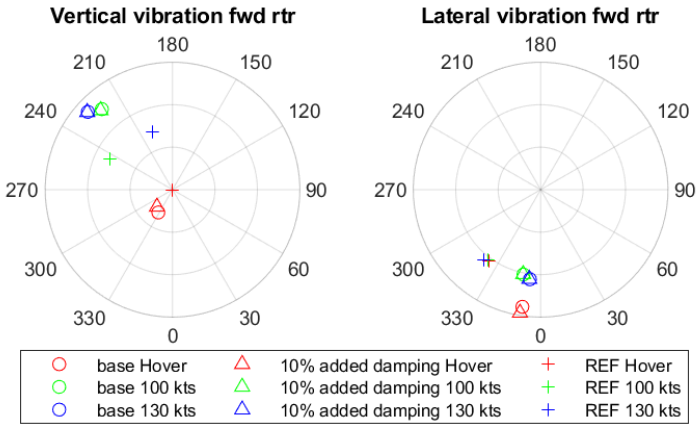

Figure 6.21: Comparison of the balance weight sensitivity for a 10% increase in blade modal damping coefficient.

Concluding from the above figure, it does not seem that additional damping would have an influence on the results.

It is known from Miller (2006) that the blade adjustment coefficients are linear. It is also known from the results section that a defect along the full span does not equal the addition of defects along smaller sections. This means that the length and location of a defect matters and cannot be captured by linear relations. It would also be interesting to check whether the same holds for the magnitude of a defect, i.e. is a 20% increase in torsional stiffness equal to twice a 10% increase? This becomes more interesting when looking for example at CG offset. In general aeroelastic stability is increased when the CG is shifted towards the leading edge. However, what would this mean for rotor vibrations? These questions were investigated and are shown in Figures 6.22 and 6.23 for the stiffness parameters and in Figure 6.24 for a section CG shift.

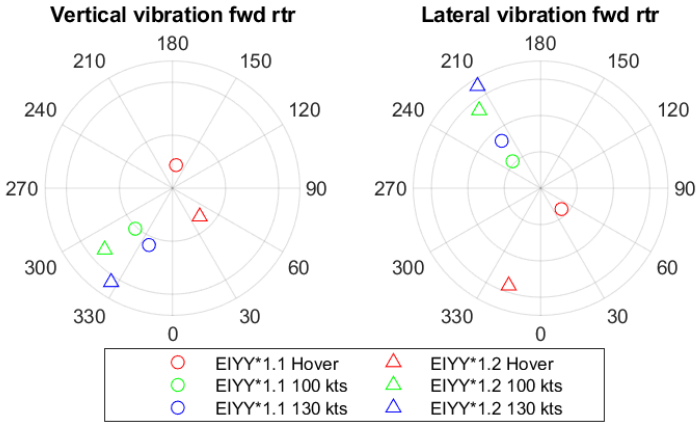

Figure 6.22: Comparison between an increase of $EIYY$ of 10% and 20% along the complete blade span.

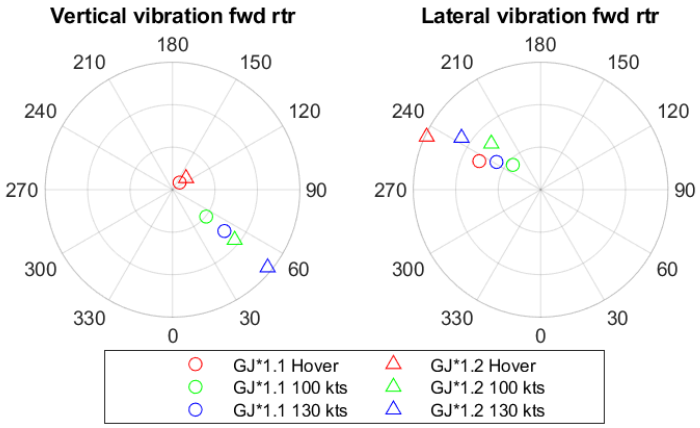

Figure 6.23: Comparison between an increase of GJ of 10% and 20% along the complete blade span.

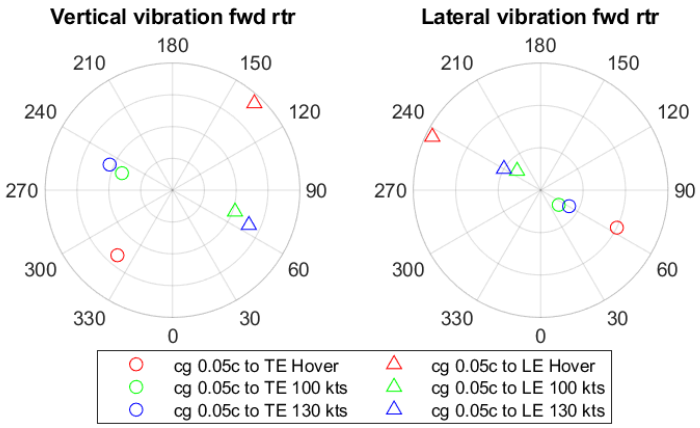

Figure 6.24: Comparison between shifting chordwise CG location $0.05c$ forward and aft.

First, looking at the increased stiffness parameters it can be concluded that the azimuth angle of the maximum vibrations does not change with increasing defect magnitude. When comparing the 10% and 20% defects it looks like the relation is not linear. Instead, it seems there are diminishing returns for increasing the defect magnitude. This would mean that more research into this relation is required before the effect of a defect of arbitrary magnitude can be predicted. When it comes to shifting the chordwise CG location in either direction it can be seen that the azimuth angle is opposite for both. The magnitude for a forward shift however has a greater effect than shifting towards the trailing edge. This is a curious result, as in general aeroelastic theory this shift would increase stability. Although, if one of the blades has reduced pitch deformation compared to the others this would still cause force imbalance at the rotor head. Another possible explanation could be that the CG is already relatively close to the leading edge, such that a shift towards the leading edge is more significant than a shift towards the trailing edge.

Lastly, it was decided to do a short investigation into whether the linearity assumption from Miller (2006) is actually true for this model. To check for this, the effect of adding one tip weight was compared to the effect of adding five weights and then dividing the result by five. The results for this analysis are shown in Figure 6.25.

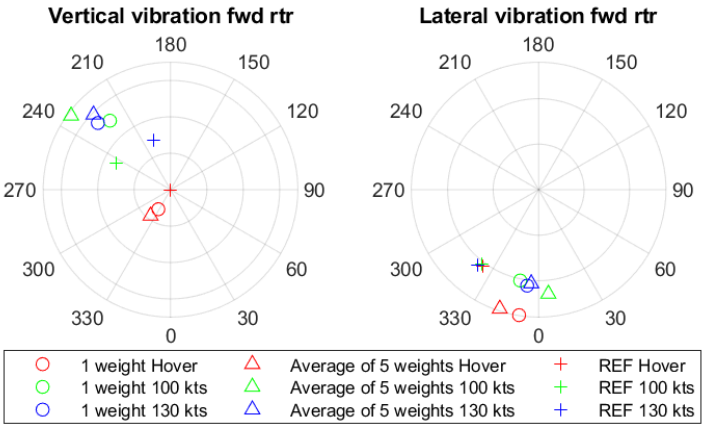

Figure 6.25: Comparison of the balance weight sensitivity taken from adding a single weight and taken from averaging the results from adding five weights.

From the above figure it can be observed that there is a minor shift in azimuth for the lateral vibrations, however the linearity assumption in this case definitely holds.

7

Conclusions

The overall goal of this research was to provide insight into what factors could cause a blade set to have poor RTB characteristics. This information would be useful for future developments into new blade property test equipment that could take advantage of both improved measuring capabilities and the knowledge on parameter significance, based on this research. In this case the research focuses on a tandem rotor helicopter system. A tandem rotor system has the added complexity of the wake of one rotor acting on the opposite rotor. The effects of this phenomenon on 1/rev vibrations is not a well researched topic. A novel inflow modeling method specifically addressing the complexity of multi-rotor wake interaction was recently introduced by the ART, the company behind the rotorcraft simulation software FLIGHTLAB, called VPM. One of the aims of this research was to investigate whether rotor vibrations on a tandem rotor system were fundamentally different from a single rotor system and whether the VPM inflow model is able to capture this effect if it exists. One of the recurring recommendations from previous investigations into rotor vibrations was the inclusion of an elastic fuselage. In this case, modal representation of the fuselage is available from earlier research at the NLR. To address the recommendations from previous works it was decided to investigate the inclusion of this modal fuselage. This fuselage model may not be optimally tuned for 1/rev, however, to not overextend the scope of this research it is only used to draw preliminary conclusions for future research efforts. Not much research has been performed with similar research questions, so it's challenging to be able to validate the vibration predictions from FLIGHTLAB. Fortunately, the sensitivities for trim tab, tip weight and pitch have been collected during flight testing. This series of measurements is highly valuable in this case since it allows for assessing the FLIGHTLAB model's validity when it comes to predicting in flight vibrations based on blade adjustments. All the above has been captured by asking the following research questions:

> MQ: "Which aeromechanical parameters of the CH-47 Chinook helicopter rotor blades have the greatest impact on the system's 1/rev vibration levels during flight?"
>
> SQ1: "What is the effect of the tandem rotor configuration of the 1/rev vibration levels of the rotor systems and how can this effect be captured in a computational model?"
>
> SQ2: "Does the inclusion of a flexible fuselage increase the accuracy of predicting the vibration coefficients?"
>
> SQ3: "What are blade adjustment sensitivity coefficient values predicted by the model and how well do they match reference literature?"

These questions will be answered in this chapter, based on the results presented in the previous chapters. First the sub-questions will be treated and lastly the main question will be discussed.

7.1. Effect of Tandem Rotor Configuration

The approach of this research to investigate the effects that the tandem rotor configuration was to compare results vibrations measured on both rotors for a model with rotor on rotor interference and a model without modeling this effect. This is the main reason why the choice was made to appy the VPM inflow model. Therefore, a conclusion shall also be made on whether this modeling approach is justified, as the VPM modeling

adds complexity and computational cost to the model. The comparisons are presented in Section 5.3, where full span adjustments of blade parameters on both rotors are shown for both modeling approaches side by side. From flight test measurements and the research by Lee et al. (2009) it could be concluded that the effectiveness of an adjustment on the rear rotor is less effective on the rear rotor than on the forward rotor. Also, the forward rotor behaves comparably to if it were just a single rotor system. Therefore, if there would be a significant impact of the rotor wake interference, one would expect to see equal results for an adjustment on the forward and aft rotor for the model without interference. The model with interference one would expect the rear rotor to show lower vibration magnitude compared to the forward rotor. Additionally both modeling approaches can be compared to the reference data, in order to investigate whether the VPM performs better.

The relation between forward and aft rotor adjustments is however not something that becomes apparent when comparing the results in Section 5.3. In many cases, for the VPM model the values on the rear rotor, relative to the forward rotor are actually higher than for the finite state inflow model. One possible cause for this could be that the VPM model influences the required rotor power, making it difficult to compare the two sets of data. One more way of comparing which modeling approach is preferable is to look at the validation plots from section chapter 6. When comparing the polar plots for the different RTB adjustments it can be concluded that the difference between the results for both models is relatively minor. Even without including the rotor wake interference the results of the finite state inflow model approach the reference data. Moreover, for the VPM model the vibrations in hover are greatly overestimated.

Based on the above statements it can be concluded that the effect of the rotor wake on the opposite rotor for 1/rev vibrations is not significant, as the model without interference effects matches the reference data quite well. This indicates that the results do not change considerably based on the rotor-wake interaction. This is true for both the forward and the rear rotor. Additionally, it is not required to use VPM to accurately estimate the vibration on the rotor opposite of the adjusted rotor. In most cases these values are too small to be significant and when these values are not small the finite state model predicts similar results as the VPM model. Therefore, considering the extra cost and complexity of the model, it is not advised to use the VPM for 1/rev vibration prediction.

7.2. Inclusion of Flexible Fuselage

The aim of investigating the effect of including an elastic fuselage model is meant to provide insight into whether future research can significantly benefit from inclusion. Creating and validating an elastic fuselage modal is a costly and time consuming process. Therefore the benefits of including an elastic fuselage model need to outweigh the additional cost. A modal representation of the fuselage that was tuned for 3/rev frequency existed from previous research at the NLR was available to try and answer this question. As this fuselage has not been validated for 1/rev this question entails a purely qualitative analysis to try and assess whether it would be advisable for future research to include an elastic fuselage. The results for this investigation have been presented in Section 6.4.

Based on the polar plots shown, it can be concluded that elastic fuselage does influence the vibration predictions. In most cases the vibration magnitudes are reduced slightly, while the azimuth angle remains mostly unchanged. The difference in most cases is minor, and does not always approach the reference data more closely. Since the differences between rigid and elastic fuselage models are not major, and the rigid model already match the reference data quite well a clear conclusion on which approach best is difficult to draw. It seems therefore that the additional cost associated with creating a flexible fuselage is not justifiable.

7.3. Comparison of Blade Adjustment Coefficients

Since it is not possible to compare the effects of changing blade aeromechanical properties to any literature, the validity of the model can only be assessed by comparing the results of the FLIGHTLAB analysis for the trim tab, tip weight and pitch link to the flight test data. The results for this analysis have been presented in sections 6.1, 6.2 and 6.3.

For the pitch link the FLIGHTLAB results almost match the experimentally determined sensitivity coefficients. The vibration magnitudes are almost equal and the difference in azimuth angle is at most 30°. The balance weight sensitivity coefficients again show a close approximation of the experimental results. The azimuth angle again has maximum error of 30°. The trim tab however does not match well with the reference. It is suspected that the aerodynamic analysis using XFOIL for the trim effects of the trim tab deflection are overestimating the effectiveness of the tab. The XFOIL analysis had two main drawbacks, namely: not being able to take into account Mach and Reynold's numbers. This was discussed in Section 4.2.3, where it was

suggested that the aerodynamic performance is likely already overestimated for $M = 0$. This due to the fact that for all flight conditions the tab is not expected to experience $M > 0.7$ at which point Mach effects sharply rise. Additionally, for the hover condition the effectiveness is already overestimated in the polar plots. The azimuth angle however of all data points however, closely approximates the reference data.

Since both the pitch link adjustment and the addition of a balance weight so closely match the reference data it is likely that the trim tab being overestimated is likely due to the XFOIL analysis instead of a FLIGHTLAB modeling error. Especially since the azimuth angle does match closely. Acknowledging this outlier, it can be concluded that model predictions match quite well with the available experimental data. Therefore the results for the analysis into the different aeromechanical parameters investigated in chapter 5 can be presented with a certain degree of confidence.

7.4. Ranking of Aeromechanical Parameters

The main goal of this research effort is to provide a ranking of the most influential aeromechanical parameters in order to support a greater research program aiming to improve the efficiency of the RTB process in the future. As was stated in the introduction of this work, an investigation into the actual occurrence and variance of specific blade defects and properties is part of a separate investigation of which the results are not yet available. Therefore this research assumed parameter variation based on engineering guess. In this case for the stiffness and aerodynamic parameters an offset of 10% was selected. For the elastic axis offset and the center of gravity offset an offset value of 5% chord was selected. This means that, while this research can conclude on which parameters are most critical, it cannot be concluded whether this defect magnitude actually occurs within the lifetime of a set of blades. It can however determine which parameters deserve more attention in the investigation into the defect occurrence within the blade inventory. In future this analysis can then be combined with aforementioned investigation to provide an actual overview of the most problematic defects for RTB.

Keeping this in mind the following conclusions can be drawn from the FLIGHTLAB analysis. When it comes to the stiffness properties of the blade, it seems that only the torsional stiffness is has a significant effect on the vibrations, since the bending stiffnesses in both directions do not cause greater vibrations than the baseline measurement. Looking at the elastic axis offset and the center of gravity offset it seems the effect of either have a similar magnitude. Even a 10% section of the span having e_d or CG shifted causes vibrations above the allowed limit for cruise. This is a greater effect than changing the torsional stiffness. When it comes to the section lift and drag coefficients the lift coefficient has a greater sensitivity than the drag coefficient. A 10% change in drag coefficient is comparable in magnitude to adjusting the torsional stiffness by 10%. The section lift coefficient however is up to nearly four times as effective. Adjusting the twist angle of the blade mainly has an effect on vertical vibrations and a minor effect on lateral vibration. Excluding the hover flight condition, the effect on vertical vibrations for a 10% increase in section twist angle along the entire span compares to a 10% change in the section lift coefficient.

Based on these results it is suggested that when analyzing the effects of blade repairs and defects, most attention be directed towards investigating the chordwise shift in center of gravity and a shift in the elastic axis. Also of great interest are a possible reduction of section lift coefficient and an increase in drag coefficient. Of similar concern are a reduction of the torsional stiffness and twist deformation of the blade. Of little concern are a reduction in flapwise and lag bending stiffness.

7.5. Recommendations

During this research a number of interesting observation were made that may prove interesting to investigate further, but were not possible due to limited time and means. In this section a number of recommendations for future research will be given. The main recommendation from this research is to investigate what the actual expected variance and upper limits of changes in aeromechanical parameters would be for blades that are in circulation. This would allow the conclusions from this research to be put into perspective.

This research was not able to accurately model the trim tab aerodynamic performance closely enough. It is assumed that the overestimation of the tab effectiveness stems from XFOIL not being designed for higher Reynold's numbers. It would be interesting to investigate whether CFD analysis would improve the sensitivities for tab deflection.

One thing that was left out of this research in order to not overextend the scope was defects on the rotor hub. This includes effects such as reduced pitch link stiffness due to wear, reduced lag damper effectiveness and other wear. It is already known from the modal analysis that was performed in this investigation that

the pitch link stiffness and lag damping influence the blade response. Rotor hub defects could equally cause trouble for the RTB process as dissimilar blades.

When the investigation started it was not expected that the finite state inflow model would perform so closely to the VPM model. Therefore this version of the model was never tested with separate rotor interference models. It would be valuable to investigate how the results for the finite state inflow model would be influenced by the inclusion of a separate interference model.

The results from this research show that a reduction in aerodynamic performance of a blade can cause vibration if the others blades are left ideal. Currently ARBI focuses mainly on measuring the effects of deficiencies on structural parameter distributions. It may be of great value to investigate the effects of deficiencies such as profile wear on aerodynamic performance.

This work mainly focused on which parameters are the major contributors to rotor vibration. Further investigation is required in order to assess the causal principles of vibration due to specific blade defects. As was briefly touched upon in the results chapter, the airloads on a blade with the CG shifted more towards the leading edge are reduced. This lift imbalance between rotors could be the cause for the measured vibration. It would be of interest to determine whether airloads increase when CG is shifted in the opposite direction. This should also be investigated for the other parameters.

Although generally not treated by RTB, the higher forcing frequencies are also causes for excessive vibration in flight. An interesting research opportunity would be to investigate whether certain higher frequencies cause excessive vibration in flight and to perform similar research on the effects of blade parameter changes on 2/rev 3/rev and so on.

A

Fast Fourier Transform

The Fast Fourier Transform (FFT) was used to generate the frequency spectrum from the FLIGHTLAB accelerometer sensors. The accelerometers included in the model record lateral and vertical accelerations in inch per second. These sensors record the accelerations at every solution step of the simulation. In the case of this research each full rotation consists of 100 time steps. When the model reaches a trimmed solution ten more full rotations are performed and the results at each timestep are stored. This leads to sinusoidal curves for the accelerations plotted against time.

In order to obtain the maximum acceleration associated with the 1/rev frequency the FFT is applied to transform the sinusoidal wave into the frequency spectrum. The FFT returns a spectrum in both real and imaginary terms, which must scaled and converted into polar coordinates to obtain the magnitude and phase angle (Cerna and Harvey (2000)). Equations A.1 and A.2 are used to determine the amplitude and phase in relation to frequency (from Cerna and Harvey (2000)).

$$\text{Amplitude spectrum in quantity peak} = \frac{\text{Magnitude}[\text{FFT}(A)]}{N} = \frac{\sqrt{[Real[\text{FFT}(A)]]^2 + [Imag[\text{FFT}(A)]]^2}}{N} \quad \text{(A.1)}$$

$$\text{Phase spectrum in radians} = \text{Phase}[\text{FFT}(A)] = \arctan\left(\frac{Imag[\text{FFT}(A)]}{Real[\text{FFT}(A)]}\right) \quad \text{(A.2)}$$

In the above equations A represents the signal and N represents the number of points. The above equation were used to create the amplitude and phase angle spectra. An example of the amplitude spectrum is presented in figure A.1.

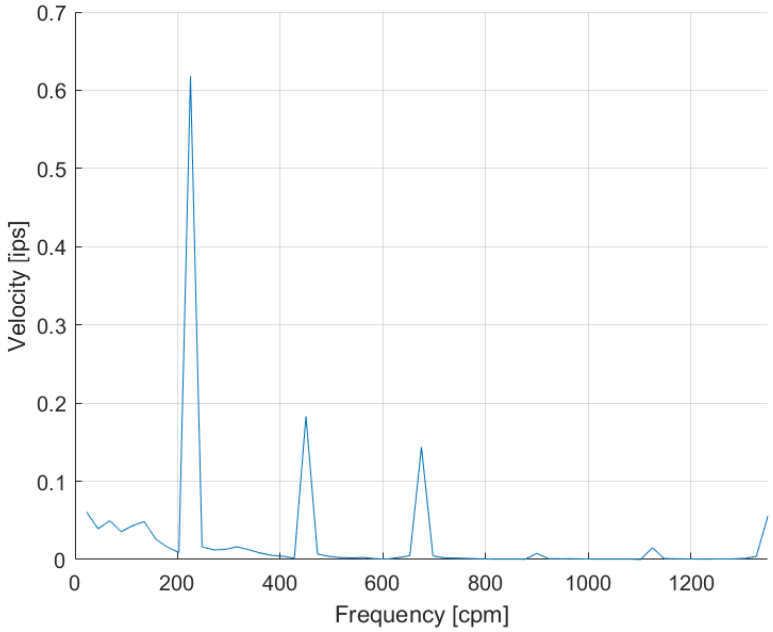

Figure A.1: Example of an amplitude spectrum for a rotor with dissimilar blades.

In the above figure the first few forcing frequencies clearly stand out. At 225 rpm the 1/rev frequency can be found followed by the 2/rev at 450 rpm and followed again by the 3/rev at 675 rpm. To obtain the 1/rev vibration magnitude in ips one simply needs to take the amplitude value at the corresponding frequency from the amplitude spectrum.

Bibliography

Advanced Rotorcraft Technology, Inc. *FLIGHTLAB Theory Manual (Vol. One)*. Sunnyvale, CA, 2011a.

Advanced Rotorcraft Technology, Inc. *FLIGHTLAB Theory Manual (Vol. Two)*. Sunnyvale, CA, 2011b.

G.L. Bender, G.M. Yamakawa, and M.K. Herbst. Airworthiness and flight characteristics test (a&fc) of the ch-47d helicopter. US Army Aviation Engineering Flight Activity, 1985. https://apps.dtic.mil/dtic/tr/fulltext/u2/a151380.pdf.

J.T. Buckel. Rotor blade static balance - art or science? Technical report, Avion, 2003. Presented to the American Helicopter Society.

R.L. Burden and J.D. Faires. *Numerical Analysis*. PWS-Kent Publishing Company, Boston, ninth edition, 1989.

M Cerna and A.F. Harvey. The fundamentals of fft-based signal analysis and measurement, 2000. Application Note 041.

R.T.N. Chen and W.S. Hindson. Influence of dynamic inflow on the helicopter vertical response. Technical report, NASA Ames Research Center, 06 1986. NASA Technical Memorandum 88327.

L.U. Dadone. Us army helicopter design datcom volume i - airfoils. Technical report, US Army Air Mobility R&D Laboratory, Ames Research Center, Moffet Field, California, May 1976. https://apps.dtic.mil/dtic/tr/fulltext/u2/a033425.pdf.

A.C. De Bruin. Survey of techniques and presentation of a research strategy for improved procedures for the royal netherlands air force. Technical report, Royal Netherlands Aerospace Center, 2010.

M. Drela. Xfoil: An analysis and design system for low reynolds number airfoils. *Conference on Low Reynolds Number Airfoil Aerodynamics*, June 1989. doi: 10.1007/978-3-642-84010-4_1.

R.W. Du Val and C He. Validation of the flightlab virtual engineering toolset. *The Aeronautical Journal*, 122: 519–555, April 2018. doi: 10.1017/aer.2018.12.

R. Ferrer, P.A. Aubourg, T. Krysinski, and S. Bellizzi. New methods for rotor tracking and balance tuning and defect detection applied to eurocopter products. *American Helicopter Society 57th Annual Forum*, 2001.

M. Gladfelter, C. He, C. Chang, M.B. Tischler, J.S. Lopez, and O. Juhasz. Enhancement and validation of vpm-derived state-space. *Vertical Flight Society 76th Annual Forum & Technology Display*, October 2020.

F. Guner, J.V.R. Prasad, C. He, and D.G. Miller. Tandem rotor inflow modeling and its effect on vehicle dynamics. *Vertical Flight Society 75th Annual Forum and Technology Display*, May 2019.

J.C. Hasty, J.A. Keller, and S.M. Krick. Improved rotor smoothing for the u.s. army ch-47d. *American Helicopter Society Specialists' Meeting on Condition Based Maintenance, Huntsville AL*, February 2008.

C. He and J. Zhao. Modeling rotor wake dynamics with viscous vortex particle method. *AIAA Journal*, 47(4), 04 2009.

C. He, M. Syal, M.B. Tischler, and O. Juhasz. State-space inflow model identification from viscous vortex particle method for advanced rotorcraft configurations. *American Helicopter Society 73rd Annual Forum*, 2017.

Helistart.com. Swashplate assembly. `http://www.helistart.com/pitchControl.aspx`.

S. Hoa. Vibration of a rotating beam with tip mass. *Journal of Sound and Vibration*, 67:369–381, 12 1979. doi: 10.1016/0022-460X(79)90542-X.

D. Hodges. Nonlinear equations for dynamics of pretwisted beams undergoing small strains and large rotations. Technical report, NASA Ames Research Center, 06 1985. NASA Technical Paper 2470.

S.J. Hulshoff. Ae4930 aeroelasticity, 2012. Course Notes.

Y. Hyun You, S. Nam Jung, Prashant M. Pawar, and E. Sup Shin. Effect of uncertainty on hub vibration response of composite helicopter rotor blades. *Journal of Aircraft*, 47(1):151–160, January-February 2010.

ierw. Transverse flow effect. `https://www.ierwtraining.com/Transverse_Flow_Effect.htm`, 2004.

W. Johnson. *Helicopter Theory*. Dover Publications inc., New York, 1980.

W. Johnson. Airloads, wakes, and aeroelasticity. Technical report, NASA Ames Research Center, 04 1990. USAAVSCOM Technical Memorandum 90-A-005.

K.C. Kim. Analytical investigation into the helicopter vibration resulting from main rotor blade (mrb) ballistic damage. Technical report, Army Research Laboratory, Aberdeen MD, 1999.

M. Krumm, V. Hämmerle, H. Cárdenez, and C. Sauerwein. 3d x-ray inspection system for helicopter rotor blade. *11th International Symposium NDT in Aerospace*, 2019.

J. Lee, S. Oh, K. Yee, and D. Kim. Numerical investigation on overlap effects of tandem rotors in forward flight. *International Journal of Aeronautical and Space Sciences*, 10, 11 2009. doi: 10.5139/IJASS.2009.10.2.063.

J.G. Leishman. Aerodynamic characteristics of a helicopter rotor airfoil as affected bysimulated ballistic damage. Technical Report ARL-CR-66, Army Research Laboratory Aberdeen Proving Ground, MD, July 1993.

J.G. Leishman. Experimental investigation into the aerodynamic characteristics of helicopter rotor airfoils with ballistic damage. Technical Report ARL-CR-295, Army Research Laboratory Aberdeen Proving Ground, MD, 1996.

N.G. Marichal, M. Tomas-Rodriguez, Angela Hernandez, Salvador Castillo-Rivera, and Pascual Campoy. Vibration reduction for vision systems on board unmanned aerial vehicles using a neuro-fuzzy controller. *Journal of Vibration and Control*, 20, 06 2013. doi: 10.1177/1077546313479632.

B. Marrant and M. Pavel. Helicopter performance, stability and control, 2002. Course Notes.

M. Maughmer and J. Coder. Comparisons of theoretical methods for predicting airfoil aerodynamic characteristics. *Journal of Aircraft*, 51:48, August 2010. doi: 10.2514/1.C032232.

P. Meinlschmidt and J. Aderhold. Thermographic inspection of rotor blades. *European Conference on Non-Destructive Testing*, 2006.

L. Meirovitch and R. Parker. Fundamentals of vibrations. *Applied Mechanics Reviews - APPL MECH REV*, 54, January 2001. doi: 10.1115/1.1421112.

N.A. Miller. A comparison of main rotor smoothing adjustments using linear and neural network algorithms. Master's thesis, Air Force Institute of Technology, Wright-Patterson Air Force Base, Ohio, 2006. https://apps.dtic.mil/dtic/tr/fulltext/u2/a446788.pdf.

S.M. Murugan, Ranjan Ganguli, and Dinesh Kumar Harursampath. Stochastic aeroelastic analysis of composite helicopter rotor. *Journal of the American Helicopter Society*, 56:12001–1, 01 2011. doi: 10.4050/JAHS.56.012001.

K.Q. Nguyen. Higher harmonic control analysis for vibration reduction of helicopter rotor systems. Technical report, NASA Ames Research Center, 10 1994. NASA Technical Memorandum 103855.

D.A. Peters and C. He. Finite state induced flow models part ii: Three dimensional rotor disk. *Journal of Aircraft*, 32(2):323–333, March-April 1995.

D.A. Peters, M.P. Rossow, A. Korn, and T. Ko. Design of helicopter rotor blades for optimum dynamic characteritics. *Computers & Mathematics with Applications*, 12A(1):85–109, 1986.

R. Pezzoni and R. Krupka. Laser-shearography for non-destructive testing of large-area composite helicopter structures. *Insight: Non-Destructive Testing and Condition Monitoring*, 43:244–248, 04 2001.

M Pitt and A. Peters. Dynamic inflow for practical applications. *Vertica*, 5(1), 1981.

M.J. Renzi. An assessment of modern methods for rotor track and balance. Master's thesis, Air Force Institute of Technology, Wright-Patterson Air Force Base, Ohio, 2004. https://apps.dtic.mil/dtic/tr/fulltext/u2/a426636.pdf.

R. Robinson. Helicopter track and balance theory. `https://www.aviationpros.com/engines-components/article/10389059/helicopter-track-and-balance-theory`, February 1999. Accessed on: 08/06/2020.

A. Rosen and R. Ben-Ari. Mathematical modelling of a helicopter rotor track and balance: Results. *Journal of Sound and Vibration - J SOUND VIB*, 200:605–620, March 1997a. doi: 10.1006/jsvi.1996.0670.

A. Rosen and R. Ben-Ari. Mathematical modelling of a helicopter rotor track and balance: Theory. *Journal of Sound and Vibration - J SOUND VIB*, 200:589–603, March 1997b. doi: 10.1006/jsvi.1996.0669.

S.C. Spring, J.R. Niemann, and G.W. Wilson. Preliminary airworthiness evaluation ch-47c with fiberglass rotor blades (with 155-l-712 engines). Technical report, United States Army Aviation Engineering Flight Activity, Edwards Air Force Base, California, April 1979. https://apps.dtic.mil/dtic/tr/fulltext/u2/a069891.pdf.

C.D. Terpening, D.L. Kunz, and S.M. Dickerson. Characterization of ch-47d rotor system fault signatures using a comprehensive model. *Journal of the American Helicopter Society*, 61, 04 2016. doi: 10.4050/JAHS.61.022012.

S. Wang, K. Danai, and M. Wilson. A probability-based approach to helicopter rotor tuning. *Journal of the American Helicopter Society*, 50:56–64, January 2005. doi: 10.4050/1.3092843.

D. Wroblewski, P. Grabill, J. Berry, and R. Branhof. Neural network system for helicopter rotor smoothing. *IEEE Aerospace Conference Proceedings*, 6:271 – 276 vol.6, February 2000. doi: 10.1109/AERO.2000.877903.